Fall 2021

Investigations on the Surface Chemistry of Colloidal Quantum Dots Towards Fluorescent Biological Probes

John Hardin Dunlap

INVESTIGATIONS ON THE SURFACE CHEMISTRY OF COLLOIDAL QUANTUM DOTS TOWARDS FLUORESCENT BIOLOGICAL PROBES

by

John Hardin Dunlap

Bachelor of Science
University of Kentucky, 2016

Submitted in Partial Fulfillment of the Requirements

For the Degree of Doctor of Philosophy in

Chemistry

College of Arts and Sciences

University of South Carolina

2021

Accepted by:

Andrew B. Greytak, Major Professor

Richard D. Adams, Committee Member

Sophya Garashchuk, Committee Member

Jochen Lauterbach, Committee Member

Tracey L. Weldon, Interim Vice Provost and Dean of the Graduate School

DEDICATION

This dissertation is dedicated to my parents, Whitney and Margaret Dunlap, for their unwavering love, guidance, and understanding throughout my graduate school journey. To my brother Thomas and his wife Julie for their advice, encouragement, and contagious optimism. To Dayna for her love, support, and helping me through the tough times. To my friends at home and abroad for the game nights, the beer-brewing, and the movie marathons that helped keep me sane. I am so grateful for your kindness, advice, and understanding, without which none of this would have been possible.

ACKNOWLEDGEMENTS

Earning a Ph.D. is not entirely a solitary achievement, the road towards it is full of twists and turns and frequent speed bumps. But with the right people by your side, it can be a pretty smooth ride. There are many whom I would like to acknowledge for their assistance and guidance which helped support me throughout the last 5 years.

I would like to give my deepest appreciation to my advisor Dr. Andrew B. Greytak. I am truly grateful for his continual guidance and support of my doctoral research. His constructive feedback and patience helped motivate me to learn new chemistries and skills, to learn from my mistakes, and to become a better scientist. He helped me look at the bigger picture, to not sweat (all) little things, and how to tell a story with our work.

I also want to acknowledge my committee members who have been my teachers not only in the classroom, but in my Ph.D. exams: Dr. Richard Adams, Dr. Sophya Garashchuk, and Dr. Jochen Lauterbach. Dr. Adams was my committee chair and was always available to advise me. During my Proposal Exam he was instrumental in helping me view the broader impacts and larger picture of my proposal topic, and his advice has stuck with me ever since. Dr. Garashchuk taught my quantum chemistry class, and it turned out to be my favorite course I took at USC. Dr. Lauterbach was not only my teacher, but my IGERT co-advisor. After my proposal exam defense, he told me to ‘work on my elevator pitch”. It was great advice I will never forget, and I have kept that thought in mind ever since.

My fellow members of the Greytak lab, Preecha Kittikhunnatham, Fiaz Ahmed, Mat Kelley, Nuwanthaka Jayaweera, and Sakiru Abiodun, have been a constant source of inspiration and support in the lab. They all made life in the lab more enjoyable, and it was great to have the opportunity to work with them. Fiaz and Preecha have become two of my greatest friends. They are truly wonderful people who helped me work through my problems and encouraged me to be a better scientist. I am honored to have had the chance to get to know them and thankful for their great advice and encouragement over the years.

I had the pleasure to teach classes for Dr. Leslie Lovelace and Dr. Amy Taylor-Perry. They were always up for a laugh and never turned down homemade baked goods whenever I brought them. Thank you for being my taste-testers!

Finally, I must acknowledge my parents Whitney and Margaret Dunlap, to whom this dissertation is dedicated. They have been a constant source of love, support, and motivation throughout graduate school and my life. Without them, I would not have achieved this dream to earn my Ph.D.

Thank you, all.

ABSTRACT

Colloidal semiconductor quantum dots (QDs) have garnered significant interest as promising materials for biological applications due to their improved photostability and narrow, tunable photoluminescence properties compared to organic fluorophores. To facilitate their utility as fluorescent bioimaging probes, QDs must undergo post-synthetic modifications to exchange their native hydrophobic ligands from synthesis with hydrophilic ones that enable colloidal dispersions in aqueous environments. Many examples exist that demonstrate surface modifications for water-soluble QDs and their efficacy in biological systems, however, there is a need to develop a more thorough understanding of how hydrophilic ligands coordinate to QD surfaces in order to develop more robust QD systems. The central themes of this dissertation are to describe how hydrophilic ligands bind to QD surfaces, what types of ligands lead to the formation of robust surface coatings, and how to identify properties of ligands that lead to stronger binding. I will begin by introducing the general applications of QDs and the necessary considerations regarding their synthesis, purification, and ligand exchange chemistry. Then, I will describe the first direct comparison of the influence of block and random copolymer ligands on QD stability in the presence of an endogenous competitor ligand. Finally, I will demonstrate the relative binding strength of molecular ligands in water as a function of ligand chain length and binding denticity. Through these systematic investigations, I aim to improve upon our understanding of ligand-QD interactions towards the development of stable and robust fluorescent QD bioimaging probes.

TABLE OF CONTENTS

LIST OF TABLES

LIST OF FIGURES

CHAPTER 1

AN INTRODUCTION TO COLLOIDAL SEMICONDUCTOR QUANTUM DOTS

1.1 Colloidal Quantum Dots: Promising Materials with Favorable Properties

Colloidal semiconductor nanocrystals (NCs) are crystalline inorganic materials synthesized in solution in the presence of coordinating molecules or ions (ligands) that serve to confine their growth to the nanoscale. They are typically 1-100 nm in size and may be prepared in a variety of morphologies, ranging from spheres and cubes to nanowires and tetrapods.[1,2] Colloidal semiconductor quantum dots (QDs) are a subset of nanocrystals that are zero-dimensional (and confined in all three dimensions), roughly spherical in shape, and on the order of 1-10 nm in diameter. Because their small size is similar to the de Broglie wavelength of an electron, QDs possess discrete quantized electronic states (**Figure 1.1**) and exhibit quantum confinement, which gives rise to their favorable electronic properties.[3]

As a consequence of their quantum confined electronic states, QDs have size-tunable bandgaps that may be changed by varying the size of the nanocrystal. The bandgap gives rise to narrow and tunable emission as photoluminescence decay occurs from the lowest excited states. In addition to their emissive properties, QDs also boast high molar extinction coefficients and enhanced photostability versus organic fluorophores. These

unique and beneficial properties have caused QDs to garner significant interest from researchers for a myriad of applications, ranging from solar energy conversion, sensing, and display technologies to photocatalysts and bioimaging probes.[4]

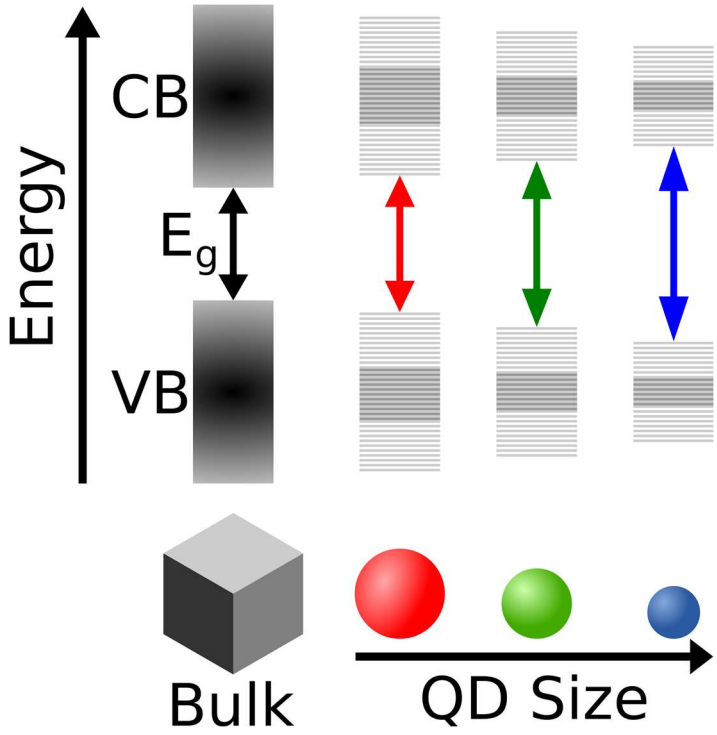

Figure 1.1 *Energy level quantization of a bulk semiconductor versus quantum dots with different sizes, and relative changes in band gap (E_g), conduction band (CB), and valence band (VB).*

1.2 Colloidal Quantum Dot Synthesis

The most common QD compositions are II-VI semiconductors, notably cadmium selenide (CdSe), cadmium sulfide (CdS), and their lead- or zinc-containing analogues (ZnSe(S), and PbSe(S)). While a variety of methods have been established to produce monodisperse colloidal QD suspensions in both organic and aqueous media, their preparation in high boiling point, non-coordinating solvents is the most widely used

because it offers the best control over the particle size distribution.[5–11] For example, 1-octadecene (ODE) is often used because its terminal alkene group can reduce elemental chalcogenide precursors to assist in NC formation, while not acting as a coordinating ligand on the particle surface.[12–14] Additionally, kinetic control and colloidal stabilization of the nanocrystals during nucleation and growth is achieved through the use of long chain aliphatic ligands, for example oleic acid (OA). The precursor conversion kinetics and ultimate size of the QDs may be fine-tuned through the reaction temperature, time, or by careful selection of the capping ligands.

The primary goal of a NC synthesis is to achieve a narrow size distribution and control over the average size and shape. The La Mer model was developed to explain the formation of colloidal samples with narrow size distributions via the concept of brief nucleation followed by extended growth from monomers, and has been used to rationalize NC growth as shown in **Figure 1.2**.[15–19] Synthetically, this involves four kinetically controlled stages: monomer supersaturation, homogeneous nucleation, growth, and growth termination.[20] The first stage begins with the formation of monomers from molecular precursors following the swift injection of a chalcogenide precursor at high temperature, upon which a brief period of monomer saturation occurs until a critical monomer concentration is reached.[21] Once a sufficient quantity of monomers has been supplied, they are rapidly consumed to form nuclei. Shortly after this "burst nucleation" begins nanocrystal growth, which can then be terminated by quenching the reaction to produce QDs in solution with narrow size distributions. Ideally, the growth period is quenched prior to a prolonged period of Ostwald ripening in which smaller particles are consumed and the monomers reassemble onto larger particles.

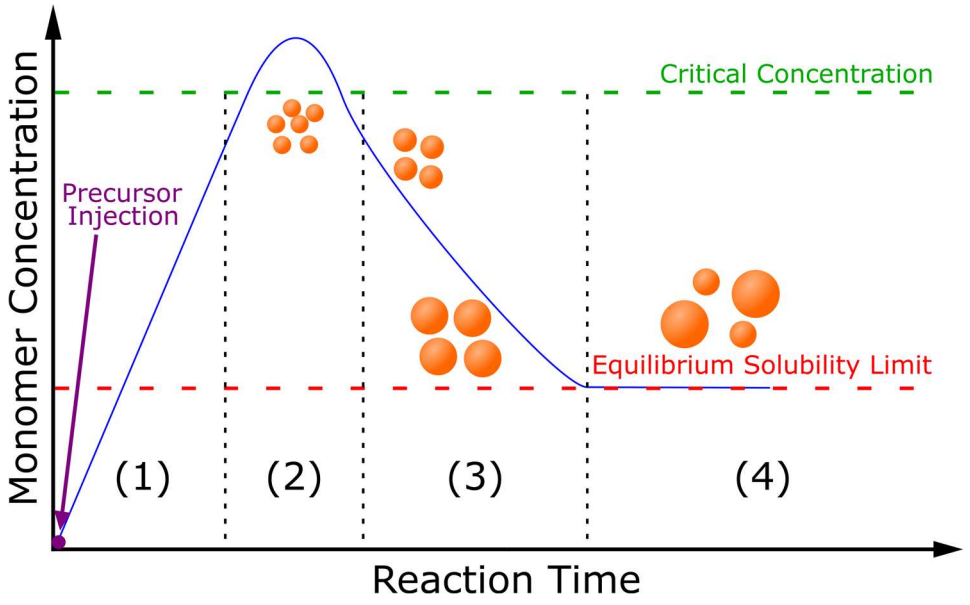

Figure 1.2 *La Mer model for the nucleation and growth of colloidal nanocrystals. (1) Formation of monomers from molecular precursors. (2) Rapid nucleation occurs as monomers are consumed. (3) Homogeneous nanocrystal growth. (4) Ostwald ripening and reaction quench.*

More recently, additional size-dependent thermodynamic and kinetic factors have been considered as a potentially more accurate explanation for size control achieved in the growth for crystalline colloidal particles.[20,22–24] In particular, there has been some debate on whether La Mer's "classical nucleation model" is applicable to systems where growth may be described by monomer reactivity or multi-step nucleation, such as InP QDs.[25,26] In this case, there is some evidence to suggest that cluster intermediates form along the reaction coordinate, rather than proceeding directly from nucleation to nanoparticle growth. While several alternative models have been presented to describe nanocrystal growth and size control, La Mer's model still appears to be applicable to QD systems synthesized in the manner used in this dissertation.[27]

1.3 Preparation of Core/Shell Quantum Dot Heterostructures

Many QD applications (such as bioimaging and display technologies) require further improvement and optimization of the nanocrystal system to improve the photoluminescence quantum yield (PLQY) and photostability. In these cases, heterostructures may be synthesized to coat an inorganic shell around the core QD which serves to isolate the core from the surrounding medium both physically and electronically.[28,29] The wider band gap shell passivates dangling orbitals on the core surface that act as electronic trap states (which limit the PLQY), and improves the QD's stability towards photo-oxidation.

Some relevant core/shell architectures include both cadmium- and zinc-based materials like CdSe/CdS, CdSe/ZnS, ZnSe/ZnS, and less toxic InP-based systems.[30–33] The selection of the shell material is vital to enforce epitaxial shell growth and produce core/shell QDs with narrow size distributions and improved photophysical properties. Generally, the shell composition should be selected such that crystal lattice mismatch is minimized, while good band alignment is achieved. This is important because the shell compresses the core, and this strain may induce formation of defects that may alter the band gap and are potentially detrimental to the QD's utility. The lattice mismatch, arising from differences in the lattice parameter between the core and shell material, is 3.9% and 11% in CdSe/CdS and CdSe/ZnS, respectively.[34] In the case of CdSe/ZnS, the mismatch does not preclude formation of thin shells, but does limit the ability to form thick shells over ~2 monolayers' thickness. To obtain thicker shells with ZnS or other shell materials with higher lattice mismatch, a gradient or multi-shell architecture can be used that offers sufficient protection of the core and high PLQYs.[35–37]

While a variety of methods have been utilized to prepare isotropic core/shell QDs, the most prevalent methods involve either the simultaneous infusion of shell materials or alternating injections of shell precursors to QD cores.[38–41] Recent work by Ou Chen's group has optimized the synthetic conditions of CdSe/CdS to produce both wurtzite and zinc blende QDs with narrow emission linewidths, high PLQY, suppressed blinking, and exceptionally narrow size distributions.[40] Their method contrasted other preparations by relying on the slow and continuous infusion of cadmium oleate ($Cd(OA)_2$) and octanethiol, the latter of which has very low reactivity relative to other chalcogenide precursors.

The prevailing synthetic method—and the one employed to synthesize colloidal core/shell QDs in this dissertation—is colloidal Successive Ion Layer Adsorption and Reaction (SILAR).[41] SILAR was developed as a tool to grow conformal thin films on planar substrates (similar to atomic layer deposition), and has since been adapted to overcoat isotropic and anisotropic shells onto colloidal nanomaterials.[42,43] The purpose of SILAR is to enforce epitaxial growth by saturating surface sites on the nanocrystal, while simultaneously preventing homogeneous nucleation of shell material with each half-cycle. In a typical SILAR synthesis, the QD cores are purified, dissolved in a weakly-coordinating solvent, and heated to a relatively mild temperature. The SILAR process begins by alternating injections of the shell metal and chalcogenide precursors, followed by some equilibration time. With each injection (or reaction half-cycle), stoichiometric doses of each reagent are added such that surface sites are hopefully saturated, but the amount of excess precursor is minimized prior to the next dose. Essentially, a self-limited monolayer of the shell should be grown after each full cycle, without excess precursors that may form nanoparticles of the pure shell material. This has been demonstrated through investigations

by the Greytak lab on the SILAR mechanism.[31,44] While the mechanism and utility of SILAR towards developing high-quality QD colloids with binary compound shells has been thoroughly investigated, there remains many questions regarding the formation and optimization of alloy-shelled QDs (such as CdSe/$Cd_xZn_{1-x}S$ used in some of the works in this dissertation).

1.4 Purification Methods for Nanocrystal Materials

Before nanocrystals and QDs can be utilized in a given application they must undergo post-synthetic purification from their crude reaction mixtures (which contain reaction byproducts, excess surfactant molecules, and unreacted precursors).[45,46] The goals of any purification are to (1) separate the nanocrystal from unwanted molecular species, (2) isolate the sample in a more desirable solvent system, and (3) provide a stable and consistent starting material for subsequent surface modifications.[47] While extraction and electrophoresis-based techniques have been employed to separate nanocrystals from their reaction mixtures, the most common and effective techniques are precipitation and redissolution (PR) and size-exclusion chromatography (SEC).[5,48–50]

Precipitation and redissolution (PR) relies on the solubility properties of the nanocrystal that are dictated by the native ligand. Because natively-capped QDs are typically soluble in nonpolar organic solvents (tetrahydrofuran, toluene, hexane, etc.), they are easily flocculated by the addition of a polar organic antisolvent (methanol, acetone, methyl acetate, etc.). As the polarity of the solvent mixture increases, the QDs aggregate and may be isolated from the mixture as depicted in **Figure 1.3**. The supernatant containing excess ligands and other components of the reaction mixture can be decanted away, leaving behind the precipitated QDs (and strongly bound native ligands) that are

readily dispersed in clean solvent. While PR is a relatively inexpensive and scalable purification, it is limited by batch-to-batch variability and concerns about similar solubilities of the QDs and impurities. Multiple PR cycles are often necessary to achieve a consistently-purified product.[50,51] When short-chain alcohols (such as methanol, a common antisolvent) are used to flocculate the QDs over several PR cycles, perturbations to the QD ligand shell may occur that limit stability.[52] Despite these limitations, the conservative use of PR can be used to effectively transfer nanocrystals into a clean solvent for subsequent impurity removal via size-exclusion purification or biphasic extraction.

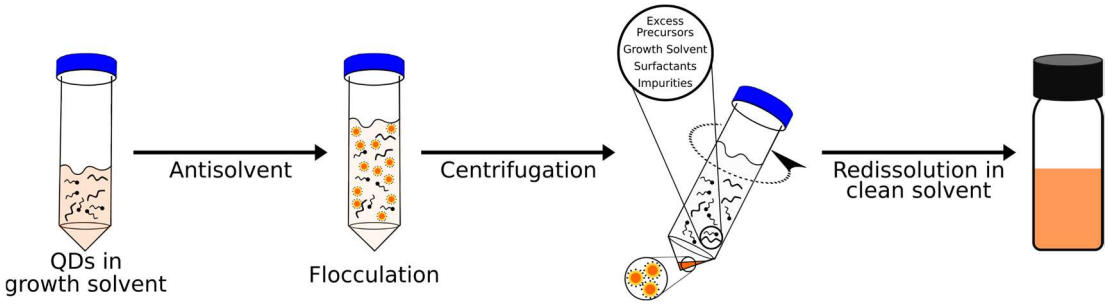

Figure 1.3 *Nanocrystal purification by precipitation and redissolution.*

To circumvent the limitations of PR the Greytak lab has employed gel permeation chromatography (GPC), a SEC technique with an anhydrous mobile phase, to purify and prepare nanocrystals with consistent surface chemistries. We have demonstrated the efficacy of GPC as a preparative technique for a variety of nanocrystal systems including CdSe and CdSe/$Cd_xZn_{1-x}S$, Au NPs, indium phosphide (InP), PbS, and cesium lead bromide ($CsPbBr_3$) perovskite QDs.[50,53–56] In GPC purification, a stationary phase consisting of polymer gel beads (such as crosslinked polystyrene) is packed in an organic

mobile phase that the QDs, ligands, and other impurities are soluble in. The mobile phase should be one in which the polymer gel is in the swollen state, and ideally one of low viscosity. One optional PR cycle may be used to bring the QDs into a GPC-compatible solvent (such as toluene) before being loaded onto the column. The GPC purification process is depicted in **Figure 1.4**. As the sample traverses the column, molecular species that are below the molecular weight cut-off (MWCO) of the polystyrene beads explore the pores and traverse the column at a slower elution rate than the QDs (which are above the MWCO and therefore travel around the beads). Thus, a size-based separation occurs as the QDs elute at a faster rate and can be isolated prior to the elution of excess ligands and other unwanted molecules. Additionally, the QDs retain only strongly bound ligands or those that desorb slowly from the surface. The advantages of GPC purification are (1) the ability to purify nanocrystals in a homogeneous solvent system without requiring precipitation, (2) repeatable purification versus PR, and (3) it routinely yields colloidally stable nanocrystals with low and consistent ligand per QD ratios. Once purified, the nanocrystal surface may be modified for any given application. GPC purification is used to purify the QDs featured in Chapter 1 of this dissertation, and PR was applied to the QDs in Chapter 2.

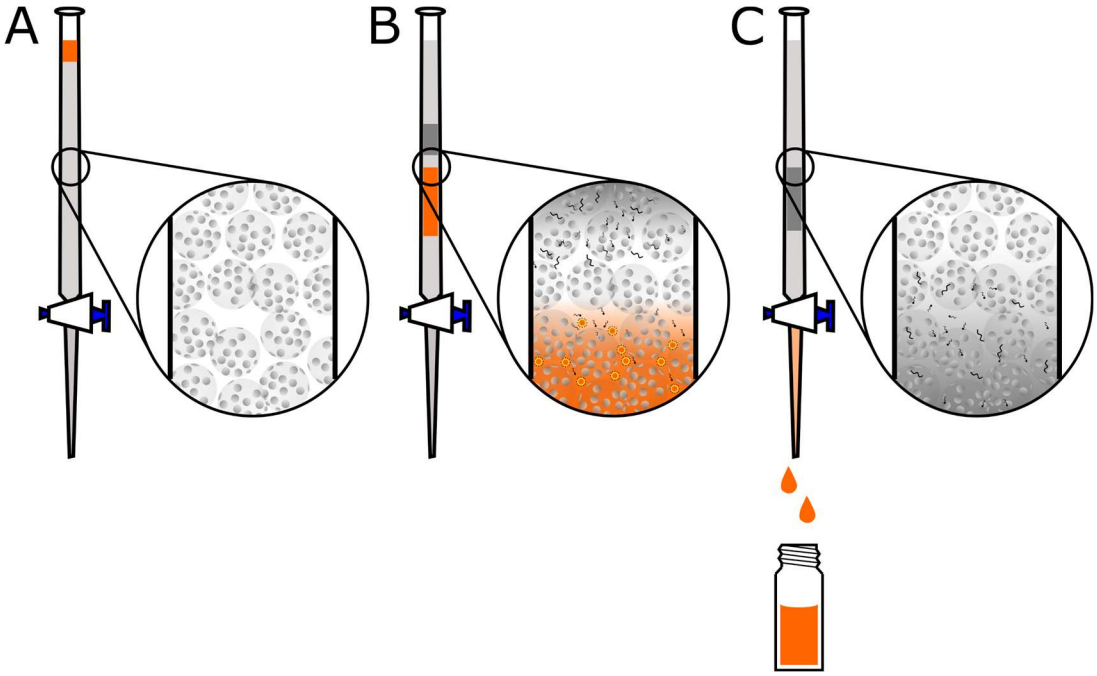

Figure 1.4 *GPC purification of colloidal QDs. (A) As-synthesized QDs are loaded onto a column of polystyrene beads in toluene. (B) The QD mixture fractionates as QDs traverse the stationary phase faster than molecular species. (C) QDs with strongly bound ligands elute first in clean solvent, leaving behind excess ligands and impurities.*

1.5 Surface Modifications on Quantum Dot Surfaces

Due to the high surface-to-volume ratio of nanocrystals, the conditions at the surface of the particle become increasingly important to both stability and function. Native organic ligands used in synthesis (such as carboxylates, amines, or phosphines) offer steric stabilization in a variety of organic solvents and help to effectively passivate dangling bonds at the QD surface. However, these native ligands are typically hydrophobic and electrically insulating, and in many cases must be exchanged with ligands more suitable towards a given application. For example, PbS QDs are synthesized with electronically insulating oleate ligands, the length of which prevents the formation of films with low inter-particle distances used in solar photovoltaics and infrared detectors. The oleate is

often exchanged with short chain ligands, such as 3-mercaptopropionic acid (MPA) to produce compact high quality films.[57] If the intended application requires QD dispersions in aqueous or polar environments the QD surface must be passivated with hydrophilic ligands such as small molecules or polymers.[58–61]

A large body of work on QD ligand exchange chemistry has provided a general understanding of the types of exchangeable ligands and how they interact with the QD surface.[62–66] To describe and categorize the immense library of available ligands, the covalent bond classification (CBC) developed by Mark Green is often used, in which ligands may be divided into three groups: X-, L-, and Z-type (**Figure 1.5**).[67–69] X-type ligands are 1-electron donors (and form strong covalent bonds to cationic surface atoms). Breaking these bonds homolytically would form radicals, while breaking them heterolytically would form separated charges. For example, carboxylates, phosphonates, and halides are considered to be X-type ligands when bound to surface metal sites on chalcogenide and pnictide NCs. They have been found to be the strongest binders in anhydrous and nonpolar solvents and are the preferred native ligands in QD synthesis.[62,66,70] L-type ligands (such as phosphines, amines, and imidazoles) are nucleophilic 2-electron donors which form dative bonds to cationic surface sites. These ligands tend to bind less strongly than X-type ligands, and are often shown to be in "dynamic equilibrium" on and off the QD surface, a term that indicates that significant surface coverage exists only in equilibrium with measurable free ligand concentrations, and these populations exchange rapidly, in some cases within the NMR dephasing time.[71–74] Z-type ligands are typically neutral 2-electron acceptors such as metal oleates ($Cd(OA)_2$, $Pb(OA)_2$, etc.) and form weaker bonds to anionic surface sites, though examples of L-type

ligands acting as Z-type coordinators have been demonstrated.[75,76] Sometimes X-type or Z-type ligand exchange may occur from the same surface depending on which bond is broken in the reaction.

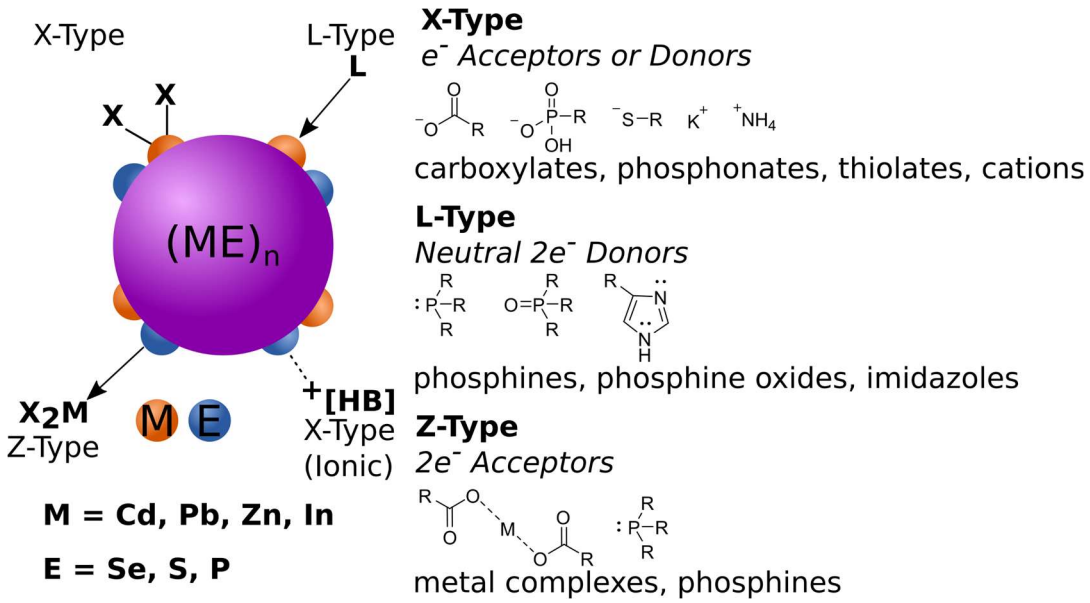

Figure 1.5 *Covalent bond classification of common ligands on nanocrystal surfaces.*

It is important to note that the coordination of a ligand is also dependent on the crystal facets present on the nanocrystal. While often described as spherical in shape (which aids in approximating the number of surface sites and ligand densities), nanocrystals are more accurately named "quasi-spherical". The crystal structure, size, and faces of the particle therefore play a key role in dictating the coordination chemistry of the ligands. A good example of the effects of nanocrystal size, shape, and surface passivation has come from recent investigations by the Greytak group and others on rock salt PbS QD synthesis and ligand densities.[55,77–79] Zherebetskyy et al. reported that PbS nanocrystals prepared from lead oleate were passivated by both oleate and hydroxide (from adventitious

water generated during synthesis). Hydroxide served as an X-type ligand which preferentially passivated the Pb-rich {111} surface where steric hindrance prevented complete passivation by oleate.[77] However, the {001} facet was terminated by lead oleate that is in dynamic equilibrium on the surface.

In a collaborative project with Adam Roberge and Fiaz Ahmed, I explored the surface passivation and role of water/hydroxide in synthesis on GPC-purified PbS QDs over a range of sizes. We found that in accordance to other literature results, PbS QDs undergo a sterically-driven shape transition from octahedral to a truncated octahedra with increasing particle diameter.[78] At larger sizes, a charge-neutral {100} facet is presented—which does not require further compensation by ligands—and the Pb-saturated {111} surface retains its passivation by $Pb(oleate)_2$ (**Figure 1.6**). Two $Pb(OA)_2$ populations were detected: one strongly bound to the QD, and another in dynamic exchange. Furthermore, when synthesized from purely anhydrous $Pb(oleate)_2$, the obtained QDs were consistently smaller under similar reaction conditions. This was likely due to the higher reactivity of anhydrous $Pb(OA)_2$, which lead to faster nucleation and slower growth.

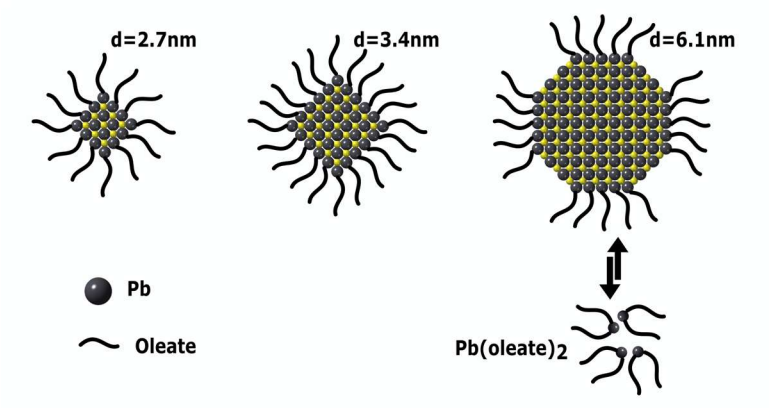

Figure 1.6 *Lead oleate passivation on GPC-purified PbS QDs as a function of size. The QDs undergo a shape transition as the diameter increases. Copyright American Chemical Society 2020.*

1.6 Biological Applications of Quantum Dots

Quantum dots have become very attractive fluorescent probes for *in vivo* and *in vitro* bioimaging studies due to their narrow and tunable emission and improved photostability relative to organic fluorophores. Core/shell QDs in particular have generated significant interest because they better maintain higher PLQYs in polar environments. The ability to prepare visible and near infrared-emitting QDs through composition and particle size has further added to their utility in biological applications.

To be useful in polar/aqueous media, additional considerations regarding the surface functionalization are necessary. Ultimately the goal is to achieve a QD with high PLQY, hydrophilic ligands that provide colloidal stability over a range of pH conditions, has low acute toxicity, and low nonspecific binding to competitor molecules. For *in vivo* and intracellular applications, the QD-ligand system should also be compact (small hydrodynamic size) in order to pass through cellular membranes or lipid bilayers.[80–82]

Stable aqueous QD dispersions that exhibit the properties above are typically prepared through (1) encapsulation of the QD and native hydrophobic ligands with an amphiphilic co-polymer or (2) ligand exchange with hydrophilic polymers or small molecules. While encapsulation is effective in dispersing the QDs, this can result in large hydrodynamic radii that hinder their utility as intracellular probes.[83] Exchange on the other hand, retains relatively compact QD-ligand systems while removing hydrophobic ligands that may induce aggregation if exposed to polar solvent while bound to the QD. Recently, significant strides in the development of stable and robust QD coatings through ligand exchange with small molecules (such as zwitterions or thiols) and polymers (with thiol or imidazole binders).[82,84–86]

Proper QD surface modification has led to a host of bioconjugation methods in the past few decades for imaging, sensing, and targeted drug delivery.[87–90] Libchaber's group demonstrated that CdSe/ZnS QDs encapsulated by phospholipid block co-polymer micelles could be conjugated to DNA and serve as fluorescent probes with low toxicity in monitoring the development of early stage *Xenopus* embryos.[91] Bruchez's group labeled a Her2 breast cancer marker with CdSe/ZnS QDs capped by an amphiphilic co-polymer coupled to streptavidin and immunoglobulin G (IgG).[92] They showed that when a common organic fluorophore, Alexa 488, and the QDs were used to label microtubules and nuclear antigens, the QDs exhibited superior photostability under continuous illumination.[92] Dubertret's group exchanged zwitterionic dihydrolipoic acid/sulfobetaine ligands on CdSe/ZnS QDs to produce stable and compact bioimaging probes at a range of pH values, and monitored intracellular traffic in G-protein-coupled receptors in living cells.[93]

1.7 Dissertation Overview

While many examples of aqueous QDs used for bioimaging and sensing have been reported, a significant number of these reports focus primarily on the efficacy of the QD-ligand system as an observable probe. Investigations into ligand binding interactions have been largely limited to organic solvents, and there remain many questions regarding the complex surface chemistry of QDs under aqueous conditions. As QDs become more widely used for biological applications, it is important to develop a more thorough understanding of QD surface chemistry. This dissertation focuses on helping to answer several key questions regarding ligand exchange chemistry and QD stability in polar environments, in an effort to prepare robust fluorescent QD probes with well-defined surface chemistries. These investigations should aid in the design of more robust and effective ligands for QDs used in biological applications and contribute to our knowledgebase of ligand interactions on QD surfaces.

The first work in this dissertation—presented in Chapter 2—addresses the question of how polymeric ligand molecular weight and monomer sequence influence the colloidal stability of core/shell QDs in the presence of an endogenous competitor ligand, L-glutathione (GSH). This was the first study that directly compared the relative stabilities of block and random co-polymer ligands on QD surfaces. Imidazole-bearing block and random co-polymer ligands were synthesized by a reversible addition-fragmentation chain-transfer (RAFT) reaction with different molecular weights, and in which the sequence of the imidazole binding groups were oriented randomly or in a block formation. It was observed that GSH was unable to displace the polymeric ligands (despite thiols being stronger binders than imidazoles) but does associate to vacant sites on the QD surface

regardless of polymer size or monomer sequence. The block co-polymer ligands yielded QDs that were more robust towards GSH association, while higher molecular weights contributed to improved stability as well.

Chapter 3 aims to describe how the length and denticity of molecular ligands influences the relative binding strengths of anionic ligands to core/shell QDs. Utilizing isothermal titration calorimetry (ITC), the competitive anionic exchange of monothiolate ligands of different chain lengths, versus a bidentate thiolate binder, to phosphonate-capped QDs under basic conditions was compared. Longer chain lengths tended to bind more strongly to the QD, and indeed to a greater extent in the case of bidentate binding, via displacement of the phosphonate. This was the first study to compare the binding strengths of mono- and di-thiolate ligands to phosphonate-capped QDs in an aqueous environment, and (one of) the first to probe coordination of chalcogenide NCs in aqueous solution using ITC.

CHAPTER 2

MULTIPLY-BINDING POLYMERIC IMIDAZOLE LIGANDS: INFLUENCE OF MOLECULAR WEIGHT AND MONOMER SEQUENCE ON COLLOIDAL QUANTUM DOT STABILITY*

2.1 Introduction

Colloidal semiconductor quantum dots (QDs) are attractive fluorophores for bioimaging and biosensing applications owing to their photostability, size-tunable emission, and high molar extinction coefficients. Core/shell QDs (e.g., CdSe/CdS, CdSe/$Cd_xZn_{1-x}S$, etc.) are widely employed for bioimaging experiments, as they better maintain their high quantum yields (QY) when transferred into aqueous media. Yet, QDs with shells of several monolayers' thickness remain sensitive to surface conditions. As-synthesized QDs possess surfaces passivated by hydrophobic ligands, which inhibit dispersion in polar solvents, but are vital to maintaining control during nucleation and growth. Post synthetic modifications with hydrophilic molecules must therefore be employed to satisfy general requirements for biological applications. These include colloidal stability in water (over time and at a range of pH values), high QYs, low acute toxicity, and low nonspecific binding.[87]

*Reprinted with permission from Dunlap, J. H.; Loszko, A. F.; Flake, R. A.; Huang, Y.; Benicewicz, B. C.; Greytak, A. B. Multiply-Binding Polymeric Imidazole Ligands: Influence of Molecular Weight and Monomer Sequence on Colloidal Quantum Dot Stability. *J. Phys. Chem. C* **2018**, *122* (46), 26756–26763. Copyright 2018 American Chemical Society.

A variety of strategies have been developed for transferring QDs into aqueous media, which rely on using surfactants or amphiphilic polymers to encapsulate the QD and native ligands, or ligand-exchange reactions to fully replace native ligands on the surface. Amphiphilic polymers effectively encapsulate natively-capped QDs via micelle-like structures, but these strategies often result in large hydrodynamic radii and limit their use as fluorescent probes.[92,94] However, smaller sizes may be retained by utilizing ligand-exchange reactions to install hydrophilic surfaces with anionic, cationic, steric, or zwitterionic stabilization. Small molecule thiols, such as cysteine, readily displace native ligands and lead to water-soluble QDs that can exhibit high QYs in some cases, particularly with ZnS-based shells in the case of CdSe QDs.[95] Multiple groups have demonstrated that QD stability may be improved by incorporating bidentate binding schemes such as poly(ethylene glycol) (PEG)-modified dihydrolipoic acid (DHLA) ligands on CdSe/CdZnS core/shell QDs.[96,97] These QDs exhibited low nonspecific binding and improved stability over a wide pH range. However, they do not provide sufficient protection of the QD surface, being prone to oxidation, poor long-term stability, and low QY in the case of thinner or less confining shells.[30,98–100]

Further improvements in stability can be achieved with polymeric ligands containing multiple anchor groups that can bind to the QD surface; such polymers can also incorporate hydrophilic moieties for solubility and functional groups for further modification.[85,101,102] This approach is exemplified by synthetic polymers bearing imidazole sidechains that mimic the polyhistidine motif that has previously been used to anchor polypeptides to QD surfaces.[103,104] More recently, Mattoussi's group has demonstrated multidentate polymer-QD systems involving both histamine and lipoic acid

functionalities to yield stable and compact QDs.[105] This multiply-binding strategy addressed concerns regarding the weak surface-imidazole bond and thiol oxidation.[74] The imidazole group possesses an affinity to under-coordinated metal sites on the QD surface, is resistant to oxidation, and has been shown to maintain high quantum yields and facilitate stable QD colloids in aqueous media.[85,106–109]

Despite numerous reports on multiply-binding co-polymer ligands, there has been relatively little exploration of differences resulting from varying monomer sequences within such polymers. A common method for forming multiply-binding or multidentate co-polymers relies on the ring opening of poly(isobutylene-*alt*-maleic anhydride) (PIMA) by nucleophilic addition of amine-modified monomers. The maleic anhydride readily reacts with primary amines, enabling formation of modified co-polymers without the need for coupling agents.[110–112] This technique has been used to form a variety of amphiphilic co-polymers for passivating nanoparticles, containing imidazole and/or thiol anchors, zwitterion motifs, and reactive groups for further functionalization, but does not offer control of the sequence of residues.[105,110–114] Another polymerization method, reversible addition-fragmentation chain transfer (RAFT), involves the free-radical polymerization of monomers through utilization of a chain transfer agent. As a living or controlled polymerization technique, it is possible to construct block co-polymers by sequentially introducing monomers in the desired order with low polydispersities and good control over the molecular weight.[115] Work by Lequeux and coworkers described the use of multidentate zwitterion/vinylimidazole block co-polymers, which demonstrated the efficacy of imidazole-binding block co-polymers to yield stable QD samples.[84,116] Alternatively, if all monomers are introduced initially, then polymer sequence is

determined statistically according to relative reactivity ratios of the monomers, resulting in disordered sequences. This method has been the approach in most published examples to date, including our own work.[107] Bawendi and coworkers pursued a strategy in which various monomers synthesized with PEG chains, imidazole groups, and derivatizable groups for further functionalization were combined into a monomer mixture of differing ratios initiated by RAFT polymerization.[85] However, the effect of sequence and length have yet to be directly compared in this or other classes of polymeric imidazole ligands.

A key characteristic for QD surface coatings to be used in imaging live cells or organisms, especially in intracellular applications, is to resist interference or ligand displacement by endogenous compounds. In particular, the intracellular stability of polymer-capped QDs is of great concern because endogenous thiol molecules, especially glutathione (GSH) and cysteine, are present at high concentrations to maintain redox homeostasis, and these could potentially displace polymers relying on imidazole as the anchoring group.

Zhu et al. used laser desorption/ionization mass spectrometry to quantify changes in dithiolate ligand monolayers on CdSe/ZnS QDs upon exposure to intracellular GSH, demonstrating that monolayer stability in HeLa cells can be compromised.[98] This provided evidence that naturally occurring thiols are capable of displacing surface ligands at biologically relevant concentrations (which can reach up to 10 mM), leading to possible aggregation, leaching of toxic metal ions, and decrease in function.[98] Understanding how endogenous thiols interact with polymer-capped QDs, and the influence of polymer structure, sequence, and length on this interaction, is essential to designing QDs appropriate for biomedical applications.

Our group has developed a family of methacrylate-based polymeric imidazole ligands (MA-PILs) synthesized by RAFT. The methacrylate backbone reduced the potential for premature reaction during synthesis compared to acrylate monomers. The polymer-capped QDs (MA-PIL-QDs) were stable and exhibited negligible nonspecific binding and cytotoxicity to human endothelial cells over a range of polymer chain lengths.[108] Ternary co-polymers with methoxy- and amine-terminated PEG sidechains enabled selective labeling of targets on cell surfaces via copper-free click chemistry and were also used to demonstrate association of MA-PILs to CdS nanowires through the use of a covalently linked fluorescent dye tracer.[109,117]

In the present study, we directly examine the stability of MA-PIL-capped CdSe/$Cd_xZn_{1-x}S$ core/shell QDs toward small thiol molecule competition, using glutathione at biologically relevant concentrations under neutral conditions in phosphate-buffered saline (PBS, pH 7.3-7.5). The core/shell QDs were prepared by selective ion layer addition and reaction (SILAR) and purified by gel permeation chromatography (GPC) in toluene prior to ligand exchange to install the MA-PILs, according to previously described methods.[50,107] Four MA-PILs were designed with a combination of PEG and imidazole sidechains using RAFT-mediated co-polymerization to define disordered (random) or block co-polymers (**Figure 2.1**). In each case, two different average polymer lengths were prepared, incorporating poly(ethylene glycol) methacrylate (PEGMA-475) and N-methacrylol succinimide (NMS) monomers. Imidazole anchoring groups were installed post-polymerization by a quantitative reaction of the succinimidyl esters with histamine. Block co-polymers were synthesized with average molecular weights of 14 kDa and 30 kDa, herein referred to as **B14K** and **B30K**. Random co-polymers were synthesized with

average molecular weights of 12 kDa and 27 kDa, herein referred to as **R12K** and **R27K**. The stability of the ligand exchanged QDs to GSH exposure was tested in two ways. First, the photoluminescence of the MA-PIL-QDs was monitored to detect surface interactions with GSH since the QY is known to be sensitive to ligand exchange or association processes, and because QY is relevant to the imaging and sensing applications of QDs. Secondly, the ligand population on the QD surface was directly measured by ultraviolet-visible (UV-Vis) absorption spectroscopy and used to quantify the ligand-to-QD ratio after removing unbound molecules via centrifugal dialysis filtration. The results to follow suggest that block co-polymers exhibit superior stability and diminished interference from small molecules, whereas in both cases the larger co-polymers appear to be more robust towards such molecules. This demonstrates the influence of molecular weight and monomer sequence on the stability of colloidal polymer-capped QDs with respect to glutathione, a representative competing ligand. To the best of our knowledge, this is the first direct comparison of polymer binding strength and resistance to small molecule competition as a function of monomer sequence. The findings that block co-polymers exhibit superior stability and diminished interference from small thiol molecules may be applicable to other classes of polymeric ligands and provides new insights into the development of stable, robust polymeric ligand coatings for *in vivo* and *in vitro* bioimaging and sensing applications.

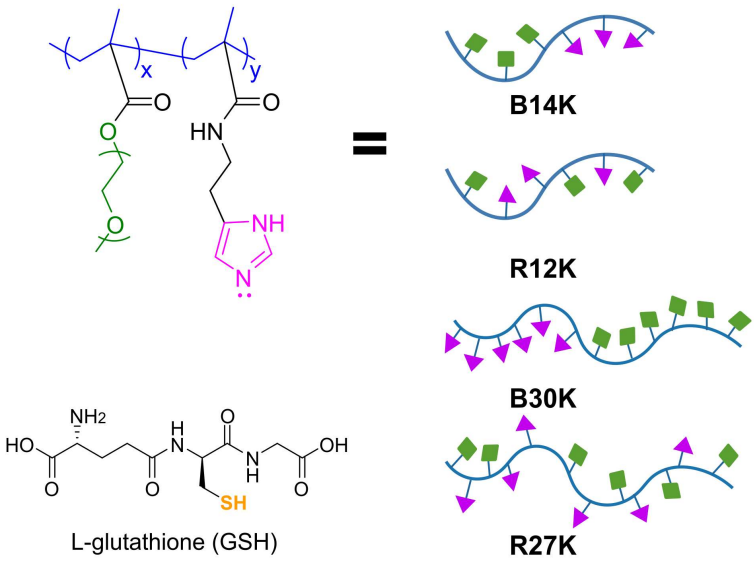

Figure 2.1 *MA-PIL Ligands and L-Glutathione Competitor.*

2.2 Synthesis of MA-PIL Ligands

A previously reported RAFT-mediated synthesis was used to prepare the poly(PEGMA-*co*-imidazole) ligands with tailored molecular weights and low polydispersities (**Table 2.1**).[107] The reactivity ratios of the NMS ($r_1 = 0.91$) and PEGMA ($r_2 = 0.69$) monomers were determined by the Kelen-Tudos method.[107] As their reactivities are relatively similar, the monomers could be co-polymerized, attaching to the methacrylate backbone in such a manner that they become randomly distributed along the polymer chain. For the block co-polymers on the other hand, poly(PEGMA-*b*-imidazole) was synthesized by sequentially polymerizing the monomers along the methacrylate backbone. In the case of the block co-polymers the PEGMA was prepared first to form PEG monomers close to the R-group, quenched, and then the NMS monomers were polymerized. Since the succinimidyl group of NMS readily reacts with primary amines, histamine was introduced after successful removal of the RAFT agent to install imidazole

anchors; the co-polymers were then isolated by dialysis. A schematic representation of the final MA-PIL ligand structures is provided in **Figure 2.1**.

Table 2.1 *Summary of Block and Random Co-Polymer Composition, Molecular Weight, Dispersity (Đ), and Degree of Polymerization (DP).*

		M_n			DP[b]	
copolymer	polymer ID	GPC	NMR	dispersity (Đ[a])	PEGMA	NMS
poly(PEGMA-b-NMS)	**B14K**	12000	13700	1.10	21	18
poly(PEGMA-b-NMS)	**B30K**	17100	29600	1.13	44	45
poly(PEGMA-co-NMS)	**R12K**	13500	12400	1.29	18	19
poly(PEGMA-co-NMS)	**R27K**	24500	27300	1.39	40	43

2.3 Preparation of Core/Shell QDs with MA-PIL Co-polymer Ligands

The CdSe/$Cd_xZn_{1-x}S$ QDs were synthesized via the previously reported SILAR method, natively capped with oleate and phosphonate ligands.[50] A four monolayer $Cd_xZn_{1-x}S$ shell was coated onto the CdSe cores with x=0.3. The shell growth was monitored by absorption and emission spectroscopy, with the QDs emitting at 572.5 nm. Prior to ligand exchange, the QDs were purified by GPC in toluene with a polystyrene size-exclusion medium to remove small molecule impurities and weakly bound ligands. Our group has previously shown the efficacy of GPC as a preparative technique for stable nanocrystal colloids with consistently low ligand-to-QD ratios, providing a surface which facilitates efficient ligand exchanges.[50,53] In the discussion to follow, the polymer-capped QDs will be referred to by the bound polymer type as follows: B14K-QD, B30K-QD, R12K-QD, and R27K-QD.

To facilitate aqueous dispersion, the native hydrophobic ligands on the QD surface were exchanged with the MA-PIL ligands by solution-phase ligand exchange. The QDs,

fully dried under vacuum after GPC purification, were dispersed in chloroform in the presence of excess ligand and stirred under ambient conditions. After stirring in chloroform for 45 minutes, methanol was added to separate the polymer-capped QDs from the organic ligands. After an additional 20 minutes, the QDs were flocculated by the addition of a 1:6 ethanol/hexane mixture, centrifuged, and the MA-PIL-QDs isolated as a solid before dispersing in PBS (pH 7.4). **Figure 2.2** shows representative absorption and emission spectra of a QD sample before and after ligand exchange. The QDs show minimal changes in the primary exciton peak line shape, with only a slight red shift in the peak wavelength following ligand e**x**change. Likewise, the emission spectrum before and after ligand exchange are quite similar, with a small blue shift following ligand exchange. This demonstrates that the ligand exchange method has little impact on the optoelectronic properties of the QDs. Prior to the glutathione exposure studies below, the aqueous MA-PIL-QDs were subjected to multiple cycles of dialysis using ultrafiltration membranes to remove excess free polymer, then diluted in PBS.

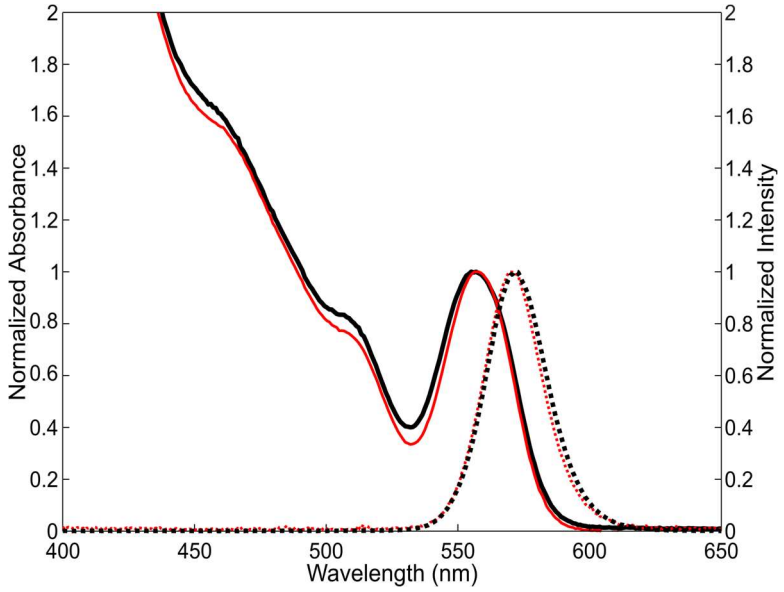

Figure 2.2 *Normalized absorption and PL emission spectra of CdSe/$Cd_xZn_{1-x}S$ QDs. Absorption (solid lines: heavy/black, after GPC in toluene; thin/red,* ***B14K-QD*** *after ligand exchange in PBS) is normalized at 557 nm. Emission of respective samples (dashed lines) is normalized at maximum intensity.*

2.4 Photoluminescence Response to Glutathione

Except in the case of very thick and electronically isolating shells, the QY of colloidal QDs can be very sensitive to ligand association and dissociation processes at the surface.[36,62] Thus, we utilized PL spectroscopy to characterize changes in PL in response to GSH at biologically relevant concentrations for each MA-PIL-QD combination. Specifically, to evaluate whether an interaction occurs between GSH and the MA-PIL-QDs, a titration experiment was designed in which the PL response was monitored continuously while GSH was introduced stepwise in a series of aliquots. Any change in QY caused by introduction of GSH could then be detected and used to compare the response of samples with random and block co-polymer ordering.

The MA-PIL-QDs were placed in an air-tight cuvette with stirring and a complete spectrum was collected every 10 seconds under 365 nm excitation. The spectra were integrated after baseline subtraction to give an intensity value that could be plotted as a function of time. With each GSH injection, the QD concentration decreased by a known amount due to the increase in total volume. Accordingly, the intensity values following injections are scaled up based on the ratio between the current and final volume following each addition of GSH. Examination of the emission spectra over the course of the experiment showed no significant change in emission line shape. Under these conditions, changes in scaled intensity are directly proportional to changes in PLQY.

Several controls were put in place to isolate the response to GSH exposure. Due to the constant light exposure necessary for successive PL response studies, the drift in the PLQY of the MA-PIL-QDs in PBS was monitored in the dark (**Figure 2.3**). In these measurements, the QDs were only exposed to light long enough to record a full spectrum and stirred for 5 minutes between subsequent measurements. All samples show an increase in PL over time, with block co-polymer-capped QDs demonstrating less drift than their random co-polymer-capped QD analogues. A control titration with N_2-sparged PBS was also conducted to account for dilution effects on the PLQY (**Figure 2.4**). The sample was stirred in PBS under constant light exposure, wherein 0.1 mL of PBS was titrated into the cuvette via syringe pump every 15 minutes, and the PL monitored over time.

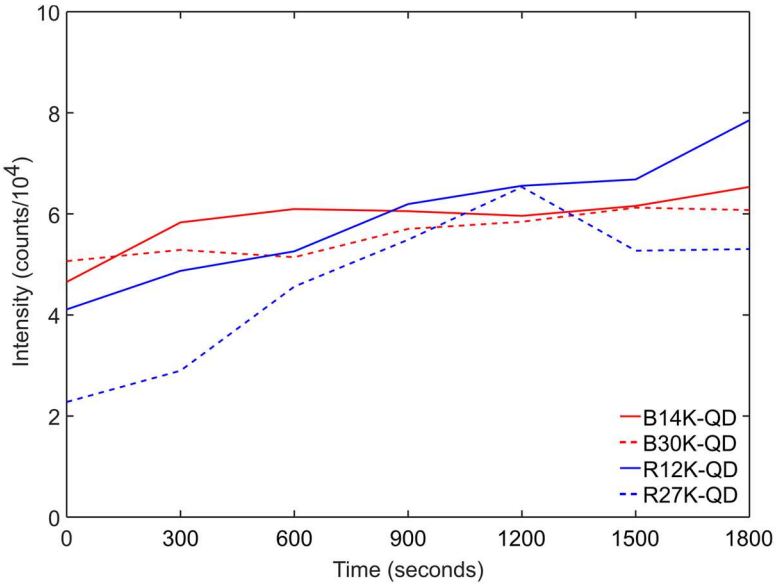

Figure 2.3 *Photoluminescence drift of MA-PIL-QDs in the dark. The average of five trials for each of the polymer-capped QD samples is represented above.*

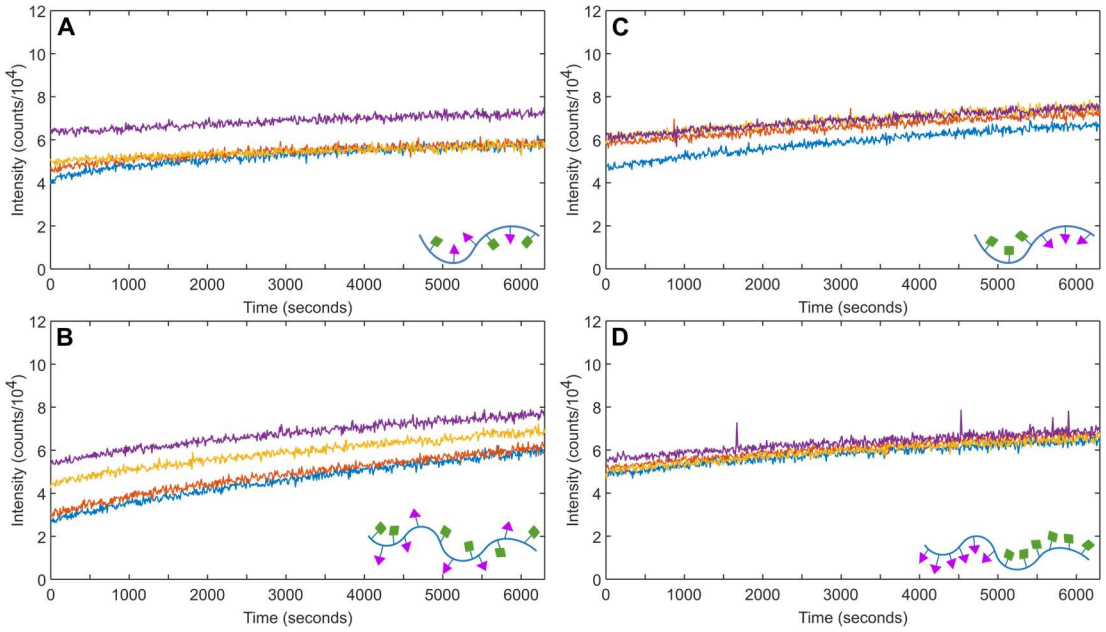

Figure 2.4 *Photoluminescence Control with PBS.* ***A-D*** *shows corresponding control trials of fluorescence stability tests in response to endogenous molecules.* ***(A) R12K-QD****,* ***(B) R27K-QD****,* ***(C) B14K-QD****, and* ***(D) B30K-QD****. Data is corrected for loss of fluorescence from dilution of the QD concentration during the titration. Measurements were repeated four times, with individual trials indicated by different colored spectra (purple, orange, red, and blue). The change in raw PL signal is exactly compensated by the change in volume.*

Figure 2.5 shows the experimental design for the GSH-response measurements and the corresponding PL traces for each MA-PIL-QD. In brief, the MA-PIL-QDs (nominally 62.6 nM in N_2-sparged PBS) were sealed in a N_2-filled cuvette (to limit oxidation of the GSH) and stirred in the dark under ambient conditions. For the first 15 minutes of each trial, the QD PL was monitored prior to addition of GSH to test their behavior under constant light exposure. The GSH was introduced via incremental titration over time and the PL intensity continuously monitored for changes in peak position and intensity, and the total GSH concentration was kept below 8 mM to avoid significant changes in the pH. Each GSH injection was administered swiftly every 900 seconds to allow sufficient time for an equilibrium to be reached, so that any rapid response to subsequent increases in [GSH] would be evident.

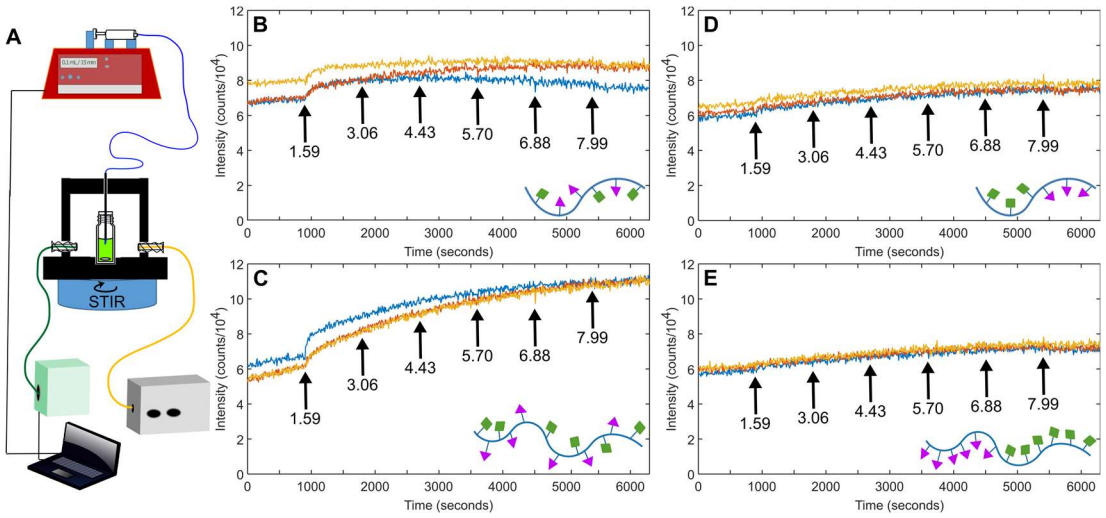

Figure 2.5 *Integrated PL intensities in response to glutathione titration. (A) Experimental design for PL measurements. (B-E) Integrated PL response to GSH for* ***R12K-QD****,* ***R27K-QD****,* ***B14K-QD****, and* ***B30K-QD****, respectively in PBS. Arrows indicate injection times and the total [GSH] in millimolar following each injection. Measurements were repeated in triplicate, with individual trials indicated by different colors (red, orange, and blue). All intensity values were corrected for dilution of the QD concentration.*

The data presented in **Figure 2.5** provides a qualitative comparison between the influence of monomer sequence and molecular weight in response to glutathione. At times prior to the first GSH injection, the QDs show a slow drift toward higher PL. However, upon initial addition of GSH, a small increase in PLQY on a timescale of several minutes is observed in all cases. The random co-polymer-capped QDs show a substantially larger increase in PL with respect to their block co-polymer-capped QD analogues. In the PBS control titrations (**Figure 2.4**), no change is discernable at the injection times. This suggests that block co-polymer MA-PILs are more resistant to interactions with GSH. We observe that the extent of change in PL at each concentration point and the equilibration time, after which the intensity no longer changes rapidly, is most pronounced at the first injection, when the GSH concentration goes from 0 to 1.59 mM, suggesting an effective association constant (K_a) $\geq 10^3$ M^{-1} for the underlying process. Though PL clearly indicates that an interaction occurs and that it is diminished for the block co-polymer-capped QDs, PL response alone is not indicative of the nature of this reaction. To gain further information regarding this interaction, we turn to absorption spectroscopy.

2.5 Quantification of Polymer Ligand Populations

In a ligand association process, the binding of an incoming molecule (i.e., GSH) does not alter the population of the native ligands on the QD surface. In a ligand exchange, however, the native ligands are displaced from the surface by a competing molecule and liberated as free ligand in solution. To distinguish between these processes, we quantified the ratios of polymer-to-QD after introduction of GSH and subsequent re-purification to remove unbound polymer using UV-Vis absorption spectroscopy. In comparison to other quantification methods such as ^{1}H NMR, UV-Vis is well suited for studying ligand

interactions, as it does not require high analyte concentrations or deuterated solvents. The histamine imidazole group served as a spectroscopic handle owing to its strong UV absorption at 213 nm, whereas the QDs absorb in the visible range at 557 nm. However, the QDs absorb strongly at short wavelengths and therefore the amounts must be measured separately, with the ligand measurement performed after completely digesting the QDs in acidic solution and dilution to known volume.

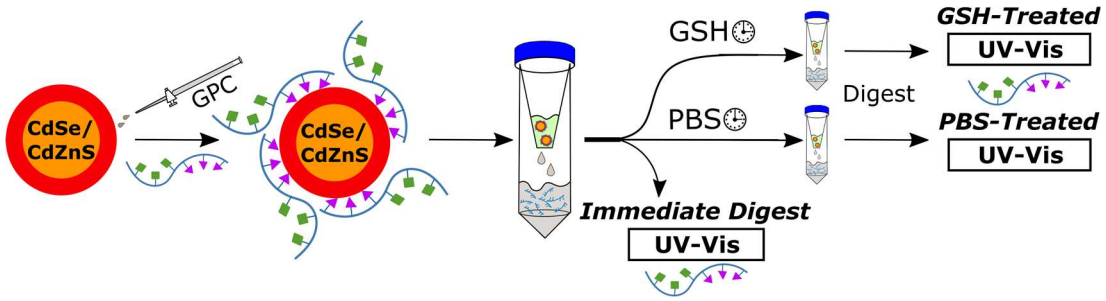

Figure 2.6 *Digestion Assay to Measure MA-PIL/QD Ratio and Detect Displacement by GSH.*

Figure 2.6 outlines the experimental approach for the digestion assay. Hydrochloric acid was found to be an effective means of degrading the QDs without destroying the polymer, allowing the polymer absorption to be resolved after digestion. Following ligand exchange to prepare the MA-PIL-QDs, 1 nmol of QDs was subjected to multiple cycles of centrifugal dialysis in PBS to remove excess free polymer and weakly bound polymer. We define this as the initially purified sample, nominally containing only QDs with bound polymer ligands. Each sample was divided into three portions of equal volume. Portion A was immediately analyzed to determine the initial ligand content. Because the largest increase in PL intensity occurred at low concentrations of GSH, we

used 2 mM GSH in PBS for the digestion assay. Portion B was exposed to the GSH under N_2, stirred for 1 hour, then dialyzed in PBS to remove excess GSH before analysis. Portion C was used as a control sample for GSH treatment and underwent an identical treatment to Portion B, but using clean PBS in place of GSH. The QD concentration before re-purification in Portion B was approximately 125 nM for each MA-PIL-QD sample. A representative trial for GSH-treated B14K-QD is provided in **Figure 2.7**.

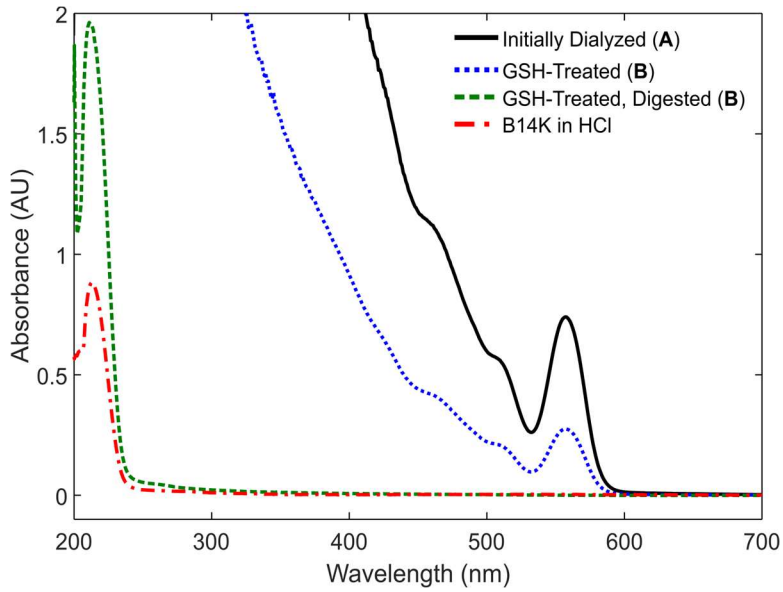

Figure 2.7 *Representative absorption spectra for **B14K-QD** after dialysis, GSH treatment, and digestion. A reference spectrum of **B14K** in HCl is shown (red dash).*

The absorption of the dialyzed, GSH-treated sample was used to measure the total QD concentration. After the addition of HCl, the sample no longer exhibits any visible absorption feature at 557 nm, indicating the efficacy of the digestion. The polymer is readily identifiable in acid, with no significant changes in line shape or peak wavelength. The QD and imidazole absorption data for each sample were used to assign the molar

quantities of QDs and surface-bound MA-PILs by comparing the visible and ultraviolet peak heights, respectively, to those of reference samples of known concentration. **Figure 2.8** compares the raw spectra and scaled reference curves for B14K-QD before (visible) and after (UV) digestion. Since no significant changes in QD absorption and emission were detected after ligand exchange, the QD concentrations were determined based on the extinction coefficient measured at 350 nm in toluene, 2.24×10^{6} $M^{-1}cm^{-1}$.

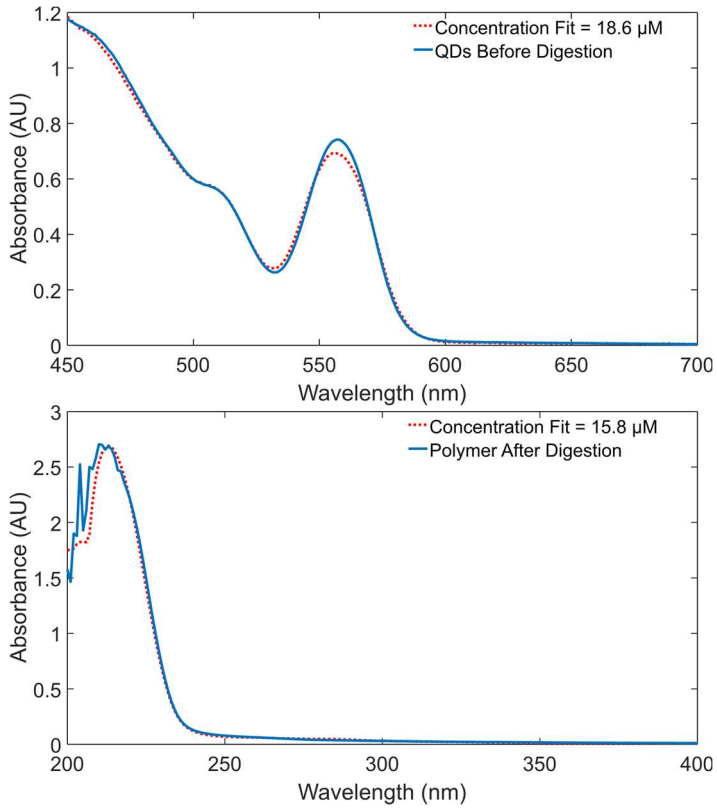

Figure 2.8 *Representative concentration fits for **B14K-QD (Portion A)** via absorption spectroscopy showing QDs before digestion (top) and polymer after digestion (bottom) absorption. The sample and fitting spectra are shown in solid and dashed lines, respectively.*

The results from the digestion assay and concentration fitting are summarized by the average polymer/QD mole ratios for each MA-PIL-QD sample in **Figure 2.9**. When comparing the block and random co-polymer ligands, the block ligand mole ratios were consistently higher, indicating a greater residual ligand population following ligand exchange and centrifugal dialysis in PBS. To understand the role of glutathione and the stability of the different polymer coatings, the GSH- and PBS-treated experiments must be compared. These samples undergo further dialysis in PBS after treatment, thus if GSH displaces the polymer, a lower polymer content should be present after digestion (with respect to the PBS control). In other words, ligand exchange by GSH would be indicated by a lower polymer/QD ratio in Portion B than Portion C, whereas indistinguishable polymer/QD ratios between these portions would be indicative of association. Considering only the effect of monomer sequence, the block co-polymer ligands were present at higher mole ratios after GSH treatment (vs. the random polymers), suggesting that block co-polymer MA-PILs have a higher affinity for the QD surface. Since there is no substantial difference between the GSH- and PBS-treated mole ratios in any of the MA-PIL formulations in this study, we conclude that GSH does not drive displacement of the polymer ligands. Yet at low concentrations and the same timescale, significant PL changes were also observed. This indicates that such PL changes are likely driven by GSH association to vacant binding sites on the QD surface. The random co-polymers exhibit lower ligand-to-QD ratios following initial dialysis and continue to lose ligand upon dilution and subsequent dialysis, which could contribute to a higher number of accessible surface sites to which GSH can bind. The larger polymers, **B30K** and **R27K**, appear to yield QDs that are more robust and resistant to interactions with GSH than the shorter

polymers of similar sequence. This is indicated by better retention of the **R27K** versus **R12K** upon repeated dilution and purification in **Figure 2.9**, and by the diminished PL response of **B30K** versus **B14K** in **Figure 2.5**.

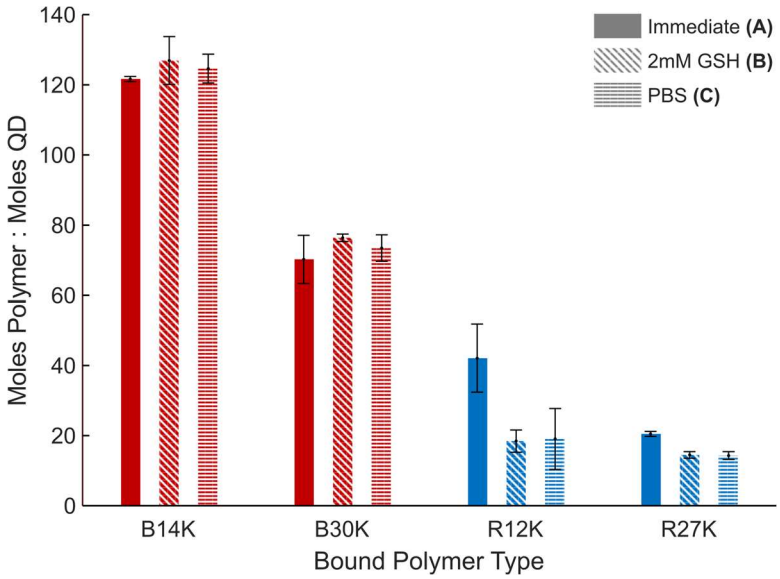

Figure 2.9 *Average MA-PIL/QD mole ratios for the three portions of each sample. All assays were repeated in triplicate and error bars indicate 1 standard deviation.*

2.6 Conclusions

We prepared stable CdSe/$Cd_xZn_{1-x}S$ core/shell QD colloids with methacrylate-based polymeric imidazole ligands. By controlling the order of monomer addition, we synthesized block- and randomly-ordered co-polymers consisting of a methacrylate backbone, PEG groups for dispersion in PBS, and imidazole anchors for binding to the QD surface. The application of RAFT-mediated synthesis facilitated the preparation of co-polymers with a high degree of molecular weight tunability. The QDs were purified by GPC to remove small molecule impurities and weakly bound organic ligands prior to ligand exchange with the polymers. We directly probed the stability of the MA-PIL-QDs towards

glutathione at biologically relevant concentrations (up to 8 mM) in PBS (pH 7.4) and studied whether GSH binds with the QD through association to vacant sites or by displacing the polymeric ligands through exchange.

PL spectroscopy revealed that upon initial titration of GSH, the random co-polymer-capped QDs exhibited a substantially greater increase in PL in contrast to the block co-polymer-capped QDs. This suggested that the block MA-PILs were more resistant to glutathione interactions. Regarding this increase in PL, we note that ligand exchange with thiols has been found previously to lead to lower QY compared to PILs. The small increases here could be a result of the rigorous dialysis protocol used to strip unbound MA-PIL ligands prior to the experiment or to the use of air-free conditions to limit thiol oxidation.

By means of a digestion assay and absorption spectroscopy, we quantified the mole ratios of polymer-to-QD. The QD and polymer concentrations were determined by fitting their visible and UV absorption with reference spectra before and after digestion in acid, respectively. The consistently higher ratios of block ligands to QDs suggest that a higher ligand population is present after ligand exchange and dialysis. When exposed to GSH, the random co-polymer populations were consistently smaller, suggesting that they have a lower affinity for the QD surface. In all cases, when comparing the GSH-exposed samples to control experiments, we find that the differences in polymer-to-QD mole ratios are not substantial, suggesting that GSH does not displace the co-polymer ligands. In the case of the differing molecular weights, we note that the higher molecular weight co-polymers (**B30K** and **R27K**) are more robust and resistant to GSH at low concentrations (2 mM). On the basis of the PL and absorption data, we conclude that GSH association occurs

regardless of polymer size or monomer sequence, albeit to a significantly higher degree for the random co-polymers. Therefore, block co-polymer imidazole ligands are more effective at stabilizing CdSe/$Cd_xZn_{1-x}S$ QDs in the presence of endogenous small thiol molecules in aqueous buffer at biologically relevant concentrations.

The superior stability and diminished interference of block co-polymers to biogenic thiols highlights the importance of monomer sequence on colloidal QD stability for live cell and intracellular applications. We believe this work serves as a steppingstone to developing more effective multiply-binding co-polymer coatings for bioimaging and biosensing. Future studies into imidazole-bearing block co-polymers could focus on analyzing their stability *in vivo*, under a range of pH conditions, and the influence of other monomers and polymer structures.

2.7 Materials and Methods

Materials for QD Synthesis, Ligand Exchange, and Analysis. All chemicals were used as received unless otherwise stated. L-glutathione (reduced form, ≥ 98%), decylamine (95%), acetone (99.5%), and methanol (≥ 99.8%) were purchased from Sigma Aldrich. Hydrochloric acid and chloroform (99.8%) were obtained from VWR. Ethanol (200 proof) was purchased from Decon Laboratories. Phosphate Buffered Saline (PBS, 10x), Hexane (99.9%), and Toluene (99.9%) were purchased from Fisher Scientific. Bio-Beads S-X1 GPC medium was obtained from Bio-Rad Laboratories. Toluene-d_8 (99.5%) was purchased from Cambridge Isotope Laboratories. Trioctylphosphine (TOP, 97%), trioctylphosphine oxide (TOPO, 99%), cadmium oxide (CdO, 99.999%), and zinc oxide (ZnO, 99.999%) were obtained from STREM Chemicals. Oleylamine (80-90%) and bis(trimethylsilyl) sulfide ($(TMS)_2S$, 95%) were purchased from Acros Organics. 1-

octadecene (ODE, 90%), 1-tetradecylphosphonic acid (TDPA, 98%), oleic acid (OA, 99%), and Se (99.999%) were obtained from Alfa Aesar. Trioctylphosphine selenide (TOPSe, 2.2M) was prepared by dissolving Se in TOP. Stock solutions (0.2 M) of $Cd(oleate)_2$ and $Zn(oleate)_2$ were prepared by heating CdO and ZnO, respectively, with excess oleic acid in ODE solvent under vacuum, then stored in a glovebox under inert atmosphere. Glutathione solution (2mM) was prepared by dissolving L-glutathione in PBS. PBS stock was diluted with DI water and sparged with N_2 to prepare an oxygen-depleted PBS solution. Optical absorption data were recorded using a Thermo Scientific Evolution Array UV-Visible spectrophotometer in a 1-cm path length quartz cuvette.

Materials for Polymer Synthesis. All chemicals were purchased from Sigma-Aldrich or Fisher unless otherwise specified. Azobis-(isobutyronitrile) (AIBN) was purchased from Sigma-Aldrich and recrystallized thrice from methanol. Poly(ethylene glycol) methacrylate (PEGMA, 475 g/mol) was obtained from Sigma-Aldrich and passed through a neutral alumina column to remove inhibitors. 4-Cyano-4-(((dodecylthio)carbonothioyl)thio)pentanoic acid (CDPA, >97%) was purchased from Boron Molecular. *N*-methacryloxysuccinimide (NMS) was synthesized from *N*-hydroxysuccinimide (NHS) as described in the literature.[118] Molecular weights (M_n) and dispersities (Đ) were determined using a gel permeation chromatograph (GPC) equipped with a Varian 290-LC pump, a Varian 390-LC refractive index detector, and three Styragel columns (HR1, HR3, and HR4, molecular weight ranges of 100−5000, 500−30 000, and 5000−500 000, respectively). THF was used as eluent for GPC at 30 °C and a flow rate of 1.0 mL/min. GPC was calibrated with polystyrene (PS) standards obtained from Polymer

Laboratories. ^{1}H NMR (Bruker Avance III-HD 300 MHz) were conducted using $CDCl_3$ or DMSO-d_6 as solvent.

Synthesis of poly(PEGMA-*b*-NMS). To form the poly(PEGMA) block, in a representative synthesis, PEGMA (4.75 g, 10 mmol), CDPA (161 mg, 0.4 mmol), trioxane (50 mg), and AIBN (0.4 mL 0.01 M in DMF, 0.04 mmol) were dissolved in 4.5 mL of DMF and added to a Schlenk tube. The solution was degassed by four freeze-pump-thaw cycles, backfilled with nitrogen, and then placed in an oil bath at 70 °C for 4.5 h. The polymerization was quenched in an ice bath. The solution was precipitated in ether. The monomer conversion was measured by ^{1}H NMR. The mixture was centrifuged at 5000 rpm for 5 min and redispersed in 10mL DMF. This precipitation-redispersion process was repeated twice to obtain poly(PEGMA) with M_n = 11000 and Đ = 1.11. To add the poly(NMS) block, poly(PEGMA) (0.60 g, 0.06 mmol), NMS (0.275 g, 1.5 mmol), trioxane (10 mg), and AIBN (0.06 mL 0.01 M in DMF, 0.04 mmol) were dissolved in 4.0 mL of DMF and added to a Schlenk tube. The solution was degassed by four freeze-pump-thaw cycles, backfilled with nitrogen, and then placed in an oil bath at 70 °C for 4.5 h. The polymerization was quenched in an ice bath. The solution was precipitated in ether. The monomer conversion was measured by ^{1}H NMR. The mixture was centrifuged at 5000 rpm for 5 min and redispersed in 5 mL DMF. This precipitation-redispersion process was repeated twice to obtain poly(PEGMA-*b*-NMS) with M_n = 12000 and Đ = 1.10.

Removal of RAFT agent. Poly(PEGMA-*b*-NMS) was dissolved in DMF and 20 eq AIBN was added. The solution was stirred at 70°C for 2 h. After cooling to room temperature, the solution was precipitated into ether, centrifuged at 5000 rpm for 5 min, and redispersed in DMF. This precipitation-redispersion process was repeated twice.

QD synthesis. CdSe/$Cd_xZn_{1-x}S$ core/shell QDs were prepared via a previously described SILAR method.[50] Briefly. phosphonate-capped CdSe cores were coated with 4 monolayers of the shell material at 0.8 monolayers/cycle. The molar extinction coefficient of the CdSe cores was estimated based on the core radius as determined from a calibration curve, and the extinction coefficient of the completed core/shell particles was calculated based on this value by considering the initial amount of cores and the final solution volume after shell growth. For the digestion assay, CdSe cores with lowest-energy absorption peak at 517 nm (~3.2 nm diameter) were coated with Cd and Zn precursors at a 1:1 ratio (x=0.5), yielding a lowest-energy absorption peak of 560 nm and a molar extinction coefficient of 2.24×10^6 $M^{-1}cm^{-1}$ at 350 nm. For the PL studies, a slightly different sample was used with x=0.3 and a lowest-energy absorption peak at 530 nm.

GPC Purification. Before ligand exchange, the CdSe/$Cd_xZn_{1-x}S$ core-shell QDs were purified via GPC using a polystyrene size-exclusion medium (Bio-Beads SX-1) in toluene solvent. The column packing and GPC purification processes were carried out as previously described.[50] Prior to GPC purification, the as-synthesized QDs were flocculated once by addition of acetone and methanol and precipitated by centrifugation (5000 rpm/5 min), followed by redissolution in toluene. The QDs were loaded onto the column dropwise and eluted as a tight band (2.8 mL total collection volume). The GPC-purified QDs were stored in toluene under ambient conditions and characterized by absorption spectroscopy.

Ligand Exchange. The ligand exchanges to install the MA-PILs were conducted as follows. For each polymer sample (**B14K**, **B30K**, **R12K**, and **R27K**), 5 nmol of GPC-purified QDs were dried by vacuum to remove toluene. An excess of each polymer (1:100

and 1:200 mole ratio QD:polymer for the higher and lower molecular weight polymers, respectively) was dissolved in 0.5 mL chloroform. The dried QDs were dissolved in the chloroform/polymer solution and stirred for 45 min at room temperature. Methanol (amount equal to 30% of total chloroform volume) was added and the mixtures stirred 20 min longer prior to adding ethanol (co-solvent) and hexane (anti-solvent) to precipitate the QDs. The samples were centrifuged (4000 rpm/5 min) and the supernatant was decanted off, followed by drying the precipitate with N_2. Each sample was then dispersed in phosphate buffered saline solution (PBS, pH = 7.4).

Centrifugal Dialysis of Polymer-Capped QDs. Centrifugal dialysis was performed using spin concentrators with a regenerated cellulose membrane to remove free and weakly-bound polymer from samples while retaining the MA-PIL-QDs. Dialysis is a commonly demonstrated purification technique that is especially suited for the present work as evidenced by efficient free polymer removal (**Figure 2.10**) and an appropriate molecular weight cut-off (50-100 kDa). The polymer-capped QD solutions initially underwent dialysis purification in DI water before subjecting the samples to the PL response tests. Before the digestion assay the polymer-capped QDs were passed through a 0.2 μm poly(ethersulfone) syringe filter and then dialyzed in PBS buffer. Samples were subject to multiple dialysis cycles to achieve consistently low retention volumes. For example, in preparation for digestion, the QDs required six cycles (5000 rpm/5-10 min) to

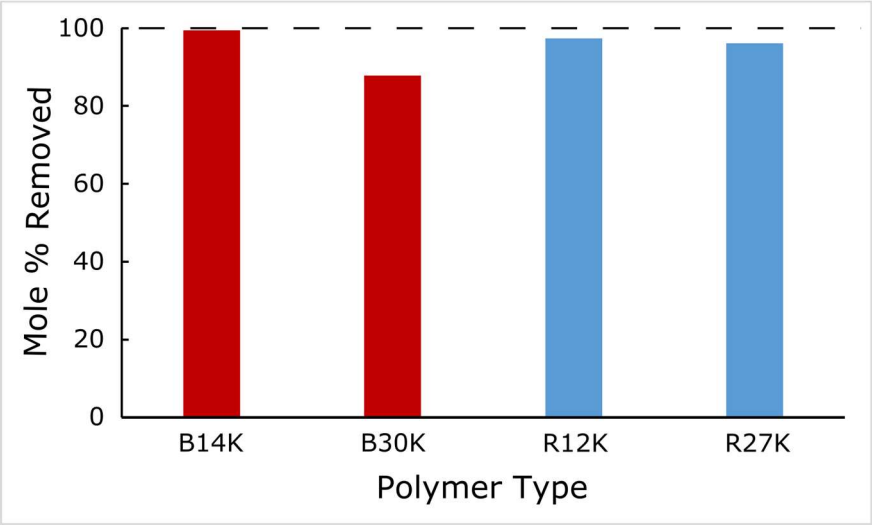

Figure 2.10 *Free polymer removal after purification through five centrifugal dialysis cycles (100 kDa MWCO). Larger retention was observed for the higher molecular weight polymers (**B30K** and **R27K**).*

achieve a retention volume of ~100 μL and effective removal of the excess polymer. The purified samples were then diluted with PBS for absorption measurements.

PL monitoring. Emission spectra were recorded by an Ocean Optics USB 4000 spectrometer using a 365 nm fiber-coupled light-emitting diode as the excitation light source. The setup is equipped with stirring, a cover to eliminate ambient light exposure, and an excitation shutter. Owing to the constant illumination required by successive PL spectroscopy measurements (described below), a control experiment was designed to test the influence of such light exposure on QY. Each of the dialyzed polymer-capped QD samples were prepared in N_2-filled, septum capped quartz cuvettes with magnetic stirring as described in the main text. The excitation shutter was opened long enough to record a single spectrum, then closed for five minutes between measurements. This process was repeated for a total of five trials (**Figure 2.3**).

Photoluminescence Spectroscopy. The MA-PIL-QDs were first dialyzed in deionized water using centrifugal spin concentrators (regenerated cellulose membrane) to

remove excess free polymer and diluted in PBS buffer (pH 7.4). The purified sample was then brought to 20 mL in N_2-sparged PBS. For each PL titration trial, a 2.5 mL aliquot of the diluted QD sample was transferred to a N_2-filled septum-capped quartz cuvette with a stir bar. The cuvette was placed in a holder atop a stir plate and covered to prevent ambient light exposure. A syringe was filled with L-glutathione (44.52 mM in PBS) and secured onto a syringe pump, configured to inject 100 µL GSH every 15 minutes via glass capillary until a total concentration of ~ 8 mM GSH was reached. Emission spectra were collected under constant 365 nm excitation. Prior to the first GSH injection, the spectrum was monitored for 15 min to account for the QD PL response. A control experiment was performed using N_2-sparged PBS in place of GSH to account for any influence of dilution on the PL response (**Figure 2.4**).

Quantification of Polymer Ligands on the QD Surface. A digestion assay coupled with UV-Vis absorption spectroscopy was used to quantify the amount of bound polymer on the QD surface after exposure to specific environmental conditions. A 1 nmol aliquot of the MA-PIL-QDs was passed through a 0.2 µm poly(ethersulfone) syringe filter and dialyzed in PBS buffer (pH 7.4). For each dialysis process, the sample was initially concentrated (5 min/5000 rpm), followed by five cycles of dialysis in PBS (5-10 min/5000 rpm) to achieve consistently low retention volumes (~100 µL). The retained QDs were diluted in PBS for analysis and divided into three portions. Portion A was immediately digested in ~2 mL HCl (3M) by stirring in the dark for 1 hour, after which the absorption spectrum was recorded. Portion B was diluted in 2 mL L-glutathione (2 mM in PBS) and sparged with N_2 for 10 minutes followed by stirring in the dark for 1 hour. Portion B was then dialyzed into PBS to remove free glutathione and the retentate diluted in PBS for

absorption measurements. Finally, the sample was digested in ~2 mL HCl with stirring in the dark for 1 hour, followed by another absorption measurement. A control sample (Portion C) was designed to account for potential dilution effects that may occur with the GSH-treated sample**.** Portion C underwent the same treatment as Portion B, using clean PBS buffer in place of the GSH solution. The polymer/QD mol ratios obtained for each individual trial and portion of the digestion assay are given in the figures below. **Figure 2.11** shows the polymer/QD ratios obtained from immediate digestion in acid (Portion A). **Figure 2.12** and **Figure 2.13** show the polymer/QD ratios for the GSH-treated (Portion B) and PBS control (Portion C), respectively.

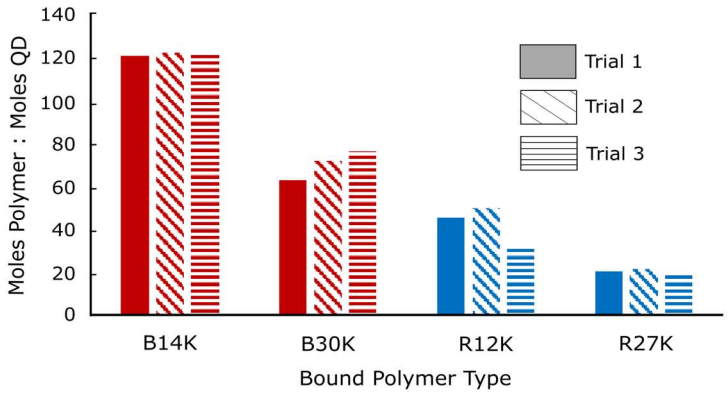

Figure 2.11 *Polymer-to-QD mole ratios of immediately digested MA-PIL-QDs. Little variation is observed among trials. Block co-polymer-capped samples of both molecular weights display a significantly higher number of bound polymers per QD. Trials were repeated in triplicate.*

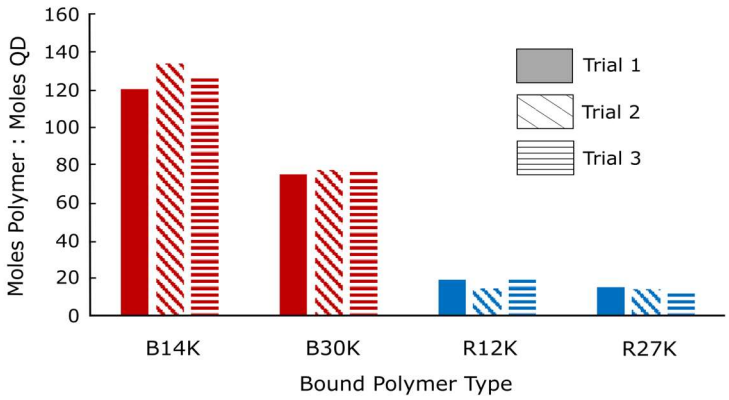

Figure 2.12 *Polymer-to-QD mole ratios of GSH-treated MA-PIL-QDs. Block co-polymer-capped samples of both molecular weights display a significantly higher number of bound polymers per QD than the random co-polymer-capped samples. Trials were repeated in triplicate.*

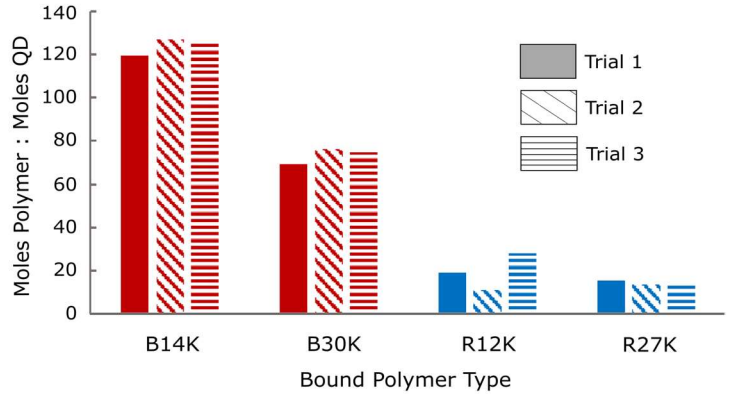

Figure 2.13 *Polymer-to-QD mole ratios of PBS-treated MA-PIL-QDs. This control was compared to GSH-treated trials to determine any change in QD-bound polymer upon exposure to endogenous molecules. Trials were repeated in triplicate.*

CHAPTER 3

COMPETITIVE ANIONIC EXCHANGE OF THIOLATE LIGANDS TO AQUEOUS PHOSPHONATE-CAPPED QUANTUM DOTS

3.1 Introduction

Colloidal semiconductor quantum dots (QDs) have emerged as promising fluorescent imaging probes for biological applications due to their enhanced photostability, narrow size-tunable emission spectra, and multifunctional surfaces compared to common organic fluorophores. When a semiconductor QD (such as CdSe, ZnSe, or InP) is overcoated with an inorganic shell (CdS(Se), ZnS(Se), etc. to produce appropriate core/shell heterostructures, the photoluminescence quantum yield (PLQY) and photostability can be further enhanced due to isolation of potential surface trap states from the excited stated centered on the core.[32,119] Core/shell QDs in particular have become the most widely used QDs for biological applications because they tend to maintain higher PLQYs upon phase transfer into polar/aqueous solvent relative to core-only particles. Achieving appropriate coordination of the inorganic surface of core/shell QDs has been a major focus in developing highly capable QD-based agents for fluorescence microscopy, diagnostics, and sensors in biological applications. Replacing initial coordinating ligands (which are typically hydrophobic) with hydrophilic ones offers a route to aqueous QDs with smaller hydrodynamic size than can be achieved with alternative encapsulation strategies, but there

are relatively few studies that directly study the relative binding strengths and quantify ligand exchanges in polar/protic solvents.

Previous studies of ligand exchanges for biological QD applications have typically focused on establishing the feasibility of various strategies for surface coordination, colloidal stability, linking chemistry, and absence of non-specific binding. Most rely on biphasic reactions or are conducted in non-aqueous solvents. Strategies include monodentate, polydentate, and polymeric ligands that can coordinate the QD surface while providing anionic, zwitterionic, or steric stabilization. In many cases, thiols are the predominant binder group, chosen for its strong affinity to QD surfaces and relative ease of exchange with native alkylcarboxylate, alkylphosphonate, amine, and phosphine ligands under anhydrous and biphasic conditions. In order to advance the prospects of QDs in aqueous and biological environments, it is necessary to evaluate the complex surface chemistry of QDs under such conditions in an organized, systematic approach that facilitates the creation of more stable, robust, and versatile QD coatings. In particular, there is a growing need to understand the coordination and intermolecular interactions that promote the stabilization of molecular ligands on QD surfaces under these conditions. While thiols can suffer from limitations in terms of fluorescence brightness and stability toward oxidation, they provide a good model for systematic variation of denticity, tail group size, and structure in order to examine their contributions to binding thermodynamics. Additionally, thiols provide access to very small hydrodynamic sizes and are also known as ligands for direct synthesis of QDs in aqueous solvent mixtures.

Rotello's group found that dithiolate anchors on pegylated ligands lead to greater intracellular stability of CdSe/ZnS vs. monothiolate-capped QDs of the same size.[98]

Heyes's group also sought to determine whether mono- or bi-dentate binders were more suitable for biological applications by monitoring nonspecific binding to CdSe/ZnS QDs capped by mercaptopropionic acid (MPA) versus dihydrolipoic acid (DHLA) in buffer.[120] They found that bidentate ligands more effectively limit nonspecific binding from competing ligands and are indeed stronger binders, though monodentate ligands could be better suited when nonspecific binding is not of concern. More sensitive metrics that directly measure ligand association or exchange are necessary to go beyond such rankings and quantify the strength of binding among different binders.

Isothermal titration calorimetry (ITC) is a well-known biochemical technique used to characterize the thermodynamics of binding interactions to proteins and other biological substrates.[121–124] Only recently has ITC been applied to coordination of nanocrystal surfaces such as Au nanoparticles and $CsPbBr_3$, InP, and CdSe, and CdSe/CdZnS QDs.[36,72,125–132] ITC offers some advantages over common spectroscopic metrics and is not limited to deuterated solvents, spectroscopic handles, or high sample concentrations. Through a single and direct measurement, the enthalpy change, equivalency, and binding constant may be obtained. However, the signal measured is an ensemble of all processes or reactions taking place during the titration, thus complementary techniques (such as NMR) are often required to characterize the reactants and final products.

Ligands for aqueous QDs generally consist of a binding headgroup, a hydrophilic tail group, and a spacer (such as an alkyl chain) between the two, all of which may have some contributions to the enthalpy and entropy of binding through coordination, interligand, and ligand-solvent interactions. Such interactions may vary on the QD composition, crystal structure, size, or shape. Therefore, systematic studies on the

independent influence of each moiety are necessary to establish how ligands bind and what leads to stronger binding. Rioux's group investigated the effect of chain length on the adsorption of alkane thiols with carboxylic acid binders (including MPA) to Au NPs in water.[126] The binding appeared to be enthalpically-driven, and increasingly exothermic with increasing chain length (C_2-C_6) regardless of Au NP diameter (5-20 nm). The effect of alkyl chain length for monothiols has also been described by Elimelech et al. on oleate-capped CdSe QDs in trichloroethylene.[132] In this X-type exchange, increases in chain length also contributed to greater exothermicity, with compensation by entropic loss observed at longer chain lengths where ligands passivate the QD less efficiently due to steric effects. Most ITC studies with QDs have been limited to nonpolar or weakly polar solvents, where it is known that thiolates bind strongly to surface atoms and displace carboxylates in approximately 1:1 stoichiometries. This may not be the case in aqueous solution where water can solvate charges and the pH can strongly influence the protonation states and binding of ligands. There is a need to extend our understanding of ligand binding to this regime relevant to bioimaging.

Here, we quantify the relative binding strengths of thiolate ligands with different alkyl chain lengths and denticity to phosphonate-capped CdSe/ZnS core/shell QDs (AEP-QDs) under basic conditions in borate buffer (pH 9.15-9.18). The zinc blende crystal structure was selected due to greater symmetry versus wurtzite QDs, which could simplify interpretation of surface sites. Overcoating of a ZnS shell onto zinc blende CdSe via the selective ionic layer adsorption and reaction (SILAR) was used to achieve zinc blende core/shell QDs. We prepared water-soluble QDs through a biphasic exchange of native oleate ligands with 2-aminoethylphosphonic acid (AEP) under basic conditions. The

ligands 3- mercaptopropionic acid (MPA), 11-mercaptoundecanoic acid (MUA), and dihydrolipoic acid (DHLA) were introduced as thiolates to the AEP-QDs in borate buffer containing a high concentration of AEP (**Figure 3.1**). We monitor this competitive exchange by NMR and isothermal titration calorimetry (ITC) to establish whether or not increases in alkyl chain length and a bidentate anchor group lead to stronger ligand binding to QDs under aqueous conditions. In each case, an exothermic signal corresponding to quantitative ligand exchange was observed. In the case of the monothiolates, we observe a larger total exothermic response for MPA versus MUA. Exchanging the AEP with DHLA led to total heat similar to the MPA exchange. Each titration was analyzed in terms of an identical, independent site model (Langmuir isotherm) with the number of sites, enthalpy, and association constant as model parameters. We find that the exchange equilibrium constant, K_{ex}, increases with increasing chain length, and is significantly larger in the case of the bidentate DHLA. From these results, we also observe that the average entropy change for MUA exchange is less negative than that of MPA, and postulate that this indicates a high degree of conformational freedom available to its longer alkyl chain when bound to the QD surface.

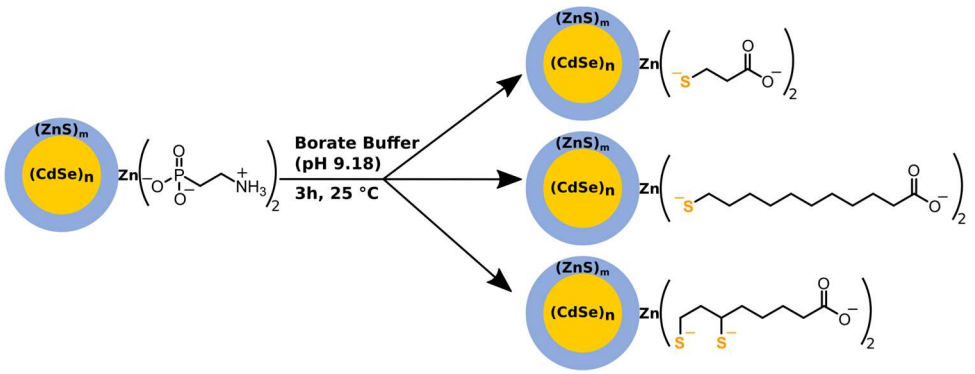

Figure 3.1 *Phosphonate to Thiolate Exchanges Investigated in This Study.*

3.2 Preparation of Phosphonate-Capped Core/Shell QDs

Many previous investigations of ligand exchange on CdSe-based core/shell QDs employed wurtzite structures. We thought it would be beneficial to investigate ligand exchanges on QDs with higher symmetry that could serve as a model system for other zinc blende nanocrystals. The role of synthetic ligands on the crystal structure of QDs has been described to show that native carboxylate ligands tend to produce zinc blende QDs, while phosphonates enforce wurtzite QD formation.[133] Wurtzite QD preparations have the potential for phosphonic acid anhydride ligands (such as tetradecyl phosphonic acid anhydride) to persist after shell growth. Alternatively, zinc blende syntheses result in QD cores capped purely with carboxylate ligands, as well as cubic symmetry, which is advantageous for investigating ligand exchange chemistries. We chose SILAR as the synthetic method due to its ability to produce QDs with quasi-spherical morphologies and high PLQYs. The oleate-capped CdSe/ZnS core/shell QDs (OA-QDs) were prepared similarly to our previous reports[44], with minor modifications: (1) the use of zinc blende CdSe cores to promote epitaxial growth of a zinc blende ZnS shell, in contrast to most previous colloidal SILAR studies which have employed wurtzite, and (2) using lower sub-monolayer equivalencies per cycle (~0.533 ML equivalents/cycle) to achieve a narrow size distribution by suppressing homogeneous nucleation of the shell material as ZnS particles. The PLQY of the OA-QDs in hexanes was measured to be 96.6 %. The oleate-capped core/shell QDs were purified by flocculation with acetone and methanol followed by redispersion in hexanes prior to ligand exchange or further analysis. **Figure 3.2** shows the initial characterizations of the OA-QDs. The crystal structures of the core and core/shell samples were confirmed to be zinc blende by powder X-ray diffraction (PXRD). Upon

overcoating of the ZnS shell, we observe a shift in lattice parameter due to compression of the CdSe core, indicated by a slight shift in peak position, confirming that shell growth proceeded epitaxially. We further characterized the QDs by scanning transmission electron microscopy (STEM) to determine the average radius of the core/shell particles (2.21 nm). The radius of the CdSe core (1.91 nm) was determined based on an established size calibration curve by Kuno using the 1st excitonic peak position (546 nm) and quantity of the CdSe cores.[134]

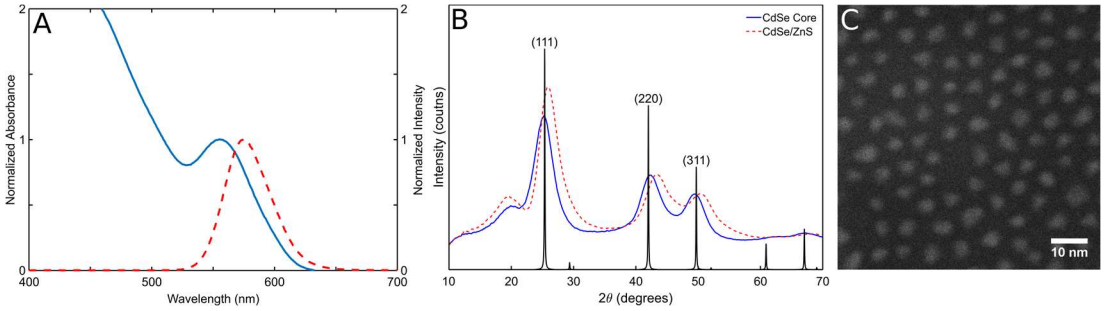

Figure 3.2 *Characterization of oleate-capped CdSe/ZnS QDs. (A) Absorption (blue, solid) and emission (red, dashed) spectra of QDs in hexanes normalized to the peak maxima. (B) Powder X-ray diffraction patterns of the zinc blende CdSe core (blue, solid) and CdSe/ZnS core/shell QD (red, dashed), and a reference pattern for bulk zinc blende CdSe (black, ICSD #41528). (C) HAADF-STEM image of the CdSe/ZnS QDs.*

To effectively describe the relative binding of thiolates by ITC, a homogeneous solvent is required. However, direct replacement of native ligands such as oleate with thiols is often conducted via biphasic reactions or in organic solvents and while effective, it would be advantageous to describe such exchanges in aqueous solvents. Recently, the Weiss group reported the formation of water-soluble CdSe and CdS QDs through X-type oleate to phosphonate exchange, with a view toward photocatalytic applications.[135–137] 2-aminoethylphosphonic acid (AEP) was shown to be a labile ligand that provided several

days of colloidal stability under basic conditions via electrostatic stabilization. We reasoned that AEP-capped core/shell QDs could serve as a starting point for investigating ligand exchanges in water, with AEP effectively serving as a leaving group. As a strategy for investigating the relative binding strength of thiolates, this approach has several advantages compared to investigating exchanges from one thiol to another. Firstly, as seen below, AEP to thiolate exchange is strongly exothermic, producing a signal that is easily distinguished from heats of dilution and probes the difference in enthalpy for phosphonate vs. thiolate coordination in aqueous buffer. Secondly, examining a reaction with a larger value of the exchange equilibrium constant K_{ex} facilitates finding unique solutions for K_{ex}, the number of sites N, and the average enthalpy change ΔH.

Aqueous AEP-QD dispersions were achieved through successful ligand exchange of the native hydrophobic carboxylate ligands as described in **Figure 3.3**. Our procedure follows that of Weiss and coworkers, however at a higher equivalency (1100 equivalents of AEP per mole QD) to help drive displacement of the native oleate ligands. Introduction of a methanolic solution of AEP and KOH induced flocculation of the OA-QDs from hexanes, followed by phase transfer into methanol with ligand exchange. The AEP-QDs were then washed several times with hexanes to remove displaced oleate and dried under vacuum to evaporate the methanol. The final AEP-QDs could be dispersed in borate buffer (pH ~9.2) and remained stable under air for several days.

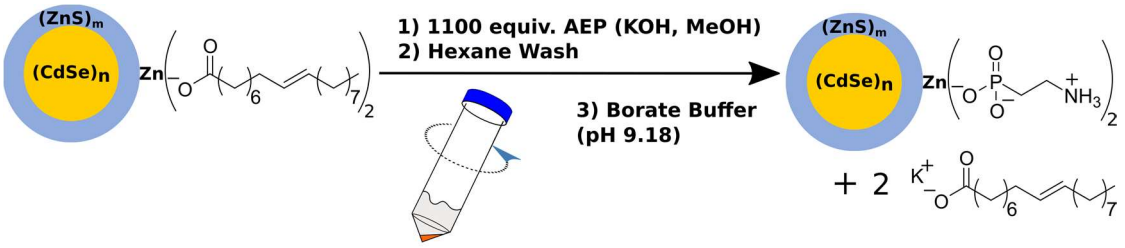

Figure 3.3 *Oleate to Phosphonate Ligand Exchange Procedure. Ligand exchange and phase transfer to methanol with AEP was accomplished by introduction of a solution of AEP and KOH in methanol (1). AEP-QDs were washed with hexanes (2), centrifuged, and redispersed in pH 9.18 borate buffer (3).*

While the phase transfer from nonpolar to polar solvent with introduction of AEP indicated a change in the QD capping layer, we monitored the phosphonate exchange by ^{1}H and ^{31}P NMR to determine whether the AEP effectively displaced the native oleate ligands (**Figure 3.4**). **Figure 3.4** shows the initially purified QD sample (blue trace), containing both a broad and slightly sharper resonance at ~ 5.6 ppm indicative of bound and free populations of oleate ligands on and off the QD surface.[55] The oleate ligand population was determined to be 242 ligands per QD with a density of 3.9 oleates per nm^2 in the initial OA-QD sample. Octadecene (ODE) from synthesis was also present that persisted through initial purification. The AEP-exchanged QDs (purple trace) in aqueous buffer after several hexane washes is also provided in **Figure 3.4**, and the appearance of AEP peaks was noted at 1.6 and 2.9 ppm, along with significant reduction of the olefin species. The hexane washes after AEP exchange were sufficient to remove the native carboxylate ligands displaced by AEP, as well as ODE, yielding AEP-QDs suitable for aqueous ligand exchange experiments. We note that the AEP-QDs retain a broad peak at 5.3 ppm, near the olefin resonances found in the OA-QD samples. This peak, along with a very broad signal at 1.25 ppm, is attributed to the presence of oleate micelles in the AEP-

QD sample that are not bound to the QD, as these are also seen in oleic acid samples brought to basic pH in D_2O. Evaluation of the ^{31}P NMR spectra of the OA-QDs in **Figure 3.4** to the AEP-QDs, demonstrates complete removal of tri-*n*-octylphosphine (TOP), a nucleophilic coordinating solvent employed in shell growth, by the washing step and the presence of AEP. It should be noted that strongly bound ligands on nanocrystal surfaces tend to have broadened resonances due to slower rotational diffusion relative to freely diffusing ligands in solution. In the case of AEP, we observe some broadening, however to a lesser extent than seen in other QD systems, and indeed for AEP-QDs prepared by Weiss and co-workers.[136] This is due to the large excess of AEP used to accomplish the ligand exchange, as well as the minimal purification conducted on the samples, leading to a large fraction of free AEP in solution that exchanges rapidly with the surface-bound population. We found that a similar synthetic approach could also be used to directly install each of the thiolate ligands investigated here, starting from OA-QD, as described in the Materials and Methods section. This supports our interpretation of thiolates binding as X-type (anionic) ligands under basic conditions, consistent with previous studies emphasizing the success of thiolate exchange under basic conditions and/or when introduced as a zinc salt.[138]

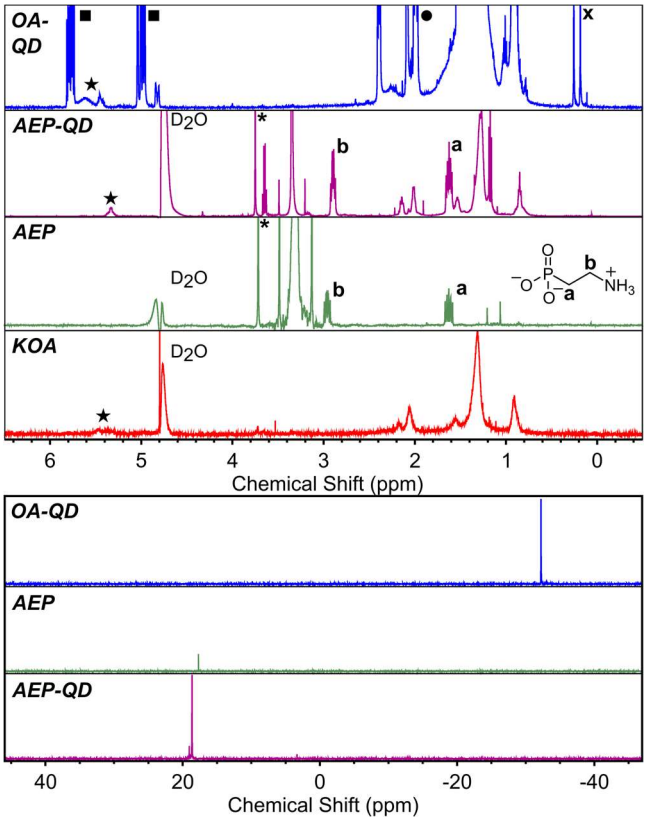

Figure 3.4 *^{1}H (top) and ^{31}P (bottom) NMR spectra of QDs and ligands showing displacement of oleate by AEP. ^{1}H NMR measurements of aqueous samples were conducted with presaturation solvent suppression to minimize the intensity of the water/D_2O peak at 4.9 ppm. The peaks for the internal standard 1,4-dioxane (*) or hexamethylcyclotrisiloxane (X), toluene (●), ODE (■), and OA (★) are indicated. Full NMR spectra are provided in the Materials and Methods section.*

3.3 Phosphonate to Thiolate Exchange

Prior to conducting thermodynamic measurements by ITC, we evaluated AEP to thiolate exchange on the benchtop to confirm that it occurs rapidly under basic conditions in buffer. Solutions of MPA, MUA, and DHLA were prepared by dissolving the free ligand into borate buffer at pH 9.15-9.18. To set up the reaction as a competitive exchange from an AEP-saturated initial state, the AEP-QDs were diluted with a 6.73 mM AEP solution in borate buffer to achieve a total AEP concentration of nominally 13 mM. The thiolate ligand

stock solutions were introduced to the AEP-QDs and stirred for 3 hours at room temperature in the dark. Conducting the exchange under basic conditions should favor deprotonated thiolates binding as X-type ligands to the QD surface. Following ligand exchange, the thiolate-QDs were purified by one cycle of dialysis in centrifugal spin concentrators to remove free thiolates and displaced AEP from the solution. The minimal dialysis purification was successful for the MUA- and DHLA-QDs, however in the case of MPA-QDs, their poor dispersibility resulted in significant sample loss and they were not robust towards purification after thiolate exchange. We initially characterized the product of the ligand exchanges using absorption and PL spectroscopy, shown in **Figure 3.5** for the representative case of DHLA exchange. Displacement of oleate to prepare AEP-QDs resulted in a high-scattering product and a red shift in the absorption and emission, indicative of some degree of aggregation among QD-AEP in aqueous buffer. Both of these changes are reduced significantly after exchange with DHLA and purification. The reduction in scattering upon introduction of the thiolate indicates better colloidal dispersion consistent with ligand exchange.

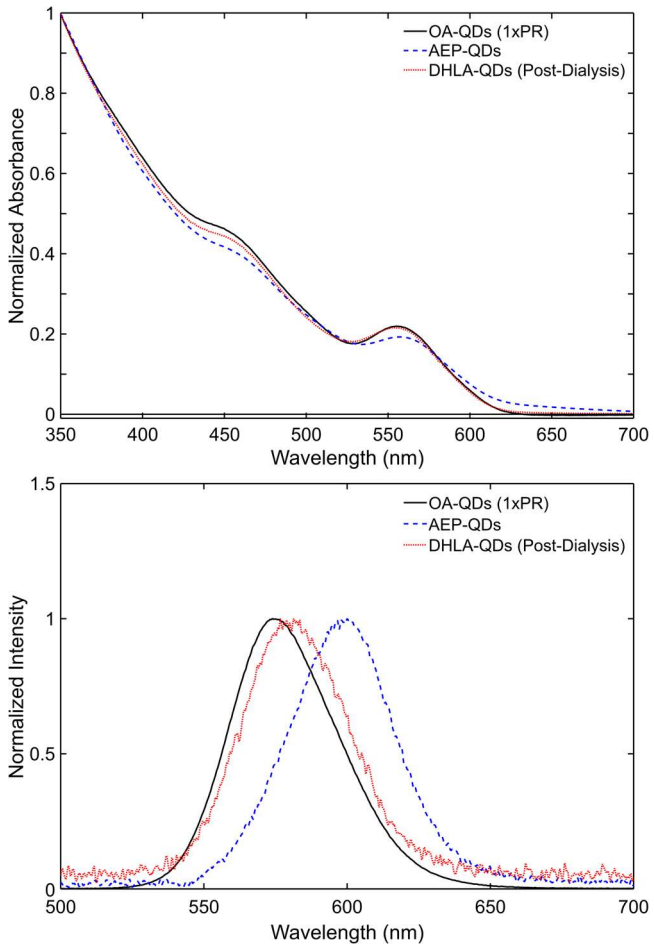

Figure 3.5 *Absorption (top) and emission (bottom) of ligand-exchanged QDs. The absorption spectra are normalized to the absorbance at 350 nm, and emission spectra are normalized to the emission maximum.*

NMR spectra for the case of AEP to DHLA exchange are presented in **Figure 3.6**. Treatment with DHLA resulted in a significant reduction of the AEP resonances, indicating successful displacement. Observation of the ^{31}P NMR shows the presence of some residual AEP in the DHLA-QD sample, though the peak intensity is greatly diminished with respect to the AEP-QDs. We attribute this reduction to displacement by DHLA, which would result in a decrease in the bound population of AEP. The presence of AEP here is most likely due to the minimal purification used to prepare the DHLA-QDs for analysis, and

further purification should effectively remove all free AEP in solution that was retained. We chose to use a minimal purification by centrifugal dialysis here to limit sample loss due to QD aggregates, because while the scattering for DHLA was quite low, the monothiol-capped QDs were not as well dispersed and prone to sticking on the centrifugal dialysis filter membrane.

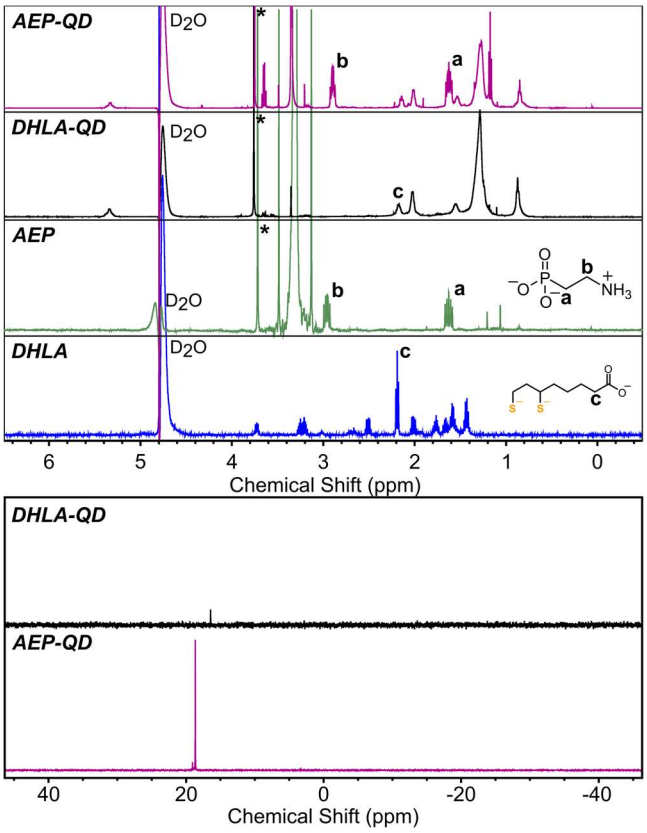

Figure 3.6 *^{1}H (top) and ^{31}P (bottom) NMR of AEP-QDs before and after exchange with DHLA. Peaks for the internal standard are indicated by (*). Full NMR spectra are provided in the Materials and Methods section.*

3.4 Isothermal Titration Calorimetry

Once we had confirmed that the thiolate exchanges occurred, we designed a competitive exchange titration experiment to probe the thermodynamics of the thiolate exchanges to AEP-QDs to determine their relative binding strengths. For each titration, solutions of the thiolates (each prepared at ~12-13 mM in borate buffer) were sparged with N_2 prior to loading into a titrant syringe under air. The sample cell was filled with 350 µL of AEP-QDs (5.2 – 7.5 µM), in buffer containing ~ 13 mM AEP. After equilibration, the titrations were conducted with a series of 30 injections of 5 µL each. Raw thermograms (showing the power compensation signal versus time) are shown in **Figure 3.7**. With each thiolate injection, a sharp exotherm is generated that quickly returns to equilibrium prior to the next injection, shown in the blue trace of **Figure 3.7**. As a control experiment to account for the heat of dilution of the ligand, the same thiolate solutions were titrated into the QD-free AEP buffer solution under identical conditions. A nonzero exothermic response was detected in each case (red trace, **Figure 3.7**), which appears to be diminished towards the end of the titration, and that we attribute to slow oxidation of the thiolate ligand.

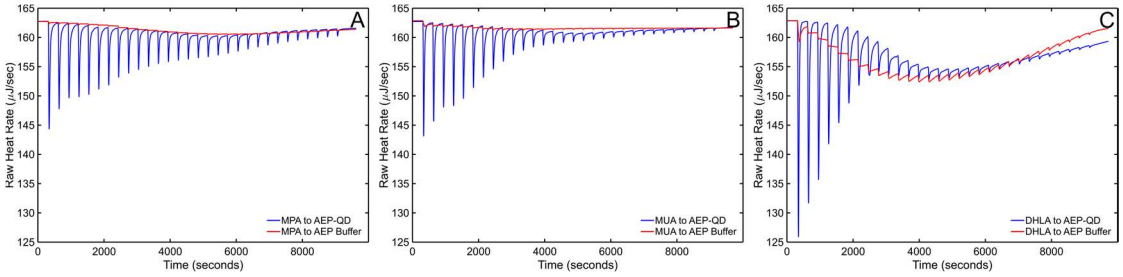

Figure 3.7 *Raw ITC Thermograms of representative Thiolate-QD titrations (blue) and thiolate-to-buffer control titrations (red). The control titration was subtracted from the QD titration and baseline corrected to generate the corrected heat thermograms prior to fitting.*

To isolate the ligand exchange contribution to the raw heat thermograms, we subtracted the free ligand background from each QD titration. The heat associated with each injection was then determined using a standard baseline correction to generate an isotherm plot indicating the enthalpy change (ΔH, plotted as kJ per mole of ligand added) versus the mole ratio of thiolate/QD at each step. The background subtracted/baseline corrected thermograms for three replicate titrations and their respective isotherms fitted to an independent site model are shown in **Figure 3.8**.

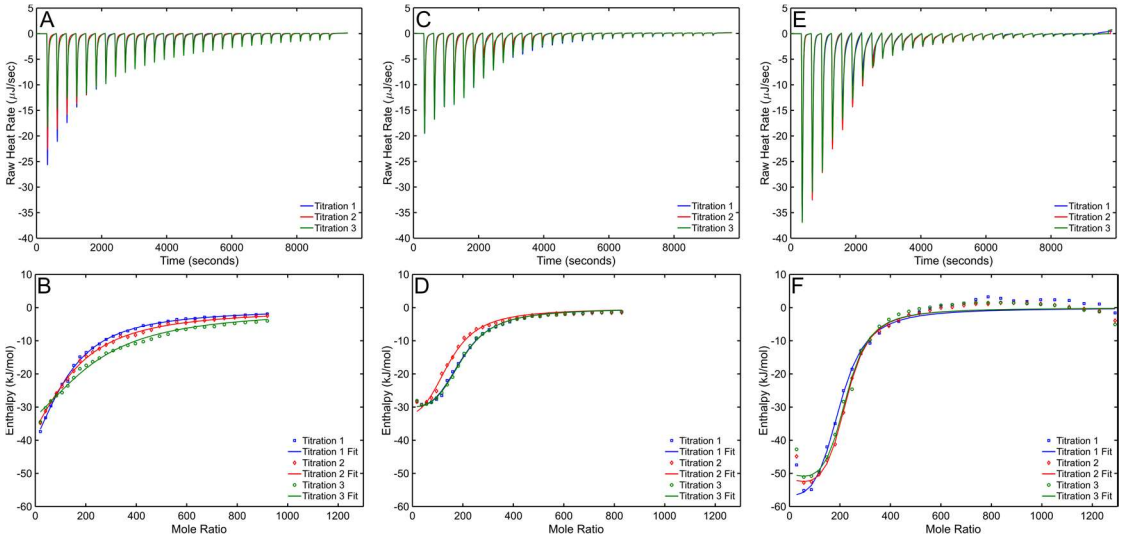

Figure 3.8 *Corrected heat response thermograms (top) and integrated heat isotherms (bottom) of three replicate thiolate titrations. The corrected thermograms were background subtracted and baseline corrected. (A, B) MPA titrations. (C, D) MUA titrations. (E, F) DHLA titrations.*

In the simple case of association of a ligand (L) to vacant sites (S), the binding equilibrium may be interpreted as follows, with the effective equilibrium association constant, K_a, determined by the fractional occupation θ of sites and ligand concentration:

$$S + L = SL \qquad \text{(Equation 1)}$$

$$K_{\mathrm{a}} = \frac{\theta}{1-\theta[L]} \qquad \text{(Equation 2)}$$

This analysis can be applied to the case of a nanoparticle with some number of identical and independent sites (Langmuir model), and within this model, the number of sites (N), enthalpy change (ΔH), and association equilibrium constant (K_{a}) can be obtained from least squares fitting of an experimental ITC isotherm. In our case, we assume no vacant sites are present on the AEP-QD surface due to the high concentration of the AEP, [L_1], relative to the number of sites. Within this limit of saturation (where the fractional occupation of unsaturated sites is negligible), no association occurs and we only detect exchange of AEP by the thiolate, which may be expressed by the exchange equilibrium constant, K_{ex}:

$$K_{\mathrm{ex}} = \frac{\theta}{1-\theta} \times \frac{[L_1]}{[L]} \qquad \text{(Equation 3)}$$

We note that in the case where there are few empty sites and $[L_1]_t \gg N[M]_t$, the fractional change in [L_1] over the course of the exchange reaction is small and $K_{\mathrm{ex}}/[L_1]$ has an approximately constant value, which we will write as the effective association constant $K_{\mathrm{a,eff}}$:

$$K_{\mathrm{ex}}/[\mathrm{L}_1] = \frac{\theta}{1-\theta} \times \frac{1}{[L]} = K_{a,\mathrm{eff}} \qquad \text{(Equation 4)}$$

The effective association constant, $K_{\mathrm{a,eff}}$, may be determined from analysis of the experimental isotherm according to the Langmuir model, along with N and ΔH. With knowledge of $[L_1]_t$, the exchange equilibrium constant K_{ex} may then be obtained and used to compare the binding strength of each thiolate compared to AEP. The ratios of K_{ex} for

the different thiolates can be used to compare their relative binding strength. The generated isotherms in **Figure 3.8** are well parameterized by the independent site model, particularly in the case of the MUA and DHLA titrations. The curvature of the MPA isotherm is quite shallow relative to MUA and DHLA, indicating that MPA may have a lower affinity to the QD surface. We note that isotherm curve shapes observed in the Langmuir model are parameterized by a single value, the Brandts *c*-parameter, and that for values of $c < 1$ it is challenging to obtain unique fits for N and ΔH.[139]

$$c = K_{\text{a,eff}} \times N \times [M]_t \qquad \text{(Equation 5)}$$

In the case of MPA, the *c* parameter is quite low (c=0.35) in comparison to that of MUA (6.6) and DHLA (17). One can also express the relative binding strength of the thiolates by comparing the effective dissociation constant, $K_{\text{d,eff}}$, which is calculated by the inverse of $K_{\text{a,eff}}$.

$$K_{d,\text{eff}} = \frac{1}{K_{a,\text{eff}}} \qquad \text{(Equation 6)}$$

We obtained $K_{\text{d,eff}}$ values of 2, 0.2, and 0.06 mM for MPA, MUA, and DHLA, respectively. This suggested that monothiolates were indeed weaker binders than the bidentate ligand and increases in chain length improved the strength of binding as well.

Each titration produced an exothermic response which decreased in magnitude with subsequent injections, and finally reaching a saturation point as the reaction reached completion and all available AEP was exchanged for the thiolate. Comparing the monothiolate ligands, a smaller exotherm is produced for the longer chain MUA versus MPA. When the denticity of the binding group was increased to two (DHLA), more heat was produced compared to the monothiolate ligands. Because of the difficulty in obtaining

unique values for N and ΔH which makes it hard to assign the number of sites with precision, a robust way to compare ΔH between reactions is to compare the total amount of heat produced from the ligand exchanges (**Figure 3.9**). This is obtained by N x ΔH, and unambiguously allows determination of the exothermicity of the exchange reactions. We found that the average heat per mole QD was similar between MPA and DHLA, and attribute this to either a higher ligand density of MPA on the QD surface (due to its compact size) or a substantially different heat of dilution between MPA and DHLA. Another potential explanation of the similar total heats could be that both thiolate binders on DHLA are not always able to bind. Theory calculations might aid in differentiating between these scenarios but is outside the scope of this work.

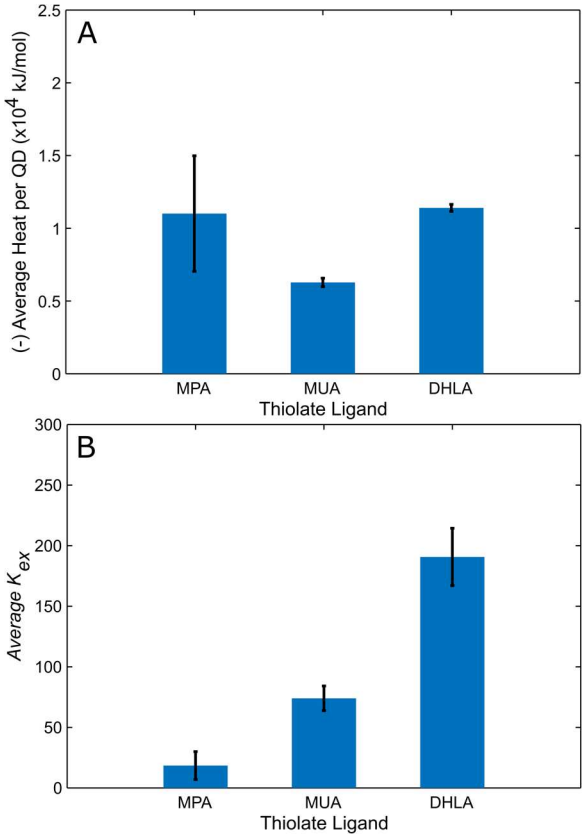

Figure 3.9 *Average heat produced per mole QD (A) and average K_{ex} (B) for each QD ITC titration. Each titration was repeated in triplicate and error bars indicate 1 standard deviation.*

In examining the relative strength of binding, we initially fit the data using a 3-parameter fit, allowing for variations in N, K_{eq}, and ΔH. This fit resulted in different numbers of sites between the ligand titrations, but as discussed above the values of N may be unreliable for curves parameterized by a smaller value of c. We considered that as the uncertainty in N for the DHLA titrations was much smaller than that of the other ligands (**Figure 3.10**), it could be informative to compare 2-parameter fits for each of the ligands with N fixed to 197 sites per QD, on the assumption that the number of anionic sites should be similar in each case. The thermodynamic parameters obtained from the 2-parameter fit are provided in **Table 3.1**.

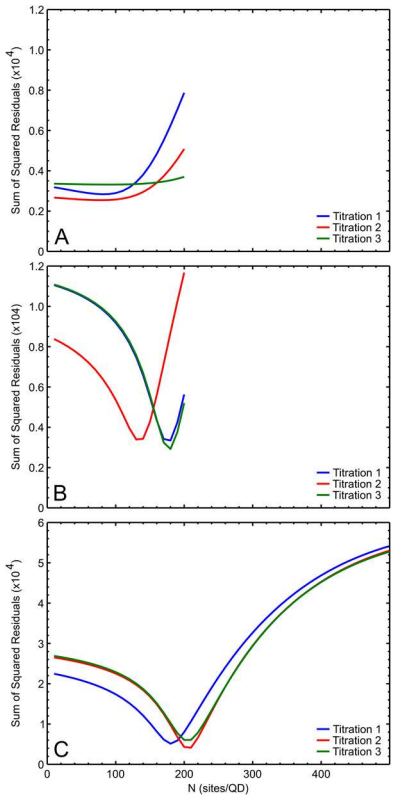

Figure 3.10 *Error analysis of sites per QD (N) as obtained from a 3-parameter fit for each QD-titration: (A) MPA, (B) MUA, and (C) DHLA.*

Table 3.1 *Thermodynamic Parameters Obtained from Thiolate Ligand Exchanges via 2-Parameter Fit. *Result of 3-parameter fit, † 2-parameter fit for K and ΔH with N held at value for DHLA fit.*

Thiol Exchange	N (Sites per QD)	ΔH (kJ mol^{-1})	ΔS (J mol^{-1} K^{-1})	ΔG (kJ mol^{-1})	Heat per QD (x10^{3} kJ mol^{-1})	K_{ex}
MPA to AEP-QD	197†	-55.9 ± 20.2	-164.5 ± 73.7	-6.8± 1.8	-11.0 ± 4.0	18.5 ± 11.5
MUA to AEP-QD	197†	-31.9 ± 1.5	-71.2 ± 3.8	-10.7 ± 0.4	-6.3 ± 0.3	74.0± 10.2
DHLA to AEP-QD	197*	-57.9 ± 1.2	-150.6 ± 4.8	-13.0 ± 0.3	-11.4 ± 0.2	190.7± 23.7

To definitively establish which molecules in this study are stronger binders, the equilibrium exchange constants (K_{ex}) may be compared. We expected the differences in binding between MPA and MUA would be subtle, despite the large difference in alkyl chain length (3 versus 11 carbons), however K_{ex} is four times larger for MUA than MPA, indicating that the increasing the chain length of a monothiolate binder increases the binding strength of the ligand. Furthermore, the value of K_{ex} for DHLA was significantly larger than both monothiolates, which reinforces the evidence that DHLA binds more strongly due to its bidentate nature. Consideration of the enthalpy and entropy obtained from the 2-parameter fits lends some insight into the driving force of the monothiolate ligands. It was expected that increases in chain length would be accompanied by greater exothermicity with decreases in ΔH and more negative ΔS as observed for alkanethiols to Au NPs in water and alkyl thiolates to CdSe in organic solvent.[126,132] In our system, we observe an increase in both ΔH and ΔS as the chain length increased. Coupled with the stronger binding of MUA over MPA, this suggests that entropy is the main driving force of MUA binding to the QD. This could be due to the longer alkyl chain of MUA having more degrees of freedom closer to the carboxylate tail that could prevent packing of MUA to adjacent sites. A significant

amount of entropy could be retained by MUA as the tail group interacts with solvent molecules, as opposed to adjacent bound MUA ligands.

3.5 Conclusions

Through the application of isothermal titration calorimetry, we compared the relative binding strength of monodentate thiolate ligands, MPA and MUA, to a representative bidentate thiolate ligand, DHLA. ITC titrations conducted in the presence of a large concentration of AEP under basic conditions in borate buffer enabled us to evaluate the influence of alkyl chain length and binding motif denticity as a competitive exchange. We found that increases in chain length led to increases in the equilibrium exchange constant, indicating stronger binding with longer-chain monothiolates. Furthermore, increasing the denticity of the binding group resulted in even stronger binding for DHLA. We also observed that, contrary to published studies on the influence of chain length in thiol ligand binding to nanoparticles, increases in chain length between MPA and MUA resulted in a higher entropy, which we attribute to ligand-solvent interactions and greater degrees of freedom in the tail group at longer chain lengths. These results have been obtained by using 2-aminoethylphosphonic acid as a common starting point for ligand exchange under mildly basic buffer conditions in water. By utilizing zinc blende colloidal CdSe/ZnS core/shell QDs, initially prepared with oleate ligands, the results offer a window into the relative stability of thiol-capped QDs employed for fluorescence imaging and sensing in biological contexts. These results also demonstrate the utility of ITC as a sensitive metric to evaluate ligand interactions on nanoparticle surfaces, as well as the need to further develop our understanding of how molecules bind to QDs. We anticipate that a

large variety of nanocrystal ligand exchange reactions can be examined in a similar manner.

3.6 Materials and Methods

Materials. All chemicals were used as received with further purification unless otherwise stated. Trioctylphosphine (TOP, 97%), cadmium oxide (CdO, 99.999%), and zinc oxide (ZnO, 99.999%) were obtained from STREM Chemicals. Tri-n-hexylamine (THA, 97%), Oleic Acid (OA, 90%), 3-mercaptopropionic acid (MPA, 99%), and 1,4-dioxane (ACS, 99+%, stab. with 1-3 ppm BHT) were purchased from Alfa Aesar. Oleic Acid (OA, 99%) was purchased from Beantown Chemical. Bis(trimethylsilyl) sulfide ($(TMS)_2S$, 95%), 1-octadecene (ODE, 90%), hexamethylcyclotrisiloxane (HMCTS, 98%), DL-Thioctic Acid ("lipoic acid", TA, 98+%), sodium bicarbonate ($NaHCO_3$, 99.5%), sodium borohydride ($NaBH_4$, 98+%) were purchased from Acros Organics. Rhodamine 640 perchlorate (R640) was purchased from Exciton. Hexanes (ACS reagent) was purchased from Avantor. Ethanol (EtOH, 200 proof) was purchased from Decon Labs. Methanol (MeOH, 99.8+%), chloroform ($CHCl_3$, 99.8+%), 11-mercaptoundecanoic acid (MUA, 95%), and 2-aminoethylphosphonic acid (AEP, 99%) were purchased from Sigma Aldrich. Boric acid (H_3BO_3, 99.9%), magnesium sulfate (anhydrous), and potassium hydroxide (KOH, tech. grade) were purchased from Fisher Scientific. Potassium chloride (KCl, 99.6%) was purchased from Mallinckrodt Chemicals. Deuterium oxide (D2O, 99.9%) and toluene-d_8 (TOL-d8, 99.5%) were purchased from Cambridge Isotope Laboratories. Trioctylphosphine selenide (TOPSe, 2.2M) was prepared by dissolving Se in TOP under inert atmosphere. $Zn(OA)_2$ was prepared by dissolving ZnO in 2.2 equivalents of oleic acid in ODE solvent under vacuum, then stored in a N_2-filled glovebox.

Borate buffer stock (20 mM) was prepared by diluting 0.2 M KCl and 0.2M H_3BO_3 in DI water with KOH to pH 9.18 and sparging with N_2 to form an oxygen-depleted buffer. Optical absorption spectra were recorded with a Thermo Scientific Evolution Array UV-Visible spectrophotometer in a quartz cuvette with a path length of 1-cm. Emission spectra were recorded with an Ocean Optics USB 4000 spectrometer equipped with a 365 nm fiber-coupled light emitting diode excitation source.

Synthesis of Dihydrolipoic Acid (DHLA). DHLA was synthesized following a previously reported method.[96] In brief, DL-thioctic acid was dissolved in 0.25 M sodium bicarbonate solution at room temperature and cooled via ice bath to 0 °C. Sodium borohydride was added over several additions and the reaction stirred at 0 °C for 2 hours, followed by acidification with 6M HCl to pH 1. The DHLA was removed from the mixture via chloroform extraction in a separatory funnel then dried over anhydrous magnesium sulfate. The slurry was filtered through vacuum filtration. The DHLA was isolated via rotary evaporation as a clear and colorless oil and dried on a Schlenk line (1.94 g yield). The final product was stored in a N_2-filled glovebox to prevent oxidation.

NMR Characterization of Ligands and QDs. ^{1}H and ^{31}P NMR measurements were conducted on a Bruker AVANCE III-HD 500 MHz spectrometer. The measurements for the free AEP ligand at different pH values was measured on a Bruker AVANCE III-HD 400 MHz spectrometer. The 1x PR QDs and hexane washes from ligand exchanges were prepared by drying the samples and dispersing in toluene-d_8 with a hexamethylcyclotrisiloxane (HMCTS) internal standard. Thiolate- and phosphonate-capped QDs were prepared for NMR by centrifugal dialysis and dilution with D_2O. 1,4-dioxane was used as an internal standard for all QD measurements in D_2O. Reference

measurements of oleic acid and free ligands in D_2O were basified to pH ~ 9.3 with potassium carbonate (0.2 M K_2CO_3 in D_2O). ^1H NMR measurements in toluene-d_8 and D_2O were conducted with a 11 s and 30 s delay, respectively (at least 5 x T_1). ^1H NMR in D_2O used a presaturation solvent suppression pulse sequence due to the significant presence of water in the samples. ^{31}P measurements were proton decoupled with 256 scans and a 1s delay time. Reference ^1H NMR spectra for the ligands used in this study are provided in **Figures 3.11-3.17**, and the ligand populations obtained before and after ligand exchange are listed in **Table 3.2** below.

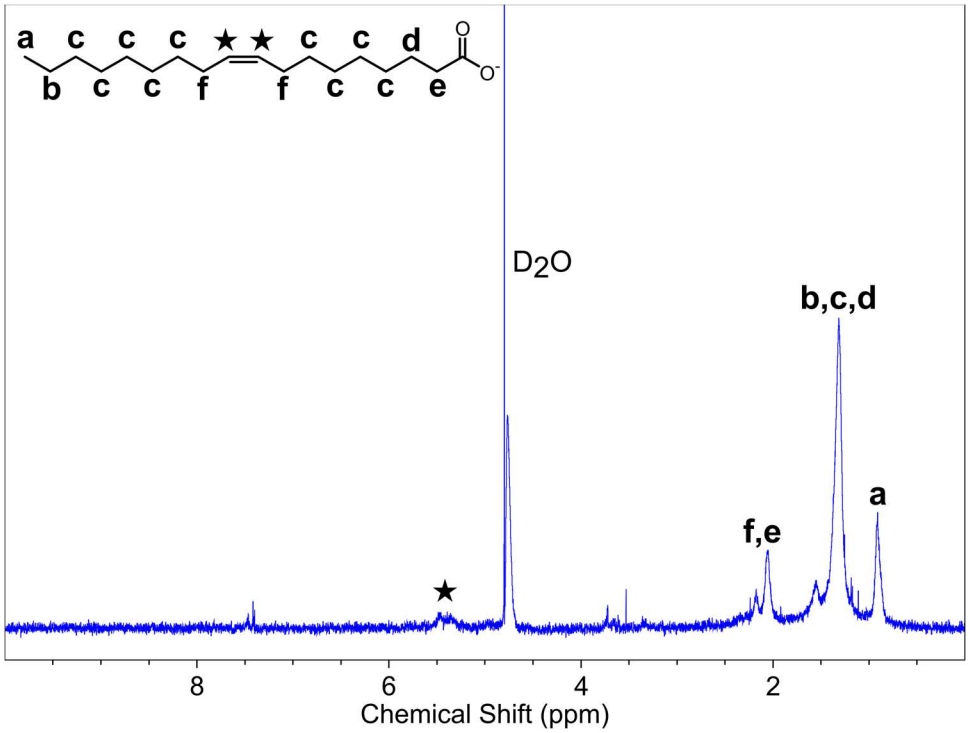

Figure 3.11 *^{1}H NMR reference spectrum of 99% oleate in D_2O, basified with K_2CO_3.*

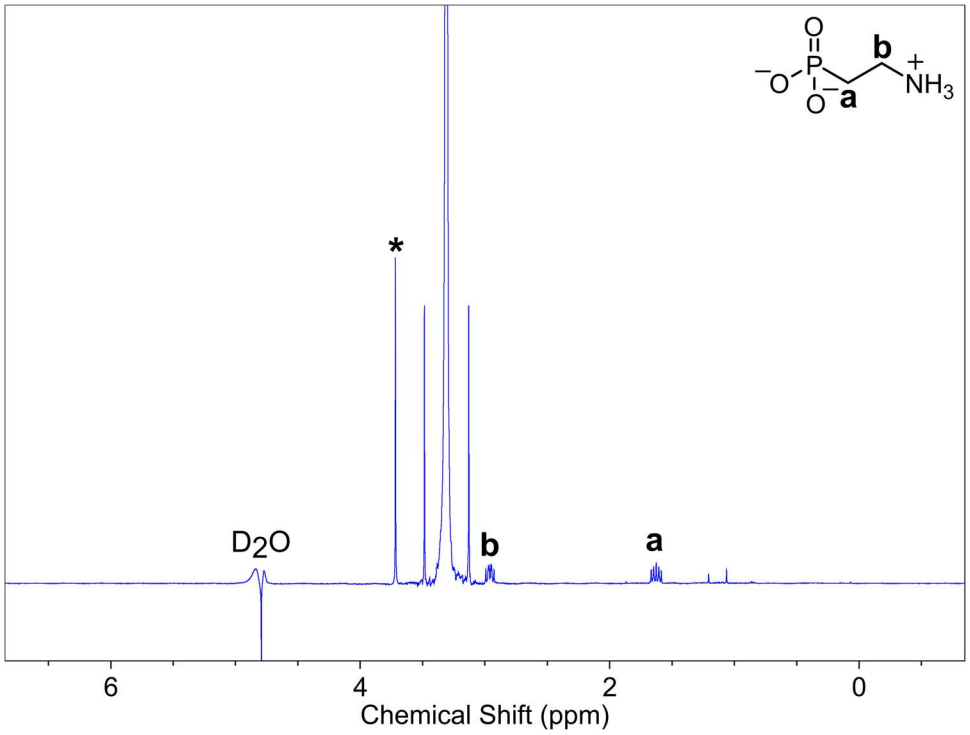

Figure 3.12 *^{1}H NMR spectrum of 2-aminoethylphosphonic acid (AEP) basified to pH 11.2 with K_2CO_3 in D_2O. The peak for the internal standard 1,4-dioxane is indicated by the (*).*

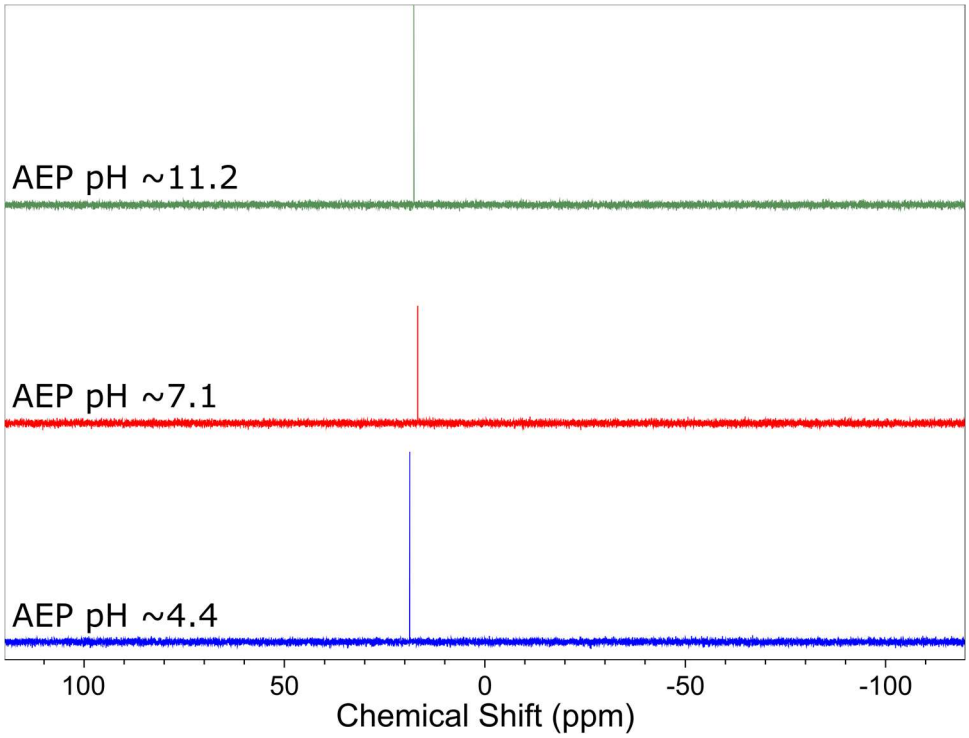

Figure 3.13 *^{31}P NMR spectrum of 2-aminoethylphosphonic acid (AEP) under different pH conditions, acidified HCl or basified with K_2CO_3 in D_2O.*

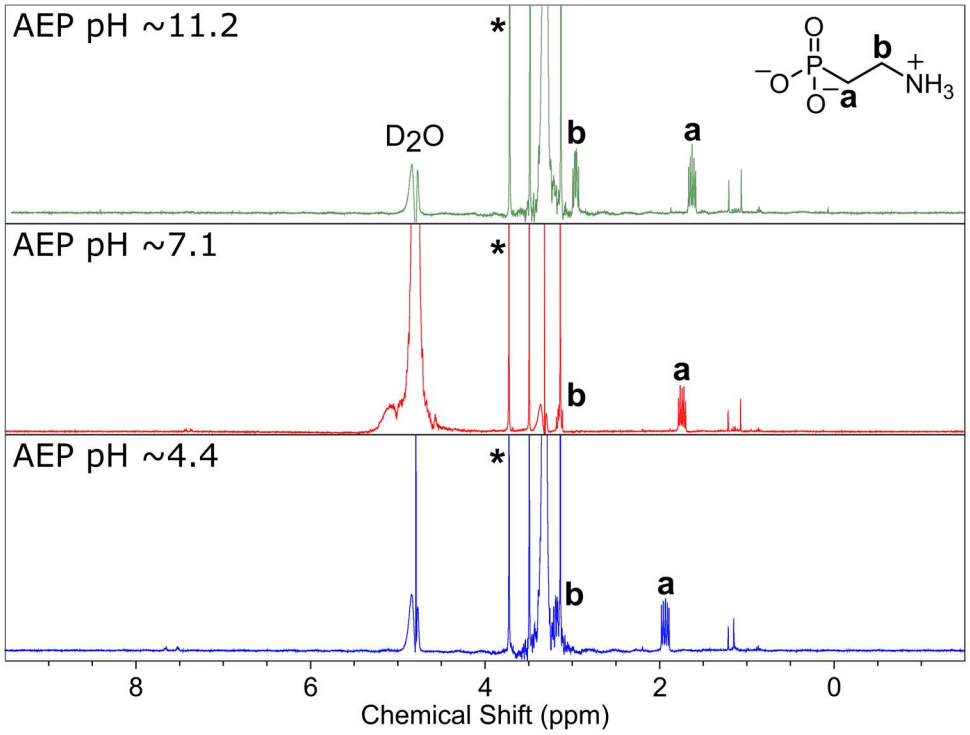

Figure 3.14 *^{1}H NMR spectrum of 2-aminoethylphosphonic acid (AEP) under different pH conditions, acidified HCl or basified with K_2CO_3 in D_2O. The peak for the internal standard 1,4-dioxane is indicated by the (*).*

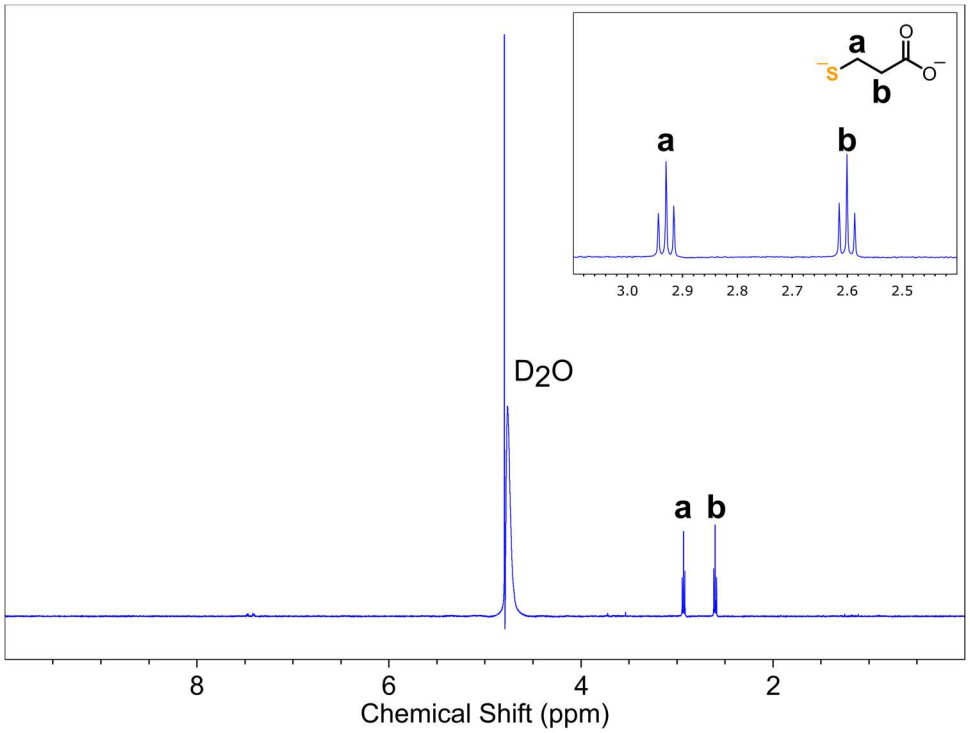

Figure 3.15 *^{1}H NMR spectrum of 3-mercaptopropionic acid, basified with K_2CO_3 in D_2O. Inset: magnification of 2.5-3 ppm region.*

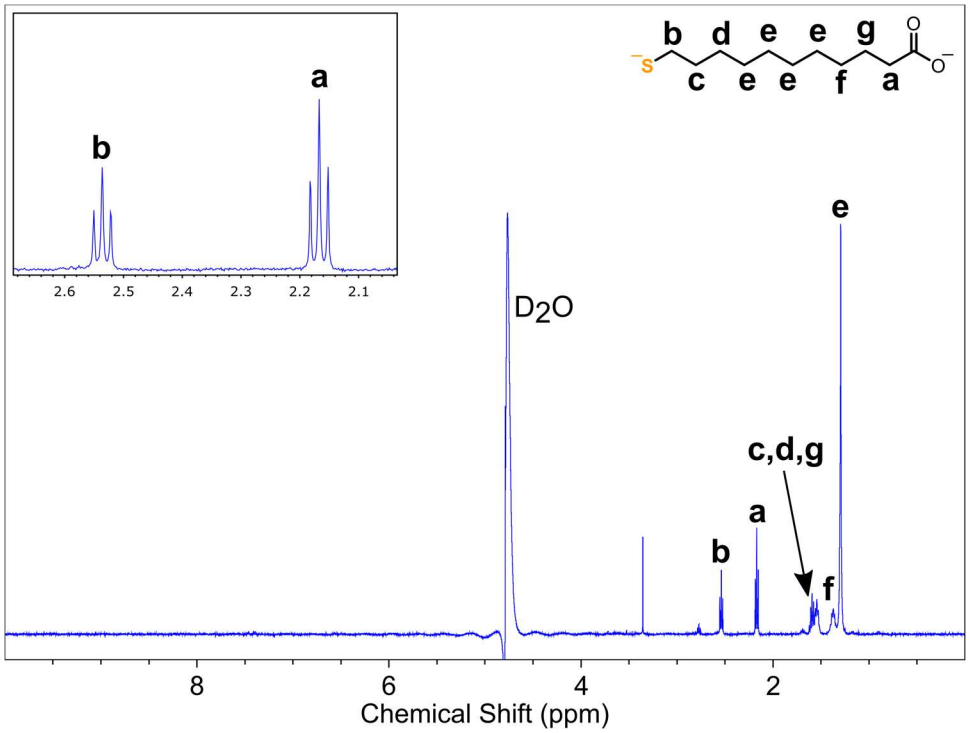

Figure 3.16 *^{1}H NMR spectrum of 11-mercaptoundecanoic acid, basified with K_2CO_3 in D_2O. Inset: magnification of 2.1-2.6 ppm region.*

Table 3.2 *Ligand populations calculated from ^1H NMR integrations relative to an internal standard: 1,4-dioxane (for NMR in D_2O) or hexamethylcyclotrisiloxane (for NMR in toluene-d_8).*

QD Type	Ligand per QD	
	AEP to Thiolate	OA to Thiolate
OA-QD	242	242
AEP-QD	951	-
MPA-QD	N/A	61
MUA-QD	37	112
DHLA-QD	347	113

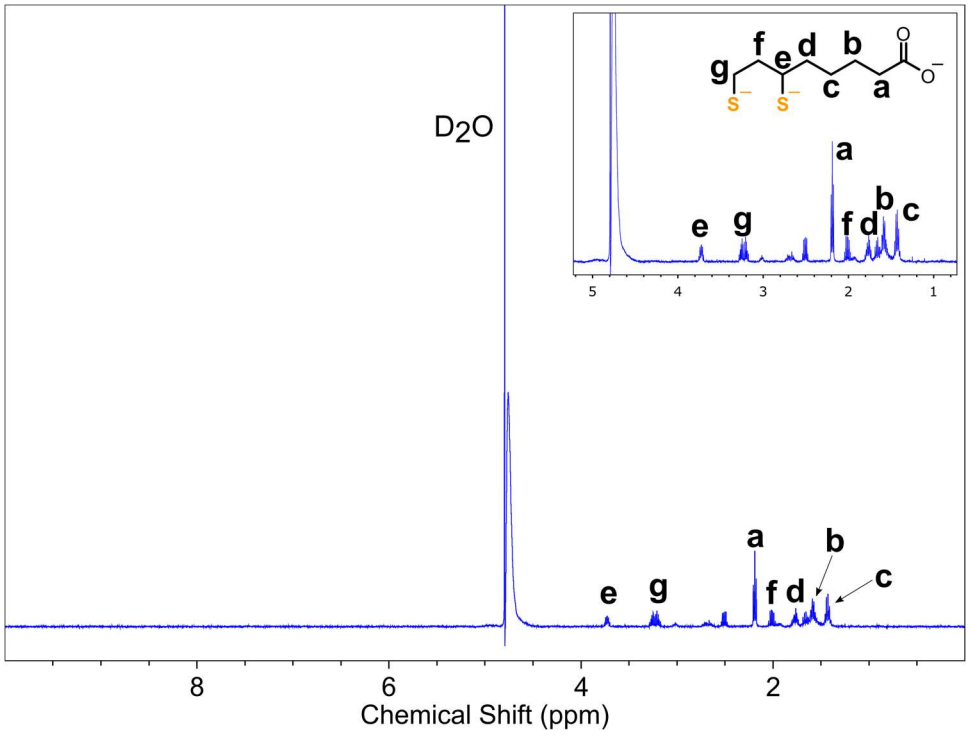

Figure 3.17 *^1H NMR spectrum of dihydrolipoic acid, basified with K_2CO_3 in D_2O. Inset: magnification of 1-5 ppm region.*

Powder X-ray Diffraction Measurements. Diffraction experiments were performed using a Bruker D8 Quest single crystal X-ray diffractometer equipped with a microfocus Mo Kα X-ray source (λ = 0.71073 Å) and a Photon II detector. Approximately 7-10 mg of CdSe cores and CdSe/ZnS QDs were purified by 1x PR into hexanes and dried under vacuum for 1 hour to obtain a viscous oil. The concentrated QD solution was loaded into a 0.81 mm ID polyimide tube and mounted in the diffractometer. A series of five phi scans (image width = 360°) were then collected with different detector orientations covering a 2θ range of 0-40° at a detector distance of 100 mm. These images were merged and integrated into a 2D powder diffraction pattern using the Bruker APEX3 software. QD powder patterns were compared to zinc blende CdSe (ICSD #41528) obtained from the Inorganic Crystal Structure Database (ICSD).

Scanning Transmission Electron Microscopy (STEM). CdSe/ZnS QDs were purified by 1x precipitation and redissolution (PR) into hexanes and drop cast onto a TEM grid (Ted Pella Inc., Type A, 400 Mesh Cu grid with Formvar and ultrathin carbon support film) and dried under vacuum for 1 hour. The samples were imaged on a JEOL 2100F 200 kV FEG-STEM/TEM. Samples were preirradiated by an electron beam shower for 15 minutes prior to imaging to polymerize hydrocarbons on the film and improve sample quality at high magnification. High angle annular dark field (HAADF) images were obtained via a Fischione model 3000 HAADF detector between 75-300 mrad. The convergence semi-angle of the probe was 17.5 mrad. Images were acquired synchronously with a 60 Hz AC electrical line frequency to minimize 60 Hz noise in the images. The average particle radius was evaluated from 795 individual particles in distinct and different areas of the TEM grid (**Figure 3.18**).

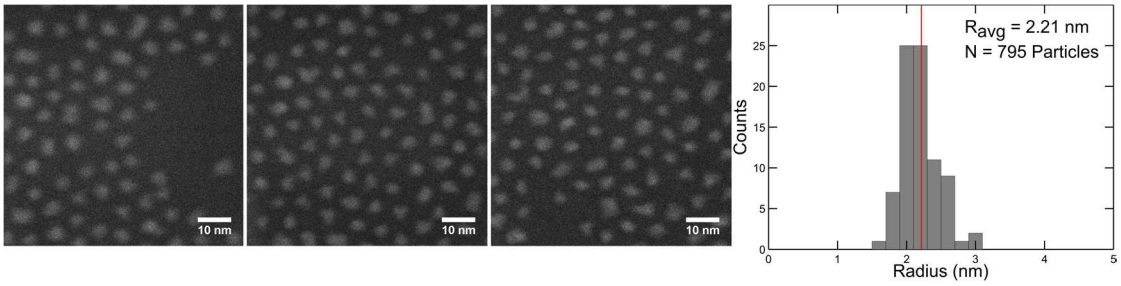

Figure 3.18 *Representative STEM images and area averaged radius histogram for the CdSe/ZnS core/shell QDs. Images were collected at distinct and different grid locations at the same magnification (2 million). Histogram shows average particle radius (red line) determined by analysis of 795 individual particles.*

Synthesis of Zinc Blende CdSe QD Cores. Oleate-capped CdSe cores were synthesized following a previously published procedure.[131] In brief, 120 mg CdO was dissolved in 660 mg oleic acid (99%) and 12 mL ODE in a three-neck round bottom flask. The mixture was degassed at 100 °C under vacuum to remove water and oxygen, then heated under N_2 to 270 °C to form cadmium oleate ($Cd(OA)_2$ as a clear and colorless solution. The reaction mixture was cooled to ~130 °C and evacuated to remove adventitious water, then heated to 270 °C under N_2. At 270 °C, 1.28 mL of a 2.2 M TOPSe precursor was rapidly injected, and the reaction mixture immediately quenched with a cool air gun. QDs were isolated from the flask with a minimal hexane rinse and stored in the dark under air. The radius of the CdSe core (1.91 nm) was determined based on an established size calibration curve by Kuno using the 1st excitonic peak position (546 nm) and quantity of the CdSe cores.[134]

Synthesis of Zinc Blende CdSe/ZnS Core/Shell QDs. Zinc blende, oleate-capped CdSe/ZnS QDs were prepared by a modification to previously reported SILAR method.[44] Our modifications were the use of zinc blende, oleate-capped CdSe cores and lower sub-monolayer equivalencies (0.533 ML/cycle). The CdSe cores were purified by 1x PR with

Acetone/MeOH into a known volume hexanes and the amount and size of the cores quantified by absorption spectroscopy and established sizing curves. The cores were diluted into a 2:1 v/v mixture of ODE/THA and degassed at 80 °C for 2 hours to remove hexanes and air. The reaction mixture was heated under N_2 to 200 °C (growth temperature). The Zn metal precursor was prepared by diluting 2.2 M $Zn(OA)_2$ in TOP with THA to a total Zn concentration of 0.1 M. The sulfur precursor was prepared by diluting $(TMS)_2S$ in TOP to a total S concentration of 0.1M. Precursors were introduced by alternating injections of the metal and chalcogenide reagents at 0.533 monolayer equivalents per cycle via a syringe pump (J-KEM Scientific Dual Syringe Pump, model 2250). Injections were performed over 3 minutes, followed by 12 minutes of equilibration time. Core/shell samples were stored at room temperature under air in the dark.

Direct Carboxylate to Thiolate Exchange. Direct exchange of carboxylates for thiolate ligands on core/shell QDs were performed via biphasic exchange. The amount/equivalents of thiolate ligand used was determined by the mole ratio of total thiolate ligand present in the active cell volume at the end of the ITC titrations to the moles QDs in the titrations. Methanolic solutions of MPA, MUA, and DHLA were prepared and basified with KOH (2:1 KOH/Thiol mole ratio). The QDs were purified by 1x PR into hexanes and the amount of QDs quantified by absorption spectroscopy. The ligand exchange was performed by adding the QD solution in hexanes to the ligand solutions in MeOH and stirring at room temperature for 3 hours in the dark. Following the exchange, the thiolate-capped QDs were centrifuged to remove poorly dispersed particles and washed with 3x 4 mL hexanes to remove displaced oleate/potassium oleate. The MeOH/hexane layers were allowed to separate before pipetting away the top hexane layer and proceeding

to the next wash, and all washes combined and saved for further analysis. After the washes, the QDs were centrifuged once more, the supernatant decanted to waste, then dried under vacuum on a Schlenk line. The dried QDs were finally dispersed in borate buffer (pH 9.18) and stored under air in a dark refrigerator.

To prepare the thiolate-capped QDs for NMR and optical analysis by removing weakly-bound or excess ligands, we performed centrifugal dialysis using Vivapsin Turbo 4 spin concentrators with a polyethersulfone membrane (50 kDa MWCO). The filters were preconditioned with DI water and borate buffer to wash the membranes prior to use with the QDs. Thiolate-capped QD samples were concentrated by 1x centrifugal filtration (5000 rpm/5 min), then diluted with borate buffer and dialyzed once. The retained QDs were diluted with borate buffer for optical measurements. For NMR, samples were further diluted with D_2O. 1,4-dioxane was used as an internal standard for aqueous NMR measurements. The ^1H NMR spectra of the thiolate-QDs after direct exchange are shown below (**Figures 3.19-3.21**).

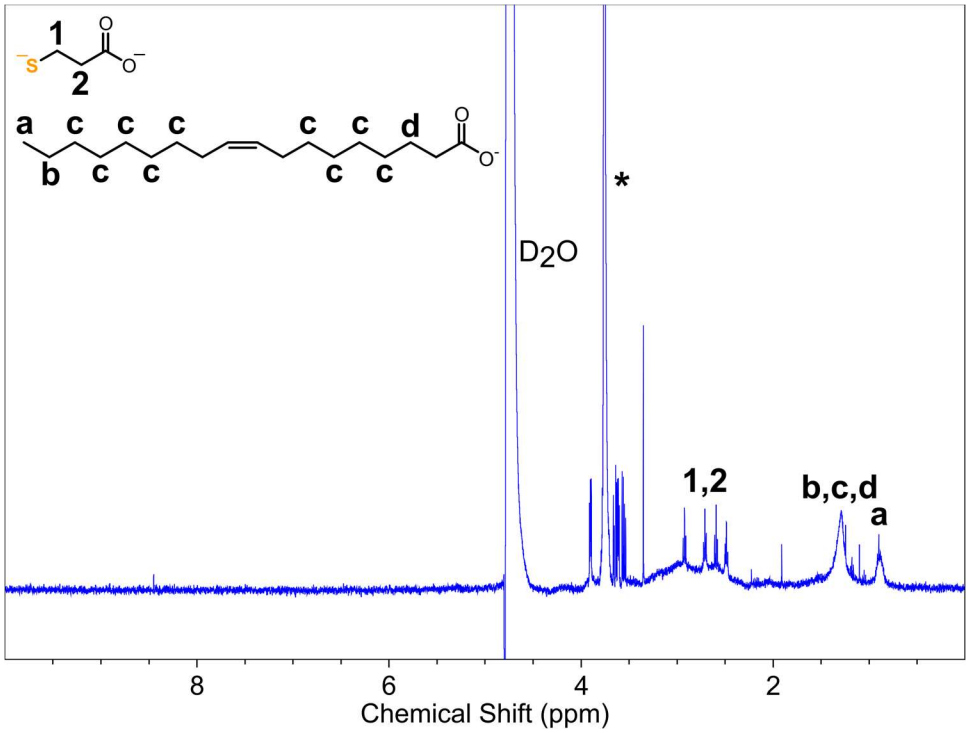

Figure 3.19 *^{1}H NMR of MPA-QDs following direct thiolate exchange in D_2O. The peak for the internal standard 1,4-dioxane is indicated by the (*).*

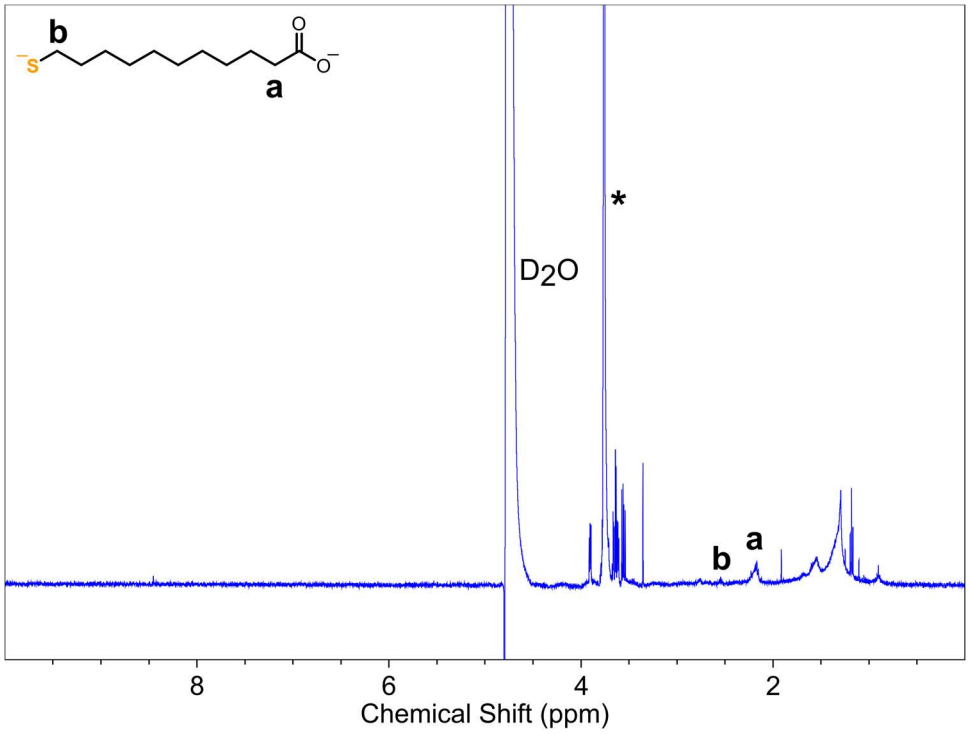

Figure 3.20 *^{1}H NMR of MUA-QDs following direct thiolate exchange in D_2O. The peak for the internal standard 1,4-dioxane is indicated by the (*).*

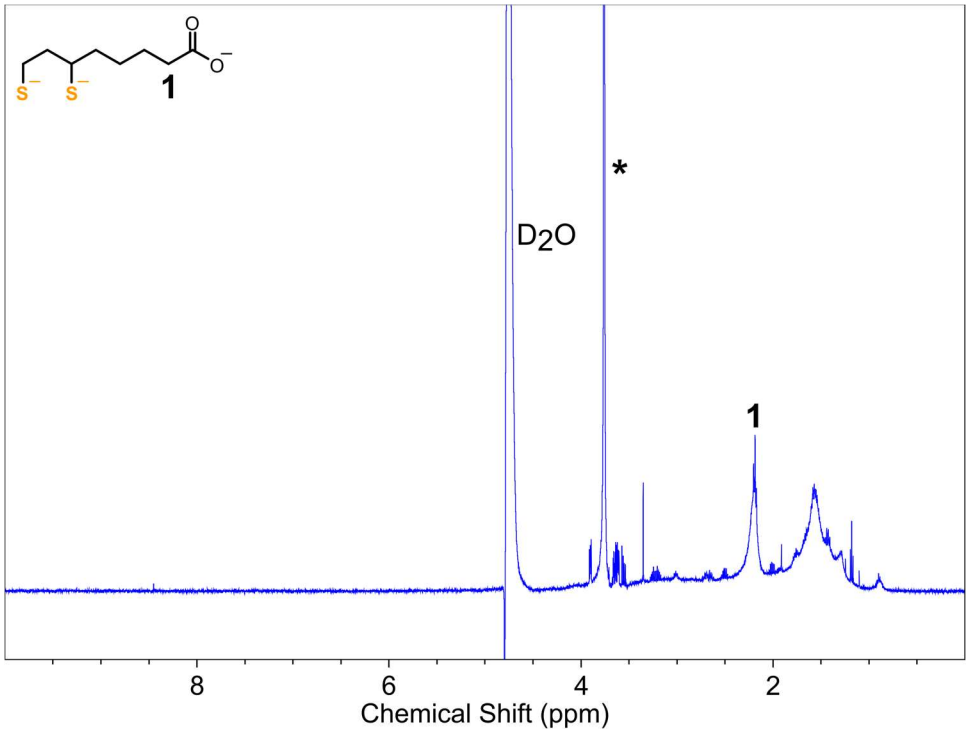

Figure 3.21 *^{1}H NMR of DHLA-QDs following direct thiolate exchange in D_2O. The peak for the internal standard 1,4-dioxane is indicated by the (*).*

Carboxylate to Phosphonate Ligand Exchange. AEP-capped QDs were prepared by biphasic ligand exchange following a modified procedure by Arcudi et al.[137] An AEP stock solution was prepared by dissolving the AEP and KOH (at a 3:1 KOH:AEP mole ratio) in MeOH to form a 0.04 M AEP solution. The QDs were purified by 1x PR into a known volume of hexanes and quantified by absorption measurements. 1100 equivalents of AEP per mole QD was injected into the QD solution, inducing flocculation and phase transfer of the QDs from hexane to methanol upon ligand exchange. The biphasic mixture was centrifuged at 9500 rpm/5 min to ensure complete separation of the hexanes and MeOH. The hexane supernatant containing impurities and excess native ligand was removed by glass pipette, then the AEP-QDs were washed three times with hexane. Each wash was performed by adding 2 mL hexane to the QDs, mixing, and

centrifuging at 9500 rpm/ 5 min to achieve phase separation before subsequent removal of the supernatant. All hexane washes were combined and saved for further analysis. After the final wash, the QDs were dried under vacuum on a Schlenk line to remove MeOH and redispersed in borate buffer.

For a parallel NMR experiment, the AEP exchange was accomplished as described above. The QDs in borate buffer were further diluted with D_2O and 1,4-dioxane (internal standard) to form an 80:20 v/v buffer/D_2O mixture. The NMR spectra for OA-QDs, AEP-QDs, and the hexane wash are shown in **Figures 3.22-3.25**.

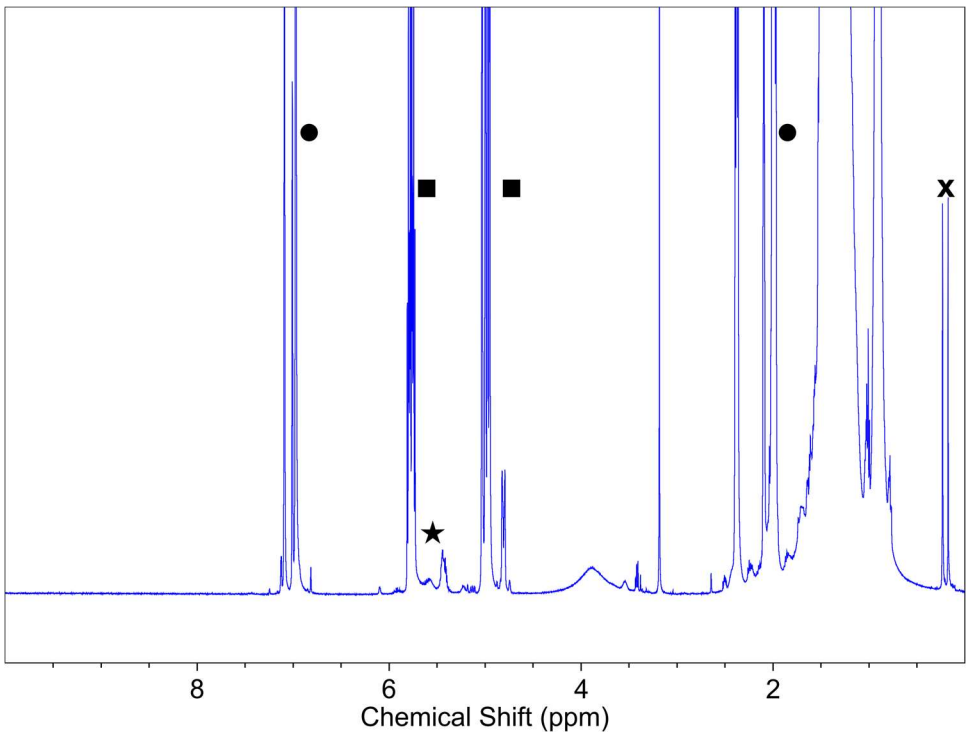

Figure 3.22 *Representative ^1H NMR spectrum of the hexane wash after AEP exchange in toluene-d_8. The peaks for the internal standard hexamethylcyclotrisiloxane (**X**), toluene (●), ODE (■), and OA (★) are indicated.*

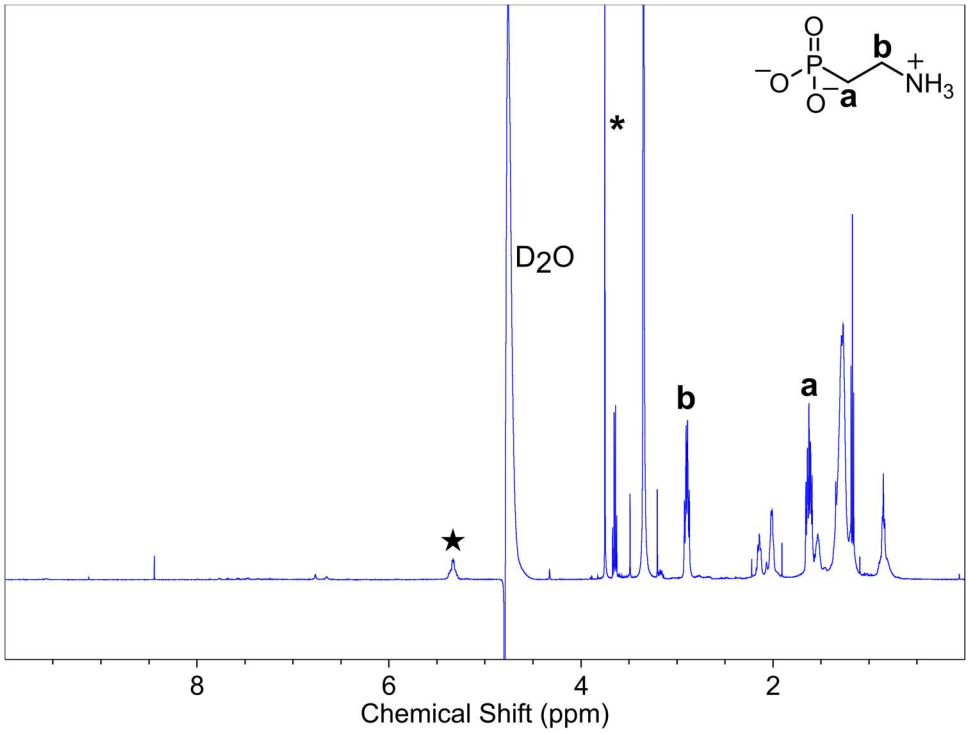

Figure 3.23 *^{1}H NMR spectrum of AEP-QDs in D_2O. The peaks for the internal standard 1,4-dioxane (*) and OA (★) are indicated.*

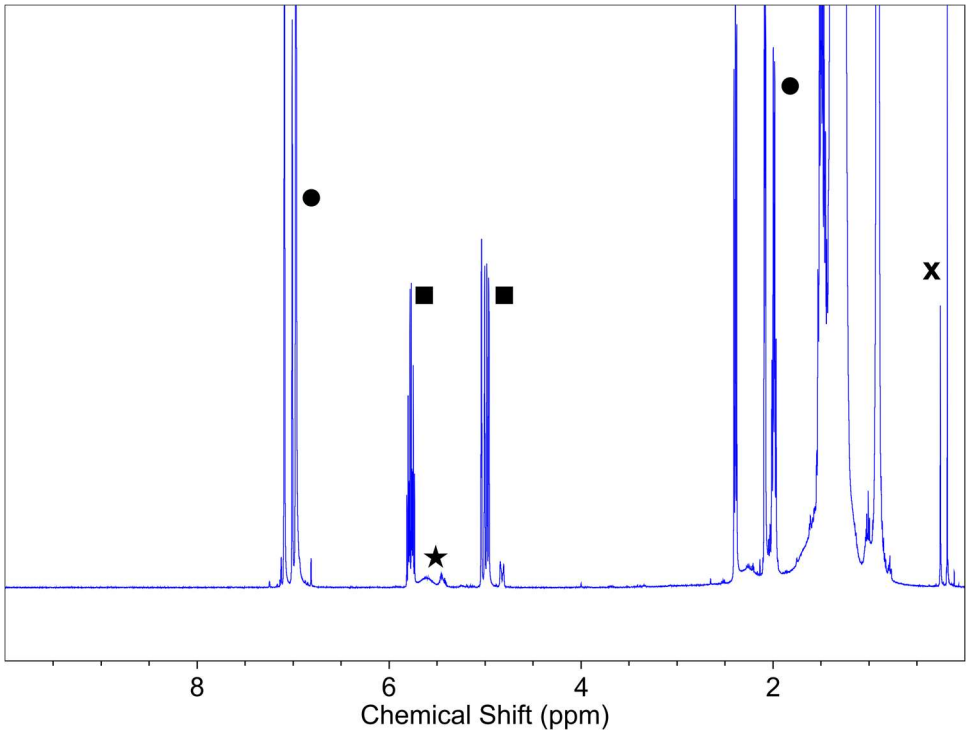

Figure 3.24 *^{1}H NMR spectrum of OA-QDs in toluene-d_8. The peaks for the internal standard hexamethylcyclotrisiloxane (**X**), toluene (●), ODE (■), and OA (★) are indicated.*

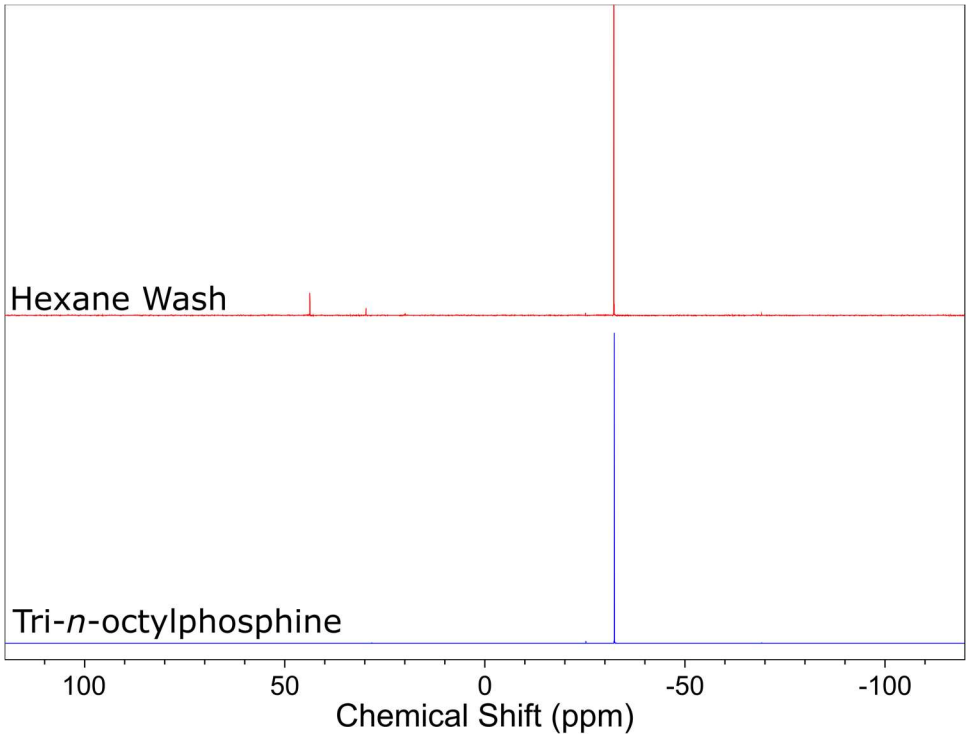

Figure 3.25 *^{31}P NMR spectrum of a representative hexane wash after AEP exchange (top) and pure tri-n-octylphosphine (bottom) in toluene-d_8.*

For the ITC experiments, the QDs were further diluted with a 6.73 mM AEP/borate buffer solution (pH 9.17) such that the nominal concentration of AEP in the QD sample was between 12-13.14 mM. The neat AEP-QDs in AEP buffer were used in the ITC titrations without further purification. The absorption of the final product after ITC was checked to observe changes in the optoelectronic properties of the QDs after ligand exchange and to evaluate the QD concentration (**Figure 3.26**).

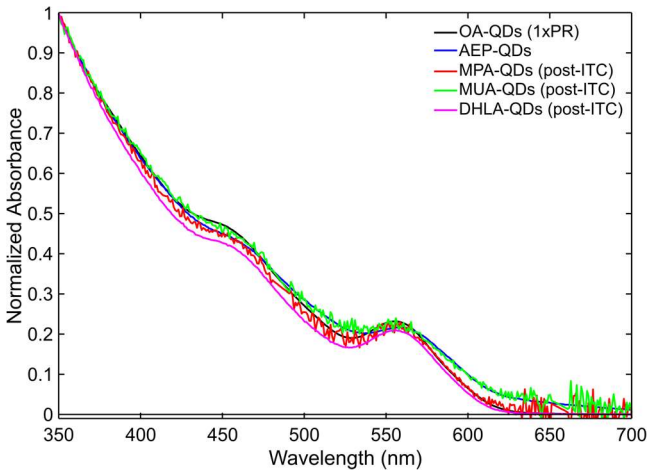

Figure 3.26 *Absorption of CdSe/ZnS QDs Pre- and Post-ITC, normalized to the absorption at 350 nm.*

Phosphonate to Thiolate Exchange for NMR. AEP-QDs were prepared as described above. Thiolate ligand stock solutions were prepared by diluting the thiol ligand in borate buffer and adjusting basifying with KOH to pH 9.15-9.18 and a nominal concentration of 5 mM. For a given exchange, the amount of thiolate ligand to introduce to the AEP-QDs was determined by the mole ratio of total thiolate ligand present in the active cell volume at the end of the ITC titrations to the moles QDs in the titrations. The thiolate ligand in borate buffer was introduced to the AEP-QDs and stirred at room temperature in the dark for 3 hours. Samples were purified by dialysis using centrifugal spin concentrators as in the direct thiolate exchanges described above. The retained thiolate-QDs were isolated and diluted with D_2O and 1,4-dioxane was included as an internal standard to form an 80:20 v/v buffer/D_2O mixture. The ligand exchange was monitored by absorption and photoluminescence spectroscopy as shown in **Figure 3.27**. The 1H and 31P NMR spectra for the ligand exchanged samples is found in **Figures 3.28-3.31**.

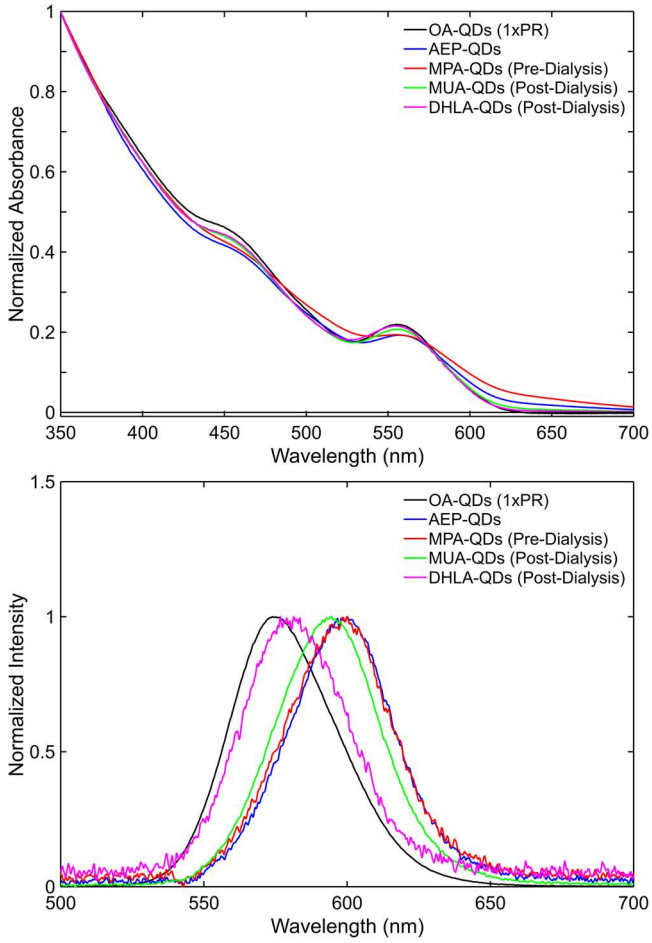

Figure 3.27 *Absorption and Emission of CdSe/ZnS QDs after ligand exchange. Absorption (top) normalized the absorption at 350 nm. Emission (bottom) normalized to the emission maximum. Thiolate-QD spectra were measured following centrifugal dialysis in borate buffer, except for the MPA-QDs, which were not robust towards centrifugal filtration.*

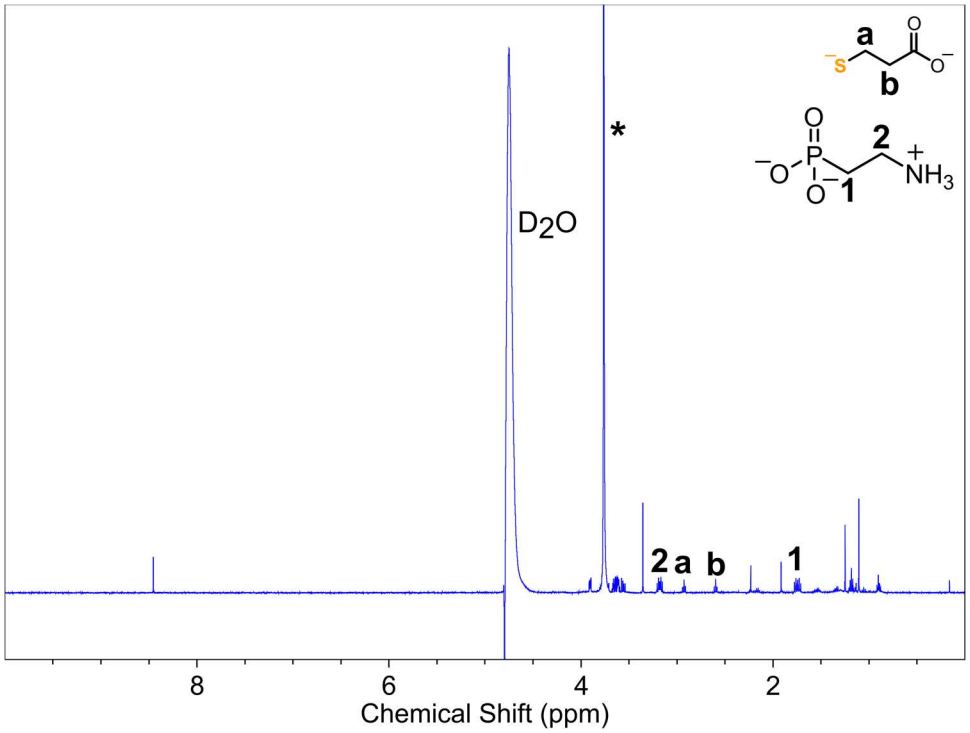

Figure 3.28 *^{1}H NMR spectrum of MPA-QDs after phosphonate-to-thiolate exchange in D_2O. The peak for the internal standard 1,4-dioxane is indicated by the (*).*

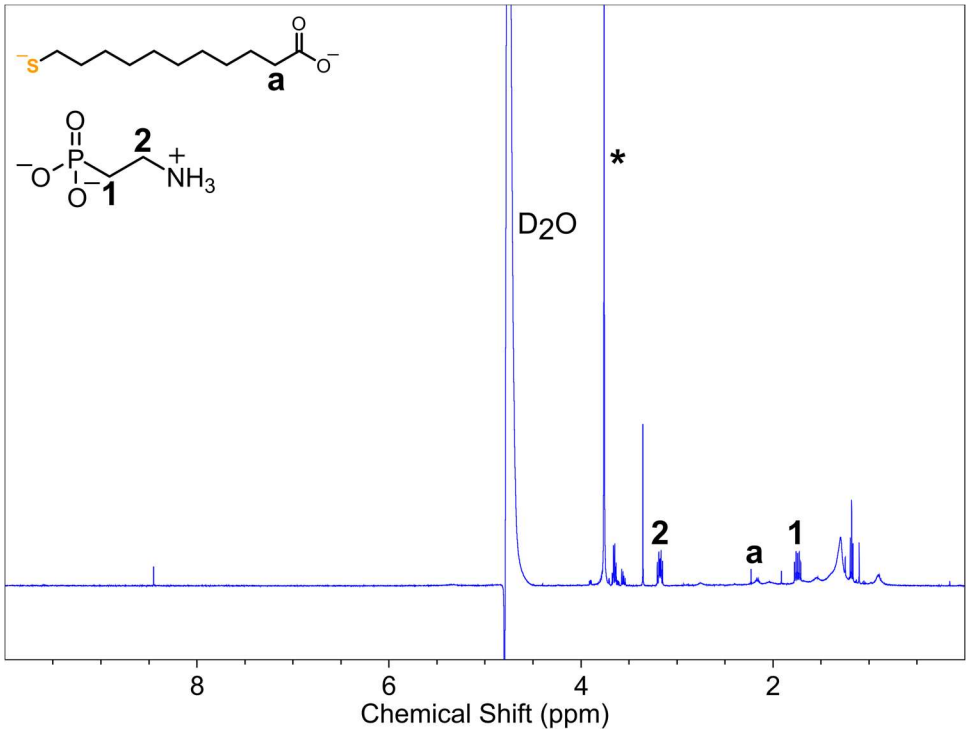

Figure 3.29 *^{1}H NMR spectrum of MUA-QDs after phosphonate-to-thiolate exchange in D_2O. The peak for the internal standard 1,4-dioxane is indicated by the (*).*

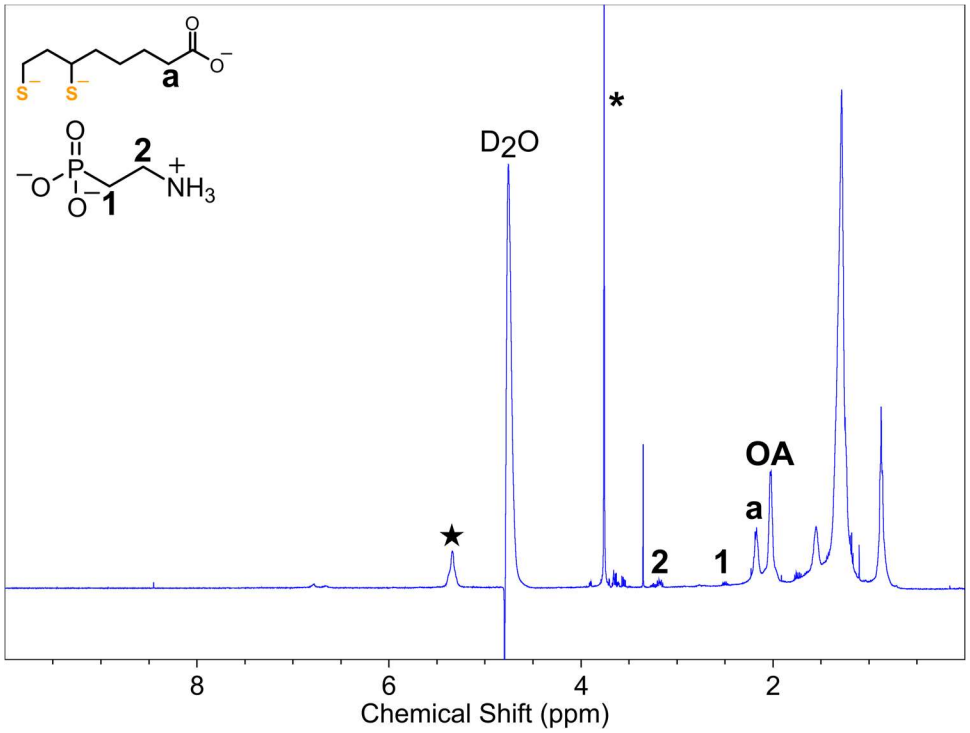

Figure 3.30 *^{1}H NMR spectrum of DHLA-QDs after phosphonate-to-thiolate exchange in D_2O. The peaks for the internal standard 1,4-dioxane (*) and OA (★) are indicated.*

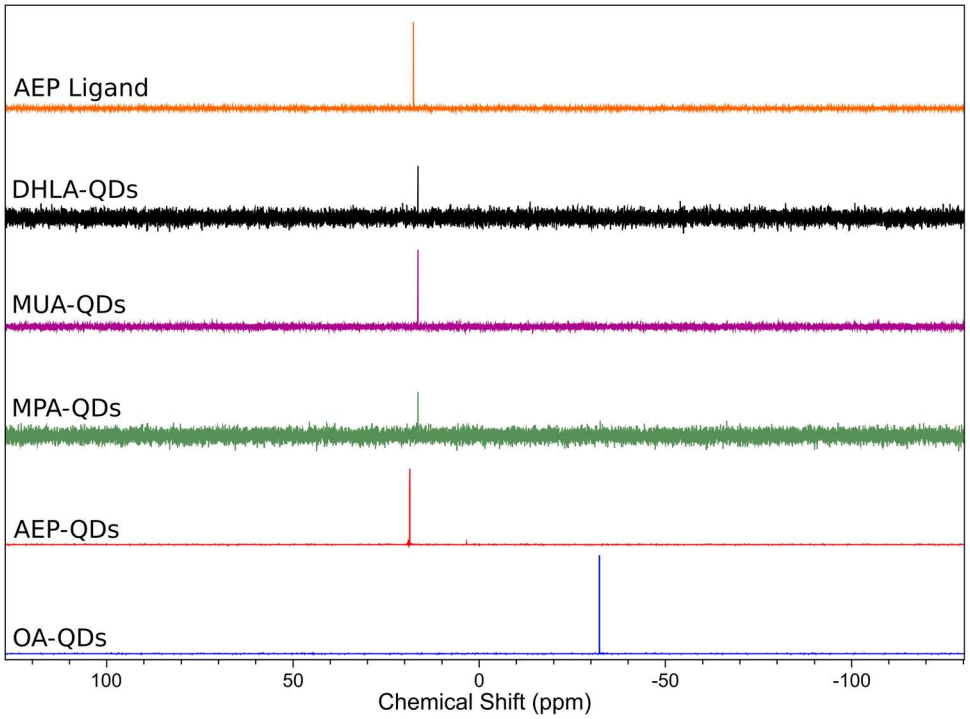

Figure 3.31 *^{31}P NMR spectra of QDs before and after AEP and thiolate exchange.*

Photoluminescence Quantum Yield (PLQY). The PLQY of the QD samples was measured relative to a rhodamine 640 perchlorate standard (R640, PLQY reported as 100% in ethanol).[140] Fluorescence spectra were measured using a Horiba Scientific FluoroMax Plus spectrofluorometer. The PLQYs for the QDs before and after ligand exchange are listed in **Table 3.3**.

Table 3.3 *Photoluminescence Quantum Yields of CdSe/ZnS QDs After Ligand Exchange. PLQY was measured relative to a rhodamine 640 perchlorate (R640) standard. *The MPA-QD PLQY could not be measured due to the poor stability of the sample and low retention after dialysis.*

	OA-QDs	AEP-QDs	*MPA-QDs	MUA-QDs	DHLA-QDs	R640
Quantum Yield (%)	96.6	4.9	N/A	17.1	1.8	100
Solvent	Hexanes	Buffer	Buffer	Buffer	Buffer	Ethanol

Isothermal Titration Calorimetry. ITC titrations were performed in a TA Instruments Affinity-ITC Low-Volume (LV) calorimeter under air at 25°C. The thiolate ligand solutions (ligand in neat borate buffer at pH 9.15-9.18) were titrated from a 250 µL syringe into a gold sample cell containing 350 µL of QDs in AEP buffer. The active cell volume of the cell was 185 µL. The power compensation required to maintain the sample cell at 25 °C (relative to a reference cell filled with an equal volume of pure DI water) was monitored over time with each injection. All experiments allowed for a midrange power variation. Each injection was followed by a 300 s interval to allow proper equilibration between ligand injections, with a total of 30 injections of 5 µL each. The cell contents were stirred continuously at 150 rpm over the course of the titration. The ligand solutions were sparged with N_2 and stored under N_2 atmosphere in the dark prior to each experiment to limit thiol oxidation. Reference titrations of neat buffer-to-buffer and thiolate ligand-to-AEP buffer were conducted under identical parameters as the ligand-to-QD titrations. The

sample cell was thoroughly cleaned with buffer or AEP buffer before each titration. Ligand-to-AEP buffer reference experiments were conducted before the ligand-to-QD runs to account for potential thiol association to the cell by saturating any possible gold sites. The raw heat thermogram were background subtracted and baseline corrected, then fit to an independent site (Langmuir) model to obtain key thermodynamic parameters (**Table 3.4**).

Table 3.4 *Thermodynamic Parameters Obtained from Thiolate Ligand Exchanges via 3-Parameter Fit.*

Thiol Exchange	N (Sites per QD)	ΔH (kJ mol^{-1})	ΔS (J mol^{-1} K^{-1})	ΔG (kJ mol^{-1})	Heat per QD (x10^{3} kJ mol^{-1})	K_{ex}
MPA to AEP-QD	83 ± 5.8	-168.5 ± 55.6	-548.6 ± 191.3	-4.9 ± 1.4	-14.2 ± 5.6	8.0 ± 4.3
MUA to AEP-QD	163 ± 24.3	-37.5 ± 2.8	-90.8 ± 10.6	-10.4 ± 0.3	-6.1 ± 0.5	66.8 ± 8.8
DHLA to AEP-QD	197 ± 14.0	-58.0 ± 5.0	-150.8 ± 19.1	-13.1 ± 0.7	-11.4 ± 0.2	200.3 ± 52.4

REFERENCES

(1) Boles, M. A.; Ling, D.; Hyeon, T.; Talapin, D. V. The Surface Science of Nanocrystals. *Nat Mater* **2016**, *15* (2), 141–153. https://doi.org/10.1038/nmat4526.

(2) O'Brien, M. N.; Jones, M. R.; Mirkin, C. A. The Nature and Implications of Uniformity in the Hierarchical Organization of Nanomaterials. *PNAS* **2016**, *113* (42), 11717–11725. https://doi.org/10.1073/pnas.1605289113.

(3) Parak, W. J.; Manna, L.; Nann, T. Fundamental Principles of Quantum Dots. In *Nanotechnology*; American Cancer Society, 2010; pp 73–96. https://doi.org/10.1002/9783527628155.nanotech004.

(4) Arquer, F. P. G. de; Talapin, D. V.; Klimov, V. I.; Arakawa, Y.; Bayer, M.; Sargent, E. H. Semiconductor Quantum Dots: Technological Progress and Future Challenges. *Science* **2021**, *373* (6555). https://doi.org/10.1126/science.aaz8541.

(5) Murray, C. B.; Norris, D. J.; Bawendi, M. G. Synthesis and Characterization of Nearly Monodisperse CdE (E = Sulfur, Selenium, Tellurium) Semiconductor Nanocrystallites. *J. Am. Chem. Soc.* **1993**, *115* (19), 8706–8715. https://doi.org/10.1021/ja00072a025.

(6) Abe, S.; Capek, R. K.; De Geyter, B.; Hens, Z. Reaction Chemistry/Nanocrystal Property Relations in the Hot Injection Synthesis, the Role of the Solute Solubility. *ACS Nano* **2013**, *7* (2), 943–949. https://doi.org/10.1021/nn3059168.

(7) Eagle, F. W.; Park, N.; Cash, M.; Cossairt, B. M. Surface Chemistry and Quantum Dot Luminescence: Shell Growth, Atomistic Modification, and Beyond. *ACS Energy Lett.* **2021**, *6* (3), 977–984. https://doi.org/10.1021/acsenergylett.0c02697.

(8) Flamee, S.; Cirillo, M.; Abe, S.; De Nolf, K.; Gomes, R.; Aubert, T.; Hens, Z. Fast, High Yield, and High Solid Loading Synthesis of Metal Selenide Nanocrystals. *Chem. Mater.* **2013**, *25* (12), 2476–2483. https://doi.org/10.1021/cm400799e.

(9) Hines, M. a.; Scholes, G. d. Colloidal PbS Nanocrystals with Size-Tunable Near-Infrared Emission: Observation of Post-Synthesis Self-Narrowing of the Particle

Size Distribution. *Adv. Mater.* **2003**, *15* (21), 1844–1849. https://doi.org/10.1002/adma.200305395.

(10) Moreels, I.; Justo, Y.; De Geyter, B.; Haustraete, K.; Martins, J. C.; Hens, Z. Size-Tunable, Bright, and Stable PbS Quantum Dots: A Surface Chemistry Study. *ACS Nano* **2011**, *5* (3), 2004–2012. https://doi.org/10.1021/nn103050w.

(11) Jing, L.; Kershaw, S. V.; Li, Y.; Huang, X.; Li, Y.; Rogach, A. L.; Gao, M. Aqueous Based Semiconductor Nanocrystals. *Chem. Rev.* **2016**, *116* (18), 10623–10730. https://doi.org/10.1021/acs.chemrev.6b00041.

(12) Yu, W. W.; Peng, X. Formation of High-Quality CdS and Other II–VI Semiconductor Nanocrystals in Noncoordinating Solvents: Tunable Reactivity of Monomers. *Angewandte Chemie International Edition* **2002**, *41* (13), 2368–2371. https://doi.org/10.1002/1521-3773(20020703)41:13<2368::AID-ANIE2368>3.0.CO;2-G.

(13) Dhaene, E.; Billet, J.; Bennett, E.; Van Driessche, I.; De Roo, J. The Trouble with ODE: Polymerization during Nanocrystal Synthesis. *Nano Lett.* **2019**, *19* (10), 7411–7417. https://doi.org/10.1021/acs.nanolett.9b03088.

(14) García-Rodríguez, R.; Hendricks, M. P.; Cossairt, B. M.; Liu, H.; Owen, J. S. Conversion Reactions of Cadmium Chalcogenide Nanocrystal Precursors. *Chem. Mater.* **2013**, *25* (8), 1233–1249. https://doi.org/10.1021/cm3035642.

(15) Mer, V. K. L. Nucleation in Phase Transitions. *Ind. Eng. Chem.* **1952**, *44* (6), 1270–1277. https://doi.org/10.1021/ie50510a027.

(16) LaMer, V. K.; Dinegar, R. H. Theory, Production and Mechanism of Formation of Monodispersed Hydrosols. *J. Am. Chem. Soc.* **1950**, *72* (11), 4847–4854. https://doi.org/10.1021/ja01167a001.

(17) Zhang, J.; Crisp, R. W.; Gao, J.; Kroupa, D. M.; Beard, M. C.; Luther, J. M. Synthetic Conditions for High-Accuracy Size Control of PbS Quantum Dots. *J. Phys. Chem. Lett.* **2015**, *6* (10), 1830–1833. https://doi.org/10.1021/acs.jpclett.5b00689.

(18) Hamachi, L. S.; Jen-La Plante, I.; Coryell, A. C.; De Roo, J.; Owen, J. S. Kinetic Control over CdS Nanocrystal Nucleation Using a Library of Thiocarbonates,

Thiocarbamates, and Thioureas. *Chem. Mater.* **2017**, *29* (20), 8711–8719. https://doi.org/10.1021/acs.chemmater.7b02861.

(19) Campos, M. P.; Hendricks, M. P.; Beecher, A. N.; Walravens, W.; Swain, R. A.; Cleveland, G. T.; Hens, Z.; Sfeir, M. Y.; Owen, J. S. A Library of Selenourea Precursors to PbSe Nanocrystals with Size Distributions near the Homogeneous Limit. *J. Am. Chem. Soc.* **2017**, *139* (6), 2296–2305. https://doi.org/10.1021/jacs.6b11021.

(20) Chu, D. B. K.; Owen, J. S.; Peters, B. Nucleation and Growth Kinetics from LaMer Burst Data. *J. Phys. Chem. A* **2017**, *121* (40), 7511–7517. https://doi.org/10.1021/acs.jpca.7b08368.

(21) Hendricks, M. P.; Campos, M. P.; Cleveland, G. T.; Plante, I. J.-L.; Owen, J. S. A Tunable Library of Substituted Thiourea Precursors to Metal Sulfide Nanocrystals. *Science* **2015**, *348* (6240), 1226–1230. https://doi.org/10.1126/science.aaa2951.

(22) Clark, M. D.; Kumar, S. K.; Owen, J. S.; Chan, E. M. Focusing Nanocrystal Size Distributions via Production Control. *Nano Lett.* **2011**, *11* (5), 1976–1980. https://doi.org/10.1021/nl200286j.

(23) Owen, J. S.; Chan, E. M.; Liu, H.; Alivisatos, A. P. Precursor Conversion Kinetics and the Nucleation of Cadmium Selenide Nanocrystals. *J. Am. Chem. Soc.* **2010**, *132* (51), 18206–18213. https://doi.org/10.1021/ja106777j.

(24) Sugimoto, T. Underlying Mechanisms in Size Control of Uniform Nanoparticles. *Journal of Colloid and Interface Science* **2007**, *309* (1), 106–118. https://doi.org/10.1016/j.jcis.2007.01.036.

(25) Cossairt, B. M. Shining Light on Indium Phosphide Quantum Dots: Understanding the Interplay among Precursor Conversion, Nucleation, and Growth. *Chem. Mater.* **2016**, *28* (20), 7181–7189. https://doi.org/10.1021/acs.chemmater.6b03408.

(26) McMurtry, B. M.; Qian, K.; Teglasi, J. K.; Swarnakar, A. K.; De Roo, J.; Owen, J. S. Continuous Nucleation and Size Dependent Growth Kinetics of Indium Phosphide Nanocrystals. *Chem. Mater.* **2020**, *32* (10), 4358–4368. https://doi.org/10.1021/acs.chemmater.0c01561.

(27) Whitehead, C. B.; Özkar, S.; Finke, R. G. LaMer's 1950 Model of Particle Formation: A Review and Critical Analysis of Its Classical Nucleation and

Fluctuation Theory Basis, of Competing Models and Mechanisms for Phase-Changes and Particle Formation, and Then of Its Application to Silver Halide, Semiconductor, Metal, and Metal-Oxide Nanoparticles. *Mater. Adv.* **2021**, *2* (1), 186–235. https://doi.org/10.1039/D0MA00439A.

(28) Reiss, P.; Protière, M.; Li, L. Core/Shell Semiconductor Nanocrystals. *Small* **2009**, *5* (2), 154–168. https://doi.org/10.1002/smll.200800841.

(29) Bodunov, E. N.; Gamboa, A. L. S. Photoluminescence Decay of Colloidal Quantum Dots: Reversible Trapping and the Nature of the Relevant Trap States. *J. Phys. Chem. C* **2019**, *123* (41), 25515–25523. https://doi.org/10.1021/acs.jpcc.9b07619.

(30) Greytak, A. B.; Allen, P. M.; Liu, W.; Zhao, J.; Young, E. R.; Popović, Z.; Walker, B. J.; Nocera, D. G.; Bawendi, M. G. Alternating Layer Addition Approach to CdSe/CdS Core/Shell Quantum Dots with near-Unity Quantum Yield and High on-Time Fractions. *Chem. Sci.* **2012**, *3* (6), 2028–2034. https://doi.org/10.1039/C2SC00561A.

(31) Tan, R.; Shen, Y.; Roberts, S. K.; Gee, M. Y.; Blom, D. A.; Greytak, A. B. Reducing Competition by Coordinating Solvent Promotes Morphological Control in Alternating Layer Growth of CdSe/CdS Core/Shell Quantum Dots. *Chem. Mater.* **2015**, *27* (21), 7468–7480. https://doi.org/10.1021/acs.chemmater.5b03588.

(32) Ji, B.; Koley, S.; Slobodkin, I.; Remennik, S.; Banin, U. ZnSe/ZnS Core/Shell Quantum Dots with Superior Optical Properties through Thermodynamic Shell Growth. *Nano Lett.* **2020**, *20* (4), 2387–2395. https://doi.org/10.1021/acs.nanolett.9b05020.

(33) Toufanian, R.; Piryatinski, A.; Mahler, A. H.; Iyer, R.; Hollingsworth, J. A.; Dennis, A. M. Bandgap Engineering of Indium Phosphide-Based Core/Shell Heterostructures Through Shell Composition and Thickness. *Front. Chem.* **2018**, *6*. https://doi.org/10.3389/fchem.2018.00567.

(34) Gong, K.; Kelley, D. F. A Predictive Model of Shell Morphology in CdSe/CdS Core/Shell Quantum Dots. *J. Chem. Phys.* **2014**, *141* (19), 194704. https://doi.org/10.1063/1.4901428.

(35) Drijvers, E.; De Roo, J.; Geiregat, P.; Fehér, K.; Hens, Z.; Aubert, T. Revisited Wurtzite CdSe Synthesis: A Gateway for the Versatile Flash Synthesis of Multishell Quantum Dots and Rods. *Chem. Mater.* **2016**, *28* (20), 7311–7323. https://doi.org/10.1021/acs.chemmater.6b02666.

(36) Shen, Y.; Tan, R.; Gee, M. Y.; Greytak, A. B. Quantum Yield Regeneration: Influence of Neutral Ligand Binding on Photophysical Properties in Colloidal Core/Shell Quantum Dots. *ACS Nano* **2015**, *9* (3), 3345–3359. https://doi.org/10.1021/acsnano.5b00671.

(37) Xie, R.; Kolb, U.; Li, J.; Basché, T.; Mews, A. Synthesis and Characterization of Highly Luminescent CdSe−Core CdS/Zn0.5Cd0.5S/ZnS Multishell Nanocrystals. *J. Am. Chem. Soc.* **2005**, *127* (20), 7480–7488. https://doi.org/10.1021/ja042939g.

(38) Pu, C.; Dai, X.; Shu, Y.; Zhu, M.; Deng, Y.; Jin, Y.; Peng, X. Electrochemically-Stable Ligands Bridge the Photoluminescence-Electroluminescence Gap of Quantum Dots. *Nature Communications* **2020**, *11* (1), 1–10. https://doi.org/10.1038/s41467-020-14756-5.

(39) Cao, W.; Chern, M.; Dennis, A. M.; Brown, K. A. Measuring Nanoparticle Polarizability Using Fluorescence Microscopy. *Nano Lett.* **2019**, *19* (8), 5762–5768. https://doi.org/10.1021/acs.nanolett.9b02402.

(40) Chen, O.; Zhao, J.; Chauhan, V. P.; Cui, J.; Wong, C.; Harris, D. K.; Wei, H.; Han, H.-S.; Fukumura, D.; Jain, R. K.; Bawendi, M. G. Compact High-Quality CdSe–CdS Core–Shell Nanocrystals with Narrow Emission Linewidths and Suppressed Blinking. *Nat Mater* **2013**, *12* (5), 445–451. https://doi.org/10.1038/nmat3539.

(41) Li, J. J.; Wang, Y. A.; Guo, W.; Keay, J. C.; Mishima, T. D.; Johnson, M. B.; Peng, X. Large-Scale Synthesis of Nearly Monodisperse CdSe/CdS Core/Shell Nanocrystals Using Air-Stable Reagents via Successive Ion Layer Adsorption and Reaction. *J. Am. Chem. Soc.* **2003**, *125* (41), 12567–12575. https://doi.org/10.1021/ja0363563.

(42) Nicolau, Y. F. Solution Deposition of Thin Solid Compound Films by a Successive Ionic-Layer Adsorption and Reaction Process. *Applications of Surface Science* **1985**, *22–23*, 1061–1074. https://doi.org/10.1016/0378-5963(85)90241-7.

(43) *Anisotropic and Shape-Selective Nanomaterials: Structure-Property Relationships*, 1st ed. 2017 edition.; Murph, S. E. H., Larsen, G. K., Coopersmith, K. J., Eds.; Springer, 2017.

(44) Tan, R.; Blom, D. A.; Ma, S.; Greytak, A. B. Probing Surface Saturation Conditions in Alternating Layer Growth of CdSe/CdS Core/Shell Quantum Dots. *Chem. Mater.* **2013**, *25* (18), 3724–3736. https://doi.org/10.1021/cm402148s.

(45) Liu, H.; Owen, J. S.; Alivisatos, A. P. Mechanistic Study of Precursor Evolution in Colloidal Group II−VI Semiconductor Nanocrystal Synthesis. *J. Am. Chem. Soc.* **2007**, *129* (2), 305–312. https://doi.org/10.1021/ja0656696.

(46) Morris-Cohen, A. J.; Malicki, M.; Peterson, M. D.; Slavin, J. W. J.; Weiss, E. A. Chemical, Structural, and Quantitative Analysis of the Ligand Shells of Colloidal Quantum Dots. *Chem. Mater.* **2013**, *25* (8), 1155–1165. https://doi.org/10.1021/cm302108j.

(47) Shen, Y.; Gee, M. Y.; Greytak, A. B. Purification Technologies for Colloidal Nanocrystals. *Chem. Commun.* **2017**, *53* (5), 827–841. https://doi.org/10.1039/C6CC07998A.

(48) Smith, A. M.; Mohs, A. M.; Nie, S. Tuning the Optical and Electronic Properties of Colloidal Nanocrystals by Lattice Strain. *Nature Nanotech* **2009**, *4* (1), 56–63. https://doi.org/10.1038/nnano.2008.360.

(49) Sperling, R. A.; Pellegrino, T.; Li, J. K.; Chang, W. H.; Parak, W. J. Electrophoretic Separation of Nanoparticles with a Discrete Number of Functional Groups. *Advanced Functional Materials* **2006**, *16* (7), 943–948. https://doi.org/10.1002/adfm.200500589.

(50) Shen, Y.; Gee, M. Y.; Tan, R.; Pellechia, P. J.; Greytak, A. B. Purification of Quantum Dots by Gel Permeation Chromatography and the Effect of Excess Ligands on Shell Growth and Ligand Exchange. *Chem. Mater.* **2013**, *25* (14), 2838–2848. https://doi.org/10.1021/cm4012734.

(51) Weir, M. P.; Toolan, D. T. W.; Kilbride, R. C.; Penfold, N. J. W.; Washington, A. L.; King, S. M.; Xiao, J.; Zhang, Z.; Gray, V.; Dowland, S.; Winkel, J.; Greenham, N. C.; Friend, R. H.; Rao, A.; Ryan, A. J.; Jones, R. A. L. Ligand Shell Structure in Lead Sulfide–Oleic Acid Colloidal Quantum Dots Revealed by Small-Angle

Scattering. *J. Phys. Chem. Lett.* **2019**, *10* (16), 4713–4719. https://doi.org/10.1021/acs.jpclett.9b01008.

(52) Hassinen, A.; Moreels, I.; De Nolf, K.; Smet, P. F.; Martins, J. C.; Hens, Z. Short-Chain Alcohols Strip X-Type Ligands and Quench the Luminescence of PbSe and CdSe Quantum Dots, Acetonitrile Does Not. *J. Am. Chem. Soc.* **2012**, *134* (51), 20705–20712. https://doi.org/10.1021/ja308861d.

(53) Shen, Y.; Roberge, A.; Tan, R.; Gee, M. Y.; Gary, D. C.; Huang, Y.; Blom, D. A.; Benicewicz, B. C.; Cossairt, B. M.; Greytak, A. B. Gel Permeation Chromatography as a Multifunctional Processor for Nanocrystal Purification and On-Column Ligand Exchange Chemistry. *Chem. Sci.* **2016**, *7* (9), 5671–5679. https://doi.org/10.1039/C6SC01301E.

(54) Roberge, A.; Stein, J. L.; Shen, Y.; Cossairt, B. M.; Greytak, A. B. Purification and In Situ Ligand Exchange of Metal-Carboxylate-Treated Fluorescent InP Quantum Dots via Gel Permeation Chromatography. *J. Phys. Chem. Lett.* **2017**, *8* (17), 4055–4060. https://doi.org/10.1021/acs.jpclett.7b01772.

(55) Roberge, A.; Dunlap, J. H.; Ahmed, F.; Greytak, A. B. Size-Dependent PbS Quantum Dot Surface Chemistry Investigated via Gel Permeation Chromatography. *Chem. Mater.* **2020**, *32* (15), 6588–6594. https://doi.org/10.1021/acs.chemmater.0c02024.

(56) Abiodun, S. L.; Pellechia, P. J.; Greytak, A. B. Effective Purification of CsPbBr3 Nanocrystals with High Quantum Yield and High Colloidal Stability via Gel Permeation Chromatography. *J. Phys. Chem. C* **2021**, *125* (6), 3463–3471. https://doi.org/10.1021/acs.jpcc.1c00207.

(57) Ahmed, F.; Dunlap, J. H.; Pellechia, P. J.; Greytak, A. B. A P-Type PbS Quantum Dot Ink with Improved Stability for Solution Processable Optoelectronics. *Chem. Commun.* **2021**, *57* (65), 8091–8094. https://doi.org/10.1039/D1CC03014K.

(58) Ostermann, J.; Schmidtke, C.; Wolter, C.; Merkl, J.-P.; Kloust, H.; Weller, H. Tailoring the Ligand Shell for the Control of Cellular Uptake and Optical Properties of Nanocrystals. *Beilstein J Nanotechnol* **2015**, *6*, 232–242. https://doi.org/10.3762/bjnano.6.22.

(59) Wagner, A. M.; Knipe, J. M.; Orive, G.; Peppas, N. A. Quantum Dots in Biomedical Applications. *Acta Biomaterialia* **2019**, *94*, 44–63. https://doi.org/10.1016/j.actbio.2019.05.022.

(60) McClelland, K. P.; Clemons, T. D.; Stupp, S. I.; Weiss, E. A. Semiconductor Quantum Dots Are Efficient and Recyclable Photocatalysts for Aqueous PET-RAFT Polymerization. *ACS Macro Lett.* **2020**, *9* (1), 7–13. https://doi.org/10.1021/acsmacrolett.9b00891.

(61) Susumu, K.; Uyeda, H. T.; Medintz, I. L.; Pons, T.; Delehanty, J. B.; Mattoussi, H. Enhancing the Stability and Biological Functionalities of Quantum Dots via Compact Multifunctional Ligands. *J. Am. Chem. Soc.* **2007**, *129* (45), 13987–13996. https://doi.org/10.1021/ja0749744.

(62) Anderson, N. C.; Hendricks, M. P.; Choi, J. J.; Owen, J. S. Ligand Exchange and the Stoichiometry of Metal Chalcogenide Nanocrystals: Spectroscopic Observation of Facile Metal-Carboxylate Displacement and Binding. *J. Am. Chem. Soc.* **2013**, *135* (49), 18536–18548. https://doi.org/10.1021/ja4086758.

(63) Roo, J. D.; Keukeleere, K. D.; Hens, Z.; Driessche, I. V. From Ligands to Binding Motifs and beyond; the Enhanced Versatility of Nanocrystal Surfaces. *Dalton Trans.* **2016**, *45* (34), 13277–13283. https://doi.org/10.1039/C6DT02410F.

(64) Owen, J. S.; Park, J.; Trudeau, P.-E.; Alivisatos, A. P. Reaction Chemistry and Ligand Exchange at Cadmium−Selenide Nanocrystal Surfaces. *J. Am. Chem. Soc.* **2008**, *130* (37), 12279–12281. https://doi.org/10.1021/ja804414f.

(65) Cass, L. C.; Malicki, M.; Weiss, E. A. The Chemical Environments of Oleate Species within Samples of Oleate-Coated PbS Quantum Dots. *Anal. Chem.* **2013**, *85* (14), 6974–6979. https://doi.org/10.1021/ac401623a.

(66) Knauf, R. R.; Lennox, J. C.; Dempsey, J. L. Quantifying Ligand Exchange Reactions at CdSe Nanocrystal Surfaces. *Chem. Mater.* **2016**, *28* (13), 4762–4770. https://doi.org/10.1021/acs.chemmater.6b01827.

(67) Green, M. L. H. A New Approach to the Formal Classification of Covalent Compounds of the Elements. *Journal of Organometallic Chemistry* **1995**, *500* (1), 127–148. https://doi.org/10.1016/0022-328X(95)00508-N.

(68) Green, M. The Nature of Quantum Dot Capping Ligands. *J. Mater. Chem.* **2010**, *20* (28), 5797–5809. https://doi.org/10.1039/C0JM00007H.

(69) Owen, J. The Coordination Chemistry of Nanocrystal Surfaces. *Science* **2015**, *347* (6222), 615–616. https://doi.org/10.1126/science.1259924.

(70) Turo, M. J.; Shen, X.; Brandon, N. K.; Castillo, S.; Fall, A. M.; Pantelides, S. T.; Macdonald, J. E. Dual-Mode Crystal-Bound and X-Type Passivation of Quantum Dots. *Chem. Commun.* **2016**, *52* (82), 12214–12217. https://doi.org/10.1039/C6CC05951A.

(71) Krause, M. M.; Jethi, L.; Mack, T. G.; Kambhampati, P. Ligand Surface Chemistry Dictates Light Emission from Nanocrystals. *J. Phys. Chem. Lett.* **2015**, *6* (21), 4292–4296. https://doi.org/10.1021/acs.jpclett.5b02015.

(72) Williams, E. S.; Major, K. J.; Tobias, A.; Woodall, D.; Morales, V.; Lippincott, C.; Moyer, P. J.; Jones, M. Characterizing the Influence of TOPO on Exciton Recombination Dynamics in Colloidal CdSe Quantum Dots. *J. Phys. Chem. C* **2013**, *117* (8), 4227–4237. https://doi.org/10.1021/jp309896e.

(73) Anderson, N. C.; Owen, J. S. Soluble, Chloride-Terminated CdSe Nanocrystals: Ligand Exchange Monitored by 1H and 31P NMR Spectroscopy. *Chem. Mater.* **2013**, *25* (1), 69–76. https://doi.org/10.1021/cm303219a.

(74) Anderson, N. C.; Chen, Peter. E.; Buckley, A. K.; De Roo, J.; Owen, J. S. Stereoelectronic Effects on the Binding of Neutral Lewis Bases to CdSe Nanocrystals. *J. Am. Chem. Soc.* **2018**, *140* (23), 7199–7205. https://doi.org/10.1021/jacs.8b02927.

(75) Jasieniak, J.; Mulvaney, P. From Cd-Rich to Se-Rich − the Manipulation of CdSe Nanocrystal Surface Stoichiometry. *J. Am. Chem. Soc.* **2007**, *129* (10), 2841–2848. https://doi.org/10.1021/ja066205a.

(76) Kirkwood, N.; Monchen, J. O. V.; Crisp, R. W.; Grimaldi, G.; Bergstein, H. A. C.; du Fossé, I.; van der Stam, W.; Infante, I.; Houtepen, A. J. Finding and Fixing Traps in II–VI and III–V Colloidal Quantum Dots: The Importance of Z-Type Ligand Passivation. *J. Am. Chem. Soc.* **2018**, *140* (46), 15712–15723. https://doi.org/10.1021/jacs.8b07783.

(77) Zherebetskyy, D.; Scheele, M.; Zhang, Y.; Bronstein, N.; Thompson, C.; Britt, D.; Salmeron, M.; Alivisatos, P.; Wang, L.-W. Hydroxylation of the Surface of PbS Nanocrystals Passivated with Oleic Acid. *Science* **2014**, 1252727. https://doi.org/10.1126/science.1252727.

(78) Choi, H.; Ko, J.-H.; Kim, Y.-H.; Jeong, S. Steric-Hindrance-Driven Shape Transition in PbS Quantum Dots: Understanding Size-Dependent Stability. *J. Am. Chem. Soc.* **2013**, *135* (14), 5278–5281. https://doi.org/10.1021/ja400948t.

(79) Beygi, H.; Sajjadi, S. A.; Babakhani, A.; Young, J. F.; van Veggel, F. C. J. M. Surface Chemistry of As-Synthesized and Air-Oxidized PbS Quantum Dots. *Applied Surface Science* **2018**, *457*, 1–10. https://doi.org/10.1016/j.apsusc.2018.06.152.

(80) Wang, T.; Bai, J.; Jiang, X.; Nienhaus, G. U. Cellular Uptake of Nanoparticles by Membrane Penetration: A Study Combining Confocal Microscopy with FTIR Spectroelectrochemistry. *ACS Nano* **2012**, *6* (2), 1251–1259. https://doi.org/10.1021/nn203892h.

(81) Betzer, O.; Shilo, M.; Opochinsky, R.; Barnoy, E.; Motiei, M.; Okun, E.; Yadid, G.; Popovtzer, R. The Effect of Nanoparticle Size on the Ability to Cross the Blood–Brain Barrier: An in Vivo Study. *Nanomedicine* **2017**, *12* (13), 1533–1546. https://doi.org/10.2217/nnm-2017-0022.

(82) Wang, W.; van Niekerk, E. A.; Zhang, Y.; Du, L.; Ji, X.; Wang, S.; Baker, J. D.; Groeniger, K.; Raymo, F. M.; Mattoussi, H. Compact, "Clickable" Quantum Dots Photoligated with Multifunctional Zwitterionic Polymers for Immunofluorescence and In Vivo Imaging. *Bioconjugate Chem.* **2020**, *31* (5), 1497–1509. https://doi.org/10.1021/acs.bioconjchem.0c00169.

(83) Pellegrino, T.; Manna, L.; Kudera, S.; Liedl, T.; Koktysh, D.; Rogach, A. L.; Keller, S.; Rädler, J.; Natile, G.; Parak, W. J. Hydrophobic Nanocrystals Coated with an Amphiphilic Polymer Shell: A General Route to Water Soluble Nanocrystals. *Nano Lett.* **2004**, *4* (4), 703–707. https://doi.org/10.1021/nl035172j.

(84) Trapiella-Alfonso, L.; Pons, T.; Lequeux, N.; Leleu, L.; Grimaldi, J.; Tasso, M.; Oujagir, E.; Seguin, J.; d'Orlye, F.; Girard, C.; Doan, B.-T.; Varenne, A. Clickable-Zwitterionic Copolymer Capped-Quantum Dots for in Vivo

Fluorescence Tumor Imaging. *ACS Appl. Mater. Interfaces* **2018**, *10* (20), 17107–17116. https://doi.org/10.1021/acsami.8b04708.

(85) Liu, W.; Greytak, A. B.; Lee, J.; Wong, C. R.; Park, J.; Marshall, L. F.; Jiang, W.; Curtin, P. N.; Ting, A. Y.; Nocera, D. G.; Fukumura, D.; Jain, R. K.; Bawendi, M. G. Compact Biocompatible Quantum Dots via RAFT-Mediated Synthesis of Imidazole-Based Random Copolymer Ligand. *J. Am. Chem. Soc.* **2010**, *132* (2), 472–483. https://doi.org/10.1021/ja908137d.

(86) Landis, R. F.; Tang, R.; Hou, S.; Yazdani, M.; Lee, Y.; Rotello, V. M. Zwitterionic Ligands Bound to Cdse/Zns Quantum Dots Prevent Adhesion to Mammalian Cells. *Phosphorus, Sulfur, and Silicon and the Related Elements* **2015**, *190* (12), 2302–2306. https://doi.org/10.1080/10426507.2015.1085049.

(87) Medintz, I. L.; Uyeda, H. T.; Goldman, E. R.; Mattoussi, H. Quantum Dot Bioconjugates for Imaging, Labelling and Sensing. *Nature Materials* **2005**, *4* (6), 435–446. https://doi.org/10.1038/nmat1390.

(88) Ximendes, E.; Benayas, A.; Jaque, D.; Marin, R. Quo Vadis, Nanoparticle-Enabled In Vivo Fluorescence Imaging? *ACS Nano* **2021**, *15* (2), 1917–1941. https://doi.org/10.1021/acsnano.0c08349.

(89) Luther, D. C.; Huang, R.; Jeon, T.; Zhang, X.; Lee, Y.-W.; Nagaraj, H.; Rotello, V. M. Delivery of Drugs, Proteins, and Nucleic Acids Using Inorganic Nanoparticles. *Advanced Drug Delivery Reviews* **2020**, *156*, 188–213. https://doi.org/10.1016/j.addr.2020.06.020.

(90) Howes, P. D.; Chandrawati, R.; Stevens, M. M. Colloidal Nanoparticles as Advanced Biological Sensors. *Science* **2014**, *346* (6205), 1247390. https://doi.org/10.1126/science.1247390.

(91) Dubertret, B.; Skourides, P.; Norris, D. J.; Noireaux, V.; Brivanlou, A. H.; Libchaber, A. In Vivo Imaging of Quantum Dots Encapsulated in Phospholipid Micelles. *Science* **2002**, *298* (5599), 1759–1762. https://doi.org/10.1126/science.1077194.

(92) Wu, X.; Liu, H.; Liu, J.; Haley, K. N.; Treadway, J. A.; Larson, J. P.; Ge, N.; Peale, F.; Bruchez, M. P. Immunofluorescent Labeling of Cancer Marker Her2 and

Other Cellular Targets with Semiconductor Quantum Dots. *Nature Biotechnology* **2003**, *21* (1), 41–46. https://doi.org/10.1038/nbt764.

(93) Muro, E.; Pons, T.; Lequeux, N.; Fragola, A.; Sanson, N.; Lenkei, Z.; Dubertret, B. Small and Stable Sulfobetaine Zwitterionic Quantum Dots for Functional Live-Cell Imaging. *J. Am. Chem. Soc.* **2010**, *132* (13), 4556–4557. https://doi.org/10.1021/ja1005493.

(94) Smith, A. M.; Duan, H.; Rhyner, M. N.; Ruan, G.; Nie, S. A Systematic Examination of Surface Coatings on the Optical and Chemical Properties of Semiconductor Quantum Dots. *Phys. Chem. Chem. Phys.* **2006**, *8* (33), 3895–3903. https://doi.org/10.1039/B606572B.

(95) Liu, W.; Choi, H. S.; Zimmer, J. P.; Tanaka, E.; Frangioni, J. V.; Bawendi, M. Compact Cysteine-Coated CdSe(ZnCdS) Quantum Dots for in Vivo Applications. *J. Am. Chem. Soc.* **2007**, *129* (47), 14530–14531. https://doi.org/10.1021/ja073790m.

(96) Uyeda, H. T.; Medintz, I. L.; Jaiswal, J. K.; Simon, S. M.; Mattoussi, H. Synthesis of Compact Multidentate Ligands to Prepare Stable Hydrophilic Quantum Dot Fluorophores. *J. Am. Chem. Soc.* **2005**, *127* (11), 3870–3878. https://doi.org/10.1021/ja044031w.

(97) Liu, W.; Howarth, M.; Greytak, A. B.; Zheng, Y.; Nocera, D. G.; Ting, A. Y.; Bawendi, M. G. Compact Biocompatible Quantum Dots Functionalized for Cellular Imaging. *J. Am. Chem. Soc.* **2008**, *130* (4), 1274–1284. https://doi.org/10.1021/ja076069p.

(98) Zhu, Z.-J.; Yeh, Y.-C.; Tang, R.; Yan, B.; Tamayo, J.; Vachet, R. W.; Rotello, V. M. Stability of Quantum Dots in Live Cells. *Nat Chem* **2011**, *3* (12), 963–968. https://doi.org/10.1038/nchem.1177.

(99) Yildiz, I.; McCaughan, B.; Cruickshank, S. F.; Callan, J. F.; Raymo, F. M. Biocompatible CdSe−ZnS Core−Shell Quantum Dots Coated with Hydrophilic Polythiols. *Langmuir* **2009**, *25* (12), 7090–7096. https://doi.org/10.1021/la900148m.

(100) Smith, A. M.; Nie, S. Minimizing the Hydrodynamic Size of Quantum Dots with Multifunctional Multidentate Polymer Ligands. *J. Am. Chem. Soc.* **2008**, *130* (34), 11278–11279. https://doi.org/10.1021/ja804306c.

(101) Petryayeva, E.; Krull, U. J. Quantum Dot and Gold Nanoparticle Immobilization for Biosensing Applications Using Multidentate Imidazole Surface Ligands. *Langmuir* **2012**, *28* (39), 13943–13951. https://doi.org/10.1021/la302985x.

(102) Palui, G.; Aldeek, F.; Wang, W.; Mattoussi, H. Strategies for Interfacing Inorganic Nanocrystals with Biological Systems Based on Polymer-Coating. *Chem. Soc. Rev.* **2014**, *44* (1), 193–227. https://doi.org/10.1039/C4CS00124A.

(103) Sapsford, K. E.; Pons, T.; Medintz, I. L.; Higashiya, S.; Brunel, F. M.; Dawson, P. E.; Mattoussi, H. Kinetics of Metal-Affinity Driven Self-Assembly between Proteins or Peptides and CdSe−ZnS Quantum Dots. *J. Phys. Chem. C* **2007**, *111* (31), 11528–11538. https://doi.org/10.1021/jp073550t.

(104) Zhou, M.; Ghosh, I. Quantum Dots and Peptides: A Bright Future Together. *Peptide Sci.* **2007**, *88* (3), 325–339. https://doi.org/10.1002/bip.20655.

(105) Wang, W.; Kapur, A.; Ji, X.; Safi, M.; Palui, G.; Palomo, V.; Dawson, P. E.; Mattoussi, H. Photoligation of an Amphiphilic Polymer with Mixed Coordination Provides Compact and Reactive Quantum Dots. *J. Am. Chem. Soc.* **2015**, *137* (16), 5438–5451. https://doi.org/10.1021/jacs.5b00671.

(106) Popović, Z.; Liu, W.; Chauhan, V. P.; Lee, J.; Wong, C.; Greytak, A. B.; Insin, N.; Nocera, D. G.; Fukumura, D.; Jain, R. K.; Bawendi, M. G. A Nanoparticle Size Series for In Vivo Fluorescence Imaging. *Angewandte Chemie International Edition* **2010**, *49* (46), 8649–8652. https://doi.org/10.1002/anie.201003142.

(107) Viswanath, A.; Shen, Y.; Green, A. N.; Tan, R.; Greytak, A. B.; Benicewicz, B. C. Copolymerization and Synthesis of Multiply Binding Histamine Ligands for the Robust Functionalization of Quantum Dots. *Macromolecules* **2014**, *47* (23), 8137–8144. https://doi.org/10.1021/ma501955t.

(108) Johnson, C. M.; Pate, K. M.; Shen, Y.; Viswanath, A.; Tan, R.; Benicewicz, B. C.; Moss, M. A.; Greytak, A. B. A Methacrylate-Based Polymeric Imidazole Ligand Yields Quantum Dots with Low Cytotoxicity and Low Nonspecific Binding. *J*

Colloid Interface Sci **2015**, *458*, 310–314. https://doi.org/10.1016/j.jcis.2015.07.069.

(109) Zhao, X.; Shen, Y.; Adogla, E. A.; Viswanath, A.; Tan, R.; Benicewicz, B. C.; Greytak, A. B.; Lin, Y.; Wang, Q. Surface Labeling of Enveloped Virus with Polymeric Imidazole Ligand-Capped Quantum Dots via the Metabolic Incorporation of Phospholipids into Host Cells. *J. Mater. Chem. B* **2016**, *4* (14), 2421–2427. https://doi.org/10.1039/C6TB00263C.

(110) Lin, C.-A. J.; Sperling, R. A.; Li, J. K.; Yang, T.-Y.; Li, P.-Y.; Zanella, M.; Chang, W. H.; Parak, W. J. Design of an Amphiphilic Polymer for Nanoparticle Coating and Functionalization. *Small* **2008**, *4* (3), 334–341. https://doi.org/10.1002/smll.200700654.

(111) Wang, W.; Ji, X.; Na, H. B.; Safi, M.; Smith, A.; Palui, G.; Perez, J. M.; Mattoussi, H. Design of a Multi-Dopamine-Modified Polymer Ligand Optimally Suited for Interfacing Magnetic Nanoparticles with Biological Systems. *Langmuir* **2014**, *30* (21), 6197–6208. https://doi.org/10.1021/la500974r.

(112) Zhang, P.; Liu, S.; Gao, D.; Hu, D.; Gong, P.; Sheng, Z.; Deng, J.; Ma, Y.; Cai, L. Click-Functionalized Compact Quantum Dots Protected by Multidentate-Imidazole Ligands: Conjugation-Ready Nanotags for Living-Virus Labeling and Imaging. *J. Am. Chem. Soc.* **2012**, *134* (20), 8388–8391. https://doi.org/10.1021/ja302367s.

(113) Wang, W.; Ji, X.; Kapur, A.; Zhang, C.; Mattoussi, H. A Multifunctional Polymer Combining the Imidazole and Zwitterion Motifs as a Biocompatible Compact Coating for Quantum Dots. *J. Am. Chem. Soc.* **2015**, *137* (44), 14158–14172. https://doi.org/10.1021/jacs.5b08915.

(114) Wang, W.; Kapur, A.; Ji, X.; Zeng, B.; Mishra, D.; Mattoussi, H. Multifunctional and High Affinity Polymer Ligand That Provides Bio-Orthogonal Coating of Quantum Dots. *Bioconjugate Chem.* **2016**, *27* (9), 2024–2036. https://doi.org/10.1021/acs.bioconjchem.6b00309.

(115) Chiefari, J.; Chong, Y. K. (Bill); Ercole, F.; Krstina, J.; Jeffery, J.; Le, T. P. T.; Mayadunne, R. T. A.; Meijs, G. F.; Moad, C. L.; Moad, G.; Rizzardo, E.; Thang, S. H. Living Free-Radical Polymerization by Reversible Addition−Fragmentation

Chain Transfer: The RAFT Process. *Macromolecules* **1998**, *31* (16), 5559–5562. https://doi.org/10.1021/ma9804951.

(116) Tasso, M.; Giovanelli, E.; Zala, D.; Bouccara, S.; Fragola, A.; Hanafi, M.; Lenkei, Z.; Pons, T.; Lequeux, N. Sulfobetaine-Vinylimidazole Block Copolymers: A Robust Quantum Dot Surface Chemistry Expanding Bioimaging's Horizons. *ACS Nano* **2015**, *9* (11), 11479–11489. https://doi.org/10.1021/acsnano.5b05705.

(117) Viswanath, A.; Paudel, P.; Kittikhunnatham, P.; Green, A. N.; Greytak, A. B.; Benicewicz, B. C. Synthesis of Random Terpolymers Bearing Multidentate Imidazole Units and Their Use in Functionalization of Cadmium Sulfide Nanowires. *Polym. Chem.* **2015**, *6* (39), 7036–7044. https://doi.org/10.1039/C5PY00685F.

(118) Batz, H. G.; Franzmann, G.; Ringsdorf, H. Model Reactions for Synthesis of Pharmacologically Active Polymers by Way of Monomeric and Polymeric Reactive Esters. *Angew. Chem. Int. Ed. Engl.* **1972**, *11* (12), 1103–1104. https://doi.org/10.1002/anie.197211031.

(119) Jang, Y.; Shapiro, A.; Isarov, M.; Rubin-Brusilovski, A.; Safran, A.; Budniak, A. K.; Horani, F.; Dehnel, J.; Sashchiuk, A.; Lifshitz, E. Interface Control of Electronic and Optical Properties in IV–VI and II–VI Core/Shell Colloidal Quantum Dots: A Review. *Chem. Commun.* **2017**, *53* (6), 1002–1024. https://doi.org/10.1039/C6CC08742F.

(120) Takeuchi, H.; Omogo, B.; Heyes, C. D. Are Bidentate Ligands Really Better than Monodentate Ligands For Nanoparticles? *Nano Lett.* **2013**, *13* (10), 4746–4752. https://doi.org/10.1021/nl4023176.

(121) Draczkowski, P.; Matosiuk, D.; Jozwiak, K. Isothermal Titration Calorimetry in Membrane Protein Research. *Journal of Pharmaceutical and Biomedical Analysis* **2014**, *87* (Supplement C), 313–325. https://doi.org/10.1016/j.jpba.2013.09.003.

(122) Dlouhy, A. C.; Li, H.; Albetel, A.-N.; Zhang, B.; Mapolelo, D. T.; Randeniya, S.; Holland, A. A.; Johnson, M. K.; Outten, C. E. The Escherichia Coli BolA Protein IbaG Forms a Histidine-Ligated [2Fe-2S]-Bridged Complex with Grx4. *Biochemistry* **2016**, *55* (49), 6869–6879. https://doi.org/10.1021/acs.biochem.6b00812.

(123) Falconer, R. J. Applications of Isothermal Titration Calorimetry – the Research and Technical Developments from 2011 to 2015. *Journal of Molecular Recognition* **2016**, *29* (10), 504–515. https://doi.org/10.1002/jmr.2550.

(124) Winiewska, M.; Bugajska, E.; Poznański, J. ITC-Derived Binding Affinity May Be Biased Due to Titrant (Nano)-Aggregation. Binding of Halogenated Benzotriazoles to the Catalytic Domain of Human Protein Kinase CK2. *PLOS ONE* **2017**, *12* (3), e0173260. https://doi.org/10.1371/journal.pone.0173260.

(125) Prozeller, D.; Morsbach, S.; Landfester, K. Isothermal Titration Calorimetry as a Complementary Method for Investigating Nanoparticle-Protein Interactions. *Nanoscale* **2019**, *11* (41), 19265–19273. https://doi.org/10.1039/c9nr05790k.

(126) Ravi, V.; Binz, J. M.; Rioux, R. M. Thermodynamic Profiles at the Solvated Inorganic–Organic Interface: The Case of Gold–Thiolate Monolayers. *Nano Lett.* **2013**, *13* (9), 4442–4448. https://doi.org/10.1021/nl402315z.

(127) Abiodun, S. L.; Gee, M. Y.; Greytak, A. B. Combined NMR and Isothermal Titration Calorimetry Investigation Resolves Conditions for Ligand Exchange and Phase Transformation in CsPbBr3 Nanocrystals. *J. Phys. Chem. C* **2021**, *125* (32), 17897–17905. https://doi.org/10.1021/acs.jpcc.1c00144.

(128) Calvin, J. J.; Swabeck, J. K.; Sedlak, A. B.; Kim, Y.; Jang, E.; Alivisatos, A. P. Thermodynamic Investigation of Increased Luminescence in Indium Phosphide Quantum Dots by Treatment with Metal Halide Salts. *J. Am. Chem. Soc.* **2020**, *142* (44), 18897–18906. https://doi.org/10.1021/jacs.0c08954.

(129) Calvin, J. J.; O'Brien, E. A.; Sedlak, A. B.; Balan, A. D.; Alivisatos, A. P. Thermodynamics of Composition Dependent Ligand Exchange on the Surfaces of Colloidal Indium Phosphide Quantum Dots. *ACS Nano* **2021**, *15* (1), 1407–1420. https://doi.org/10.1021/acsnano.0c08683.

(130) Jharimune, S.; Sathe, A. A.; Rioux, R. M. Thermochemical Measurements of Cation Exchange in CdSe Nanocrystals Using Isothermal Titration Calorimetry. *Nano Lett.* **2018**, *18* (11), 6795–6803. https://doi.org/10.1021/acs.nanolett.8b02661.

(131) Gee, M. Y.; Shen, Y.; Greytak, A. B. Isothermal Titration Calorimetry Resolves Sequential Ligand Exchange and Association Reactions in Treatment of Oleate-

Capped CdSe Quantum Dots with Alkylphosphonic Acid. *J. Phys. Chem. C* **2020**, *124* (43), 23964–23975. https://doi.org/10.1021/acs.jpcc.0c07338.

(132) Elimelech, O.; Aviv, O.; Oded, M.; Banin, U. A Tale of Tails: Thermodynamics of CdSe Nanocrystal Surface Ligand Exchange. *Nano Lett.* **2020**, *20* (9), 6396–6403. https://doi.org/10.1021/acs.nanolett.0c01913.

(133) Gao, Y.; Peng, X. Crystal Structure Control of CdSe Nanocrystals in Growth and Nucleation: Dominating Effects of Surface versus Interior Structure. *J. Am. Chem. Soc.* **2014**, *136* (18), 6724–6732. https://doi.org/10.1021/ja5020025.

(134) Kuno, M. K. Band Edge Spectroscopy of CdSe Quantum Dots. Thesis, Massachusetts Institute of Technology, 1998.

(135) Calzada, R.; Thompson, C. M.; Westmoreland, D. E.; Edme, K.; Weiss, E. A. Organic-to-Aqueous Phase Transfer of Cadmium Chalcogenide Quantum Dots Using a Sulfur-Free Ligand for Enhanced Photoluminescence and Oxidative Stability. *Chem. Mater.* **2016**, *28* (18), 6716–6723. https://doi.org/10.1021/acs.chemmater.6b03106.

(136) Westmoreland, D. E.; Nap, R. J.; Arcudi, F.; Szleifer, I.; Weiss, E. A. PH-Dependent Structure of Water-Exposed Surfaces of CdSe Quantum Dots. *Chem. Commun.* **2019**, *55* (38), 5435–5438. https://doi.org/10.1039/C9CC01339C.

(137) Arcudi, F.; Westmoreland, D. E.; Weiss, E. A. Colloidally Stable CdS Quantum Dots in Water with Electrostatically Stabilized Weak-Binding, Sulfur-Free Ligands. *Chemistry – A European Journal* **2019**, *25* (63), 14469–14474. https://doi.org/10.1002/chem.201903908.

(138) Liu, D.; Snee, P. T. Water-Soluble Semiconductor Nanocrystals Cap Exchanged with Metalated Ligands. *ACS Nano* **2011**, *5* (1), 546–550. https://doi.org/10.1021/nn1025934.

(139) Freyer, M. W.; Lewis, E. A. Isothermal Titration Calorimetry: Experimental Design, Data Analysis, and Probing Macromolecule/Ligand Binding and Kinetic Interactions. In *Methods in Cell Biology*; Biophysical Tools for Biologists, Volume One: In Vitro Techniques; Academic Press, 2008; Vol. 84, pp 79–113. https://doi.org/10.1016/S0091-679X(07)84004-0.

(140) Beaumont, P. C.; Johnson, D. G.; Parsons, B. J. Photophysical Properties of Laser Dyes: Picosecond Laser Flash Photolysis Studies of Rhodamine 6G, Rhodamine B and Rhodamine 101. *J. Chem. Soc., Faraday Trans.* **1993**, *89* (23), 4185–4191. https://doi.org/10.1039/FT9938904185.

APPENDIX A

COPYRIGHT PERMISSIONS

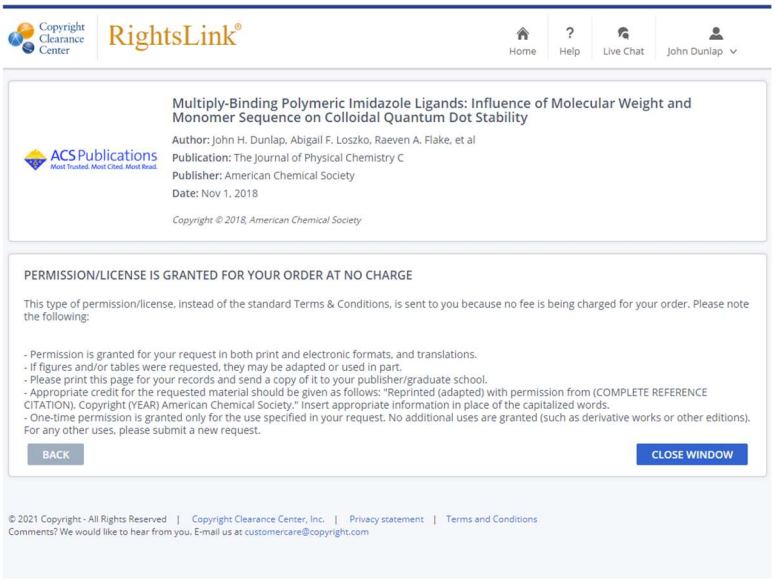

Copyright Clearance Center | RightsLink®

Home | Help | Live Chat | John Dunlap

ACS Publications
Most Trusted. Most Cited. Most Read.

Multiply-Binding Polymeric Imidazole Ligands: Influence of Molecular Weight and Monomer Sequence on Colloidal Quantum Dot Stability

Author: John H. Dunlap, Abigail F. Loszko, Raeven A. Flake, et al
Publication: The Journal of Physical Chemistry C
Publisher: American Chemical Society
Date: Nov 1, 2018

Copyright © 2018, American Chemical Society

PERMISSION/LICENSE IS GRANTED FOR YOUR ORDER AT NO CHARGE

This type of permission/license, instead of the standard Terms & Conditions, is sent to you because no fee is being charged for your order. Please note the following:

- Permission is granted for your request in both print and electronic formats, and translations.
- If figures and/or tables were requested, they may be adapted or used in part.
- Please print this page for your records and send a copy of it to your publisher/graduate school.
- Appropriate credit for the requested material should be given as follows: "Reprinted (adapted) with permission from (COMPLETE REFERENCE CITATION). Copyright (YEAR) American Chemical Society." Insert appropriate information in place of the capitalized words.
- One-time permission is granted only for the use specified in your request. No additional uses are granted (such as derivative works or other editions). For any other uses, please submit a new request.

BACK | CLOSE WINDOW

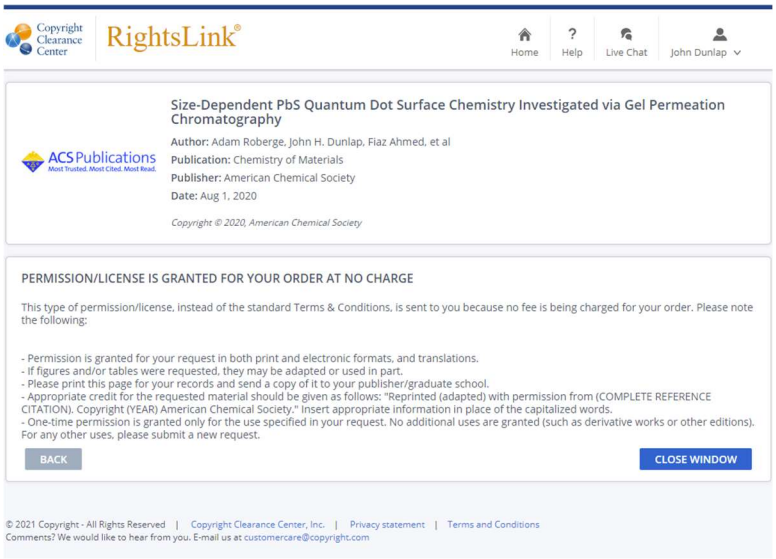

Copyright Clearance Center | RightsLink®

Home | Help | Live Chat | John Dunlap

ACS Publications
Most Trusted. Most Cited. Most Read.

Size-Dependent PbS Quantum Dot Surface Chemistry Investigated via Gel Permeation Chromatography

Author: Adam Roberge, John H. Dunlap, Fiaz Ahmed, et al
Publication: Chemistry of Materials
Publisher: American Chemical Society
Date: Aug 1, 2020

Copyright © 2020, American Chemical Society

PERMISSION/LICENSE IS GRANTED FOR YOUR ORDER AT NO CHARGE

This type of permission/license, instead of the standard Terms & Conditions, is sent to you because no fee is being charged for your order. Please note the following:

- Permission is granted for your request in both print and electronic formats, and translations.
- If figures and/or tables were requested, they may be adapted or used in part.
- Please print this page for your records and send a copy of it to your publisher/graduate school.
- Appropriate credit for the requested material should be given as follows: "Reprinted (adapted) with permission from (COMPLETE REFERENCE CITATION). Copyright (YEAR) American Chemical Society." Insert appropriate information in place of the capitalized words.
- One-time permission is granted only for the use specified in your request. No additional uses are granted (such as derivative works or other editions). For any other uses, please submit a new request.

BACK | CLOSE WINDOW